Development of nanocatalytic-based assay for the detection of an endocrine disrupting compound in aqueous solution

by

Yazmin Bustami

A thesis
presented to the University of Waterloo
in fulfillment of the
thesis requirement for the degree of
Doctor of Philosophy
in
Chemical Engineering

Waterloo, Ontario, Canada, 2016

AUTHOR'S DECLARATION

I hereby declare that I am the sole author of this thesis. This is a true copy of the thesis, including any required final revisions, as accepted by my examiners.

I understand that my thesis may be made electronically available to the public.

Abstract

Endocrine disrupting compound (EDC) pollutants raise a concern among researchers as these pollutants are implicated in the increasing incidence of testicular, breast and thyroid cancers. Some of these chemicals are widely used for plastics production and discharged into the water system as industrial effluents that could harm the ecosystem as well as plant, animal and human life. Thus, rapid detection and quantification of EDCs in water is desired for screening and investigative purposes. For this purpose, nanoparticle-based methods appear to be potentially efficient, quick and cost-effective techniques to rapidly assess this toxic pollutant.

The main focus of this study was to synthesize heterogeneous nanoparticles, iron oxide/gold nanoparticles (IONPs/AuNPs) and to manipulate their synergistic effects for the development of a nanoparticles-based assay, specifically for the EDC compound, 17β-estradiol. As the first step, IONPs and AuNPs were synthesized separately and heterogeneous nanoparticles were formed by a simple electrostatic- self- assembly technique. The unique physiochemical properties of this hybrid nanoparticle were investigated as a supporting material for biomolecules, as well for its intrinsic peroxidase-like activity using a hydrogen peroxidase dependent system.

The formation of the IONPs/AuNPs was verified using several characterization tools such as UV-Vis spectrophotometry, Dynamic Light Scattering (DLS), Transmission Electron Microscope (TEM), Energy Dispersive X-ray (EDX) and X-ray Photoelectron Spectroscopy (XPS). The diameter calculated from TEM was 16.1 ± 11.1 nm and EDX confirmed the presence of the Fe and Au elements. From a heterostructural analysis using HRTEM and

XPS data, an alloy-like morphology (Fe/Au) was suggested for the heterogeneous nanoparticles, rather than a core-shell structure. The Fe/Au nanoparticles showed good potential for the basis of a colorimetric assay for glucose detection using glucose oxidase immobilized on the Fe/Au surface. In addition, the Fe/Au nanoparticles also showed a significant peroxidase-like activity. A nanocatalytic-based assay was developed by modifying the nanoparticles surface with an aptamer in order to specifically "capture" the target molecule, 17β-estradiol. The formation of a Fe/Au-17β-estradiol complex significantly hampered the peroxidase-like catalytic activity resulting in the development of a unique nanosensor system based on the extent of loss of peroxidase activity.

Development of the nanocatalytic-based assay suggests the potential application of Fe/Au nanoparticles to capture, separate and detect a selective target as well as a basis for the development of a rapid, simple and reliable detection tool. The heterogeneous Fe/Au nanoparticles show a remarkable synergistic property for application in nanosensor system. Therefore, some of the work presented here can be extended in certain major directions such as heterostructure formation and optimization of nanocatalytic-based assay.

Acknowledgements

All praises to Allah (God) for the strengths and His blessing for me to complete this thesis. Special appreciation goes to my supervisor, Prof. William Anderson for his supervision and constant support. His invaluable help of constructive comments and suggestions throughout the experimental and thesis works have contributed to the success of this research. Not forgotten, my appreciation to my co-supervisor, Prof. Murray Moo-Young for his support and encouragement. I also would like to thank my committee members, Prof. Boxin Zhao, Prof. Ariel Chan, and Prof. Sigrid Peldszus for their great advices.

My sincere thanks to my lab members Mina, Caitlin, Cibele, Ram and Dr Shazia for their advice and timely help. Also to Dr. Zengian Shi and Chong Meng for their generosity for allowing me to use equipment vital for my research work. My special thanks to Arifa Syahira, our former internship student from UMP and to all Department of Chemical Engineering staffs for the kind helps.

My fellow Malaysian clan, especially Abdul Halim and Siti Nordeyani, for the endless support and for making my study journey in Canada a wonderful and enjoyable moment. I would like to express my gratitude to USM Academic Staff Training Scheme (ASTS) and Ministry of Higher Education, Malaysia for the financial assistance during my study.

Last but not least, a heartfelt appreciation to my husband, kids, my mum, my siblings, and my family in laws; thank you for the inspiration and for the warmth love and blessing.

Dedication

Dedicated to my beloved husband, *Mohamad Salihin Abdul Wahab*, my wonderful kids; *Siti Khadijah Amani*, *Amru Rayyan* and *Aryan Haikal*, my mother, *Jamalah Rosni*, my late father *Bustami Hassan*, and the rest of my family members.

Table of Contents

List of Figures

x

List of Tables

List of Abbreviations

A nucleobase	Adenine
Au III	aurum/gold (III)
Au4f	primary XPS region for gold
ABTS	2,2-azino-bis (3-ethylbenzothiazoline-6-sulfonic acid)
APEOs	alkylphenolethoxylates
APnEOs	nonylphenol ethoxylate
Au-O	aurum-oxygen bond
Au/Pt	gold-platinum nanoparticles
Au/PdPt	gold-padmium-platinum nanoparticles
$Au_{core}Pd_{shell}$	gold (core)-padmium (shell)
AuNPs	gold nanoparticles
Ag	silver nanoparticles
bR	bacteriorhodopsin
BLM	bilayer lipid membrane
BPA	bisphenol A
C nucleobase	Cytosine
C1s	primary XPS region for Carbon
cm	centimeter
cRGD	cancer targeting ligands
CLEIA	chemiluminescence enzyme immunoassay
CS	cation chitosan
CS-MNPs	chitosan-magnetic nanoparticles
CoS	cobalt sulfide
CuPt	copper-platinum nanoparticles
CuS	copper sulfide
CV	coefficient of variation
Cy5.5	cyanine fluorescent dye
d	diameter
d_h	hydrodynamic diameter
d-spacing	interplanar spacing
dH_2O	distilled water

ds-DNA	double stranded DNA
DDT	dichlorodiphenyltrichloroethane
Dh1A	haloalkane dehalogenase
DNA	Deoxyribonucleic acid
DLS	Dynamic Light Scattering
EDCs	endocrine disrupting chemicals
e.g. or i.e.	examples
et al.,	and others
eV	electron volt
E1	estrone
E2	17β-estradiol
E3	estriol
EE2	ethinylestradiol
EDC-linker	N-ethyl-N'- (3-dimethylaminoprophyl) carbodiimide hydrochloride
EDX	Energy Dispersive X-Ray Analysis
ELISA	Enzyme-linked Immunosorbent Assay
ER	estrogen receptor
fcc	face center cubic
fl-apt	probe aptamer
fM	femtomolar
γ-Fe_2O_3	maghemite
Fe2p	primary XPS region for iron
Fe^{3+}	ferric ion
Fe^{2+}	ferrous ion
Fe/Co	iron-cobalt nanoparticles
Fe/Au-fl-apt	probe aptamer tagged to iron-gold nanoparticles
Fe/Au	iron-gold nanoparticles
Fe/Au-Gox	immobilized glucose oxidase on iron-gold nanoparticles
Fe_3O_4	magnetite
Fe_3O_4-CA	anion citrate modified feroferric oxide nanoparticles
FFT	Fast Fourier Transform
$FeSO_4$	ferrous sulfate

FeSO$_4$.7H$_2$O	ferrous sulfate heptahydrate
FTIR	Fourier transform infrared spectroscopy
G nucleobase	Guanine
GOx	Glucose oxidase
GnRH	gonadotropins
GO-AuNPs	graphene oxide-gold nanoparticles
hr	hour
hkl	Miller indices
H$_2$O$_2$	hydrogen peroxide
H-GNs	hemin-graphene
HAuCL$_4$	hydrogen tetrachloro-aurate (III)
HNO$_3$	nitric acid
HPTE	(2,2-bis(*p*-Hydroxyphenyl)-1,1,1-trichloroethane)
HRP	horseradish peroxidase
HRTEM	High-resolution Transmission Electron Microscopy
IgG	Immunoglobulin G
IONPs	iron oxide nanoparticles
IMS	Immunomagnetic Separation
IPCR	Immune-Polymerase Chain Reaction
K$_m$	Michaelis constant for the particular enzyme
KBr	potassium bromide
mg/mL	milligram permililiter
min	minute
mV	milivolts
M$_w$	molecular weight
MES buffer	2-(*N*-morpholino) ethanesulfonic acid buffer
MWTPs	municipal wastewater treatment plants
ng L^{-1} or ng/L	nanogram per litre
nm	nanometer
NaAc	sodium acetate buffer
NaBH$_4$	sodium borohydride

Na$_3$C$_6$H$_5$O$_7$	trisodium citrate
NaOH	sodium hydroxide
NH$_4$OH	ammonium hydroxide
NHS	N- hydroxysuccinimide
NP or 4NNP	nonylphenol
NP1EO	nonylphenol monoethoxylate
NP2EO	nonylphenol diethoxylate
OP	octylphenol
OPs	organophosphorous insecticides
pg/mL	picograms per mililitre
PAEs	phthalates or phthalic acid esters
PBMNPs	Prussian blue magnetic nanoparticles
PBS-T	phosphate-buffer saline with Tween 20
PBBs	polybrominatd biphenyls
PCBs	polychlorinated biphenyls
PCB77	3,4,3',4'- tetrachlorobiphenyl
PDA	polydopamine
PDI	polydispersity index
PM	purple membrane
PVC	polyvinyl chloride
PZC	point of zero charge
rpm	revolutions per minute
ROS	reactive oxygen species
[S]	substrate concentration
s	seconds
ss-DNA	single stranded DNA
S.D	standard deviation
SNPs	single-nucleotidepolymorphisms
SMCC	sulfosuccinimidyl-4-[N-maleimidomethyl]cyclohexane-1-carboxylate
SELEX	Systematic Evolution of Ligand by Exponential Enrichment
SH-apt	thiolated aptamer

SPA	staphylococcal protein A
SWCNTs	single-walled carbon nanotubes
T nucleobase	Thymine
TEM	Transmission Electron Microscopy
TMB	3,3,5,5-tetramethylbenzidine
Tyr	tyrosinase
V_{max}	maximal velocity
VTG	vitellogenin
WS_2	tungsten disulfides
WWTP	wastewater treatment plants
XPS	X-ray photoelectron spectroscopy
11-MUDA	11-Mercaptoundecanoic acid
^{o}C	degree Celsius
μM	micomolar
μL	microliter

Chapter 1
Introduction

1.1   Motivation:

Environmental pollution is one of the main contributors towards health hazards in humans. With the constant and continuous development of modern industrial processing, environmental pollution seems unavoidable. Industrial processing activities such as the production of synthetic plastics, dyes, drugs, antioxidants, polymers, detergents, oil refinery and pulp and paper tends to release highly toxic compounds, for example endocrine disrupting chemicals (EDCs) as industrial effluents. Many of the EDCs are known to cause toxic effects to animals and plants as they easily penetrate the skin and cell membranes, resulting in a wide range of genotoxicity, mutagenicity, hepatotoxic effects and affecting the rate of biocatalyzed reactions, and the processes of respiration and photosynthesis (Rodriguez-Mozaz et al., 2004). The focal urge for environment quality monitoring is based on the main concern that the EDCs are found to accumulate in the environment and subsequently harm plant, animal and human life. Thus, an efficient, rapid and cost-effective analytical technique for screening for these toxic pollutants is highly desirable.

The expansion of the nanotechnology field into biotechnology and material technology has made possible research into magnetic materials and new technology applications. The utilization of nanoparticles for monitoring systems is extensively adapted to biosensor applications. It has become an interesting multidisciplinary area for applications in bioscience and biotechnology, biomedical and environment technology. A number of studies have focused on the hybrid nanoparticles, iron oxide-gold nanoparticles (IONPs-AuNPs). IONPs are favourable particles due to their remarkable material properties with functional versatility. They

are known to be inexpensive to produce, physically and chemically stable, biocompatible and environmentally safe (Haun et al., 2010). The unique properties of magnetic nanoparticles also show new phenomena such as superparamagnetism (Beveridge et al., 2011). However, the pure magnetic nanoparticles themselves may not be very useful in practical applications (Zhao et al., 2005) as they easily aggregate and have limited available groups for biofunctionalization. The addition of gold nanoparticles (AuNPs) will provide a platform for surface modification, functionalization, tuning magnetic properties and biocompatibility (Cho et al., 2005).

The IONPs-AuNPs show unique physiochemical properties as they have been demonstrated to exhibit improved catalytic performance, better selectivity and stability for the synergistic effect (Duan and Wang, 2013; Ferrando et al., 2008). It is known that IONPs-AuNPs can be manipulated for interfacial interaction between nanoparticles and biomolecules such as enzymes, DNAzymes, antibodies and aptamers. These biomolecules can be immobilized on the modified nanoparticle surfaces by several conjugation methods. For examples, direct conjugation to the surface and to surface-bound stabilizing ligands or coatings, either directly or using small cross-linking molecules and other intermediaries (Sapsford et al., 2013). In recent years, nanoparticles have been discovered to have intrinsic peroxidase-like catalytic activity (Chen et al., 2013, Sun et al., 2013, He et al., 2011, Kwon et al., 2011, Chen et al., 2011). Therefore, the combination of both interesting properties could provide a useful platform for biosensing purposes, particularly; nanoparticles-based assays for easy handling of samples as well as selective detection of EDCs.

1.2   Research objectives:

The first objective of this thesis was to construct and acquire a qualitative understanding of the formation of heterogeneous nanoparticles of iron oxide/gold nanoparticles (IONPs-AuNPs) by using an electrostatic- self- assembly technique of the positively charged IONPs and negatively charged citrate coated AuNPs.

The second objective was to study the physiochemical property of the hybrid IONPs-AuNPs. To investigate the nanoparticles as a biomolecule supporting material, glucose oxidase was immobilized on the carboxylate-modified IONPs-AuNPs and tested for glucose detection. Then, to investigate the intrinsic peroxidase-like catalytic activity of IONPs-AuNPs, a steady-state kinetic analysis using a hydrogen peroxidase dependent system was carried out.

Finally, to assess the application of IONPs-AuNPs as supporting materials and their catalytic activity, development of a nanocatalytic-based assay was performed, specifically to detect an endocrine disrupting chemical; 17β-estradiol.

1.3   Thesis structure

This thesis consists of five chapters. Chapter 1 focuses on the research motivation and objectives. Chapter 2 summarizes the literature on iron oxide nanoparticles and the heterogeneous nanoparticles of IONPs-AuNPs, endocrine disrupting chemicals (EDC) and application of heterogenous nanoparticles in nanosensor systems. Chapter 3 explains in detail the heterostructure of IONPs-AuNPs and their application for glucose detection as a model system. Chapter 4 explains the manipulation of the nanoparticles peroxidase-like activity for development of a nanocatalytic-based assay. Finally, Chapter 5 summarizes the main conclusions and recommendations for future directions.

References

Beveridge JS, Stephens JR, and Williams ME. (2011) The use of magnetic nanoparticles in analytical chemistry. *Ann Rev of Anal Chem* (4): 251-273

Birnbaum LS. (2013) State of the Science of Endocrine Disruptors. *Environ Health Perspect* 121(4): a107

Chen H, Li Y, Zhang F, Zhang G, and Fan X. (2011) Graphene supported Au-Pd bimetallic nanoparticles with core-shell structures and superior peroxidase-like activities. *J Mater Chem* 21(44): 17658–17661

Chen L, Feng T, Wang P, and Xiang Y. (2013) Transition metal (Fe, Co) and organic silanol modified mesoporous titanium phosphates as catalysts for the oxidation of benzyl alcohol in water. *React Kin, Mech & Catal* (110:2): 485-496

Cho SJ, Idrobo JC, Olamit J, Liu K, Browning ND, and Kauzlarich SM. (2005) Growth mechanisms and oxidation resistance of gold-coated iron nanoparticles. *Chem Mater* (17): 3181-3186

Duan S, and Wang R. (2013) Bimetallic nanostructures with magnetic and noble metals and their physicochemical applications. *Prog In Nat Sci-Mater Intl* 23(2): 113-126

Ferrando R, Jellinek J, and Johnston RL. (2008) Nanoalloys: from theory to applications of alloy clusters and nanoparticles. *Chem Rev* 108(3): 845-910

Haun JB, Yoon T, Lee H, and Weissleder R. (2010) Magnetic nanoparticle biosensors. *Nanomed Nanobiotechnol* (2): 291–304

He W, Liu Y, Yuan J, Yin JJ, Wu X, Hu X, Zhang K, Liu J, Chen C, Ji Y, and Guo Y. (2011) Au@Pt nanostructures as Oxidase and Peroxidase Mimetics for Use in Immunoassays. *Biomater* (32): 1139–1147

Kwon T, Min M, Lee H, and Kim BJ. (2011) Facile preparation of water soluble CuPt nanorods with controlled aspect ratio and study on their catalytic properties in water. *J Mater Chem* 21(32): 11956–11960

Rodriguez-Mozaz S, Marco MP, J. Lopez de Alda M, and Barceló D. (2004) Biosensors for environmental applications: Future development trends *Pure Appl Chem* 76(4): 723–752

Sapsford KE, Algar WR, Berti L, Gemmill KB, Casey BJ, Oh E, Stewart MH, and Medintz IL. (2013) Functionalizing nanoparticles with biological molecules: Developing chemistries that facilitate nanotechnology. *Chem Rev* 113(3): 1904–2074

Sun H, Jiao X, Han Y, Jiang Z, and Chen D. (2013) Synthesis of Fe_3O_4-Au Nanocomposites with Enhanced Peroxidase-Like Activity. *Eur J Inorg Chem* 109–114

Zhao G, Feng JJ, Zhang QL, Li SP, and Chen HY. (2005) Synthesis and characterization of Prussian blue modified magnetite nanoparticles and its application to the electrocatalytic reduction of H_2O_2. *Chem Mater* (17): 3154-3159

Chapter 2

Literature review

2.1   Magnetic nanoparticles

In the past two decades, nanoparticles have received considerable attention among researchers in multidisciplinary areas such as biotechnology, medical, environmental technology and metallurgy technology due to the interesting properties related to their size (Racuciu et al., 2008). Nanoparticles can be divided into certain categories such as metallic nanoparticles including gold, silver, alloy and other metal nanoparticles, oxide nanoparticles consisting of magnetic and nonmagnetic oxide nanoparticles, sulfide nanoparticles, and other miscellaneous nanoparticles.

Magnetic nanoparticles show importance as they have been developed into a new entity, due to their finite size and surface effects which dominate the magnetic behavior of the individual nanoparticles (Batlle and Labarta, 2002). Due to this composition, the particles attain superparamagnetism, high field irreversibility, high saturation field, extra anisotropy contributions or shifted loops after field cooling (Tartaj et al., 2003). Superparamagnetic properties, which means the magnetic nanoparticles have no "magnetic memory" is advantageous because they can be easily dispersed in solvent without attractive magnetic forces inducing particle aggregation (Beveridge et al., 2011).

Many types of magnetic nanoparticles can be synthesized such as iron oxide, ferrites of cobalt, manganese, nickel, and magnesium. The most commonly employed magnetic nanoparticles are made from iron oxide as they are easily synthesized with size-monodisperse products with high magnetic moments (Beveridge et al., 2011) and also are known to be biocompatible (Li et al., 2011). Magnetic iron oxides come in several forms, including

maghemite (γ-Fe_2O_3) and magnetite (Fe_3O_4), but these can be difficult to distinguish in particles that are not single crystals. These particles are also known to be spherical in shape (Beveridge et al., 2011), which may be an advantage for applications. These ferrite colloids are characterized by a spinel crystal structure with oxygen ions forming a close-packed cubic lattice and iron ions located at the interstices (Figure 2.1). The magnetization of Fe_3O_4 arises from antiferromagnetic coupling (super-exchange through oxygens) between the Fe^{3+} ions in octahedral and tetrahedral interstices, leaving the magnetic moments of the Fe^{2+} ions (in octahedral positions) as responsible for the magnetization of the unit cell (Reddy et al., 2012).
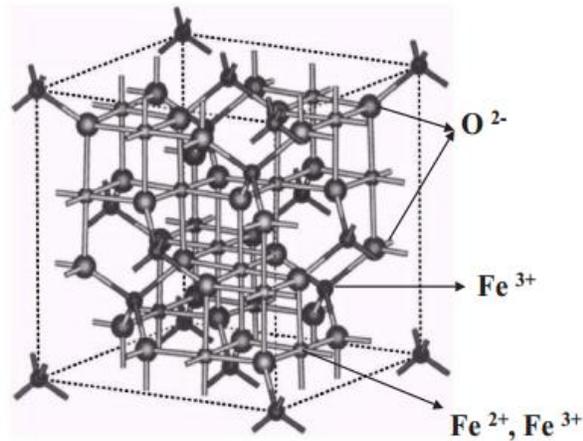
Figure 2.1 **Inverse spinel structure of Fe_3O_4. The large spheres represent the oxygen atoms, the small dark spheres the A-site and the small bright spheres denote the B-site (from Jeng and Guo, 2002).**

The characteristic of magnetic nanoparticles which exhibit responses to the external magnetic field supports diverse application and several important properties of magnetic materials are crucial for these applications, namely (Safarik and Safarikova, 2009; Arruebo et al., 2007) :

1) For selective separation (removal) of magnetic nano- and micro- particles and composites from the complex samples using an external magnetic field (e.g. using an appropriate magnetic separator, permanent magnet, or electromagnet). This process is very important for bioapplication and environmental technology because most of the biological materials and contaminants have diamagnetic properties or no magnetic properties. When this biological material is magnetically modified, an efficient selective separation from the complex mixture is enabled.

2) For mobility purposes, where the magnetic particles are able to move to a desired place and making sure they remain there, using an external magnetic field. This property is beneficial especially for magnetic drug targeting applications.

3) For generation of heat when magnetic particles are subjected to an alternating magnetic field. This phenomenon can be efficiently employed especially for cancer therapy using magnetic fluid hyperthermia.

4) For generation of negative T2 contrast during magnetic resonance imaging in the presence of magnetic iron oxides nanoparticles.

5) For magnetic modification of diamagnetic biological materials (e.g. cells) and magnetic labeling of biologically active compounds by magnetic nano- and microparticles.

2.1.1 Synthesis of magnetic nanoparticles

One of the latest tendencies in materials science is to tailor-make classical products with controlled properties for special uses (Tartaj et al., 2003). It is important to carefully synthesize the magnetic nanoparticle since it could modify the magnetic physicochemical properties that might affect the final application, and particle aggregation must be minimized. Many chemical procedures have been used such as classical co-precipitation, microemulsion, sol-gel syntheses, sonochemical, microwave reaction, hydrothermal reactions, hydrolysis and thermolysis (Safarik et al., 2011). Generally, most of the methods aim to synthesize a uniform nanoparticles size and shape; however this is a complex process because of their colloidal nature (Laurent et. al., 2008). There are two main challenges that need to be taken into consideration in order to produce a good nanoparticle. The first main chemical challenge consists of defining experimental conditions, leading to a monodisperse population of magnetic grains of suitable size. The second critical point is to select a reproducible process that can be industrialized without any complex purification procedure, such as ultracentrifugation (Sjogren et al., 1997), size-exclusion chromatography (Nunes and Yu, 1987), magnetic filtration (Babes et al., 1999), or flow field gradient (Thurm and Odenbach, 2002). These methods have been used to prepare particles with homogeneous composition and narrow size distribution. However, the most common method for the production of magnetite nanoparticles is the chemical co-precipitation technique of iron salts.

2.1.1.1 Solution co-precipitation method

The solution co-precipitation offers a simple and most efficient approach. It shows the potential for rigorous control of the nanoparticles size and shape. However the control of the particle size is difficult sometimes and tends to generate a broader size of distribution.

In principle, there are two main mechanisms for formation of particles in solution; nucleation and growth. LaMer and Dinegar (1950) first explained this mechanism in sulfur colloids experiments. In a homogenous precipitation, a short single burst of nucleation occurs when the concentration of constituent species reaches critical supersaturation. Then the nuclei obtained are allowed to grow uniformly by diffusion of solutes from the solution to their surface until the final size is attained. To achieve size monodispersity, nucleation should be avoided during the period of growth. In general, the co-precipitation process involves the precipitation of iron salts such as iron precursors Fe^{2+} and Fe^{3+} in the ratio of $1:2$ in aqueous alkaline medium. Most commonly, sodium hydroxide (NaOH) or ammonium hydroxide (NH_4OH) is used, which leads to the formation of green rust at the early stage of precipitation, followed by the black precipitation as the process is completed. Different wet-chemical synthesis parameters such as the Fe^{2+}/Fe^{3+} ratio, ionic strength, ions concentration and pH value affect the resulting iron oxide characteristics. The overall reaction equation may be indicated as follows:

$$Fe^{2+} + 2\,Fe^{3+} + 8OH^- \rightarrow Fe_3O_4 + 4H_2O$$

However, magnetite (Fe_3O_4) is not very stable and is sensitive to oxidation which results in the formation of maghemite (γ-Fe_2O_3) (Safarik et al., 2011). In this co-precipitation method, the pH value of the solution changes rapidly and locally. Accordingly, it is difficult to synthesize the smaller and more uniform-shaped products that are desirable for practical uses (Mizukoshi et al., 2009). Thus, to achieve a good monodispersity, reaction parameters such as solution pH and temperature, the stirring mixing rate, the anion salt, and the concentration of metal ions need to be strictly control because these reactions are governed by thermodynamic (e.g., temperature, reduction potential) and kinetic parameters (e.g., reactant concentration, diffusion, solubility, reaction rate) (Beveridge et al., 2011).

Since the nanoparticle size is crucial for its final application, several modification strategies have been carried out. The addition of chelating organic anions (carboxylate, citric, gluconic and oleic acids) or polymer surface complexing agents (dextran, carbodextran, starch, or polyvinyl alcohol) during the formation of magnetite can help to achieve more uniform nanoparticle size and shape (Safarik et al., 2011). According to the molar ratio between the organic ion and the iron salts, the chelation of these organic ions on the iron oxide surface can either prevent nucleation and then lead to the larger particles or inhibit the growth of the crystal nuclei, leading to small nanoparticles (Laurent et al., 2008; Berger et al., 1999). Other strategies could be applied such as performing the synthetic and biological nanoreactors. For instance, water-swollen reversed micellar structures in non-polar solvents, apoferritin protein cages, and formation of dendrimers, cyclodextrins and liposomes (Laurent et al., 2008).

2.1.1.2 Reverse co-precipitation method

The main drawback of classical co-precipitation is the difficulty of size and shape control; hence researchers introduced a new technique which utilizes the basic fundamentals of the co-precipitation technique with slight modifications (Kazemzadeh et al., 2012; Mahmed et al., 2011; Aono et al., 2005; Teraoka et al., 1995). Teraoka et al. (1995) explored the reverse co-precipitation method to synthesize fine powders of poly-metallic oxides. The reverse co-precipitation method is opposite from the classical co-precipitation system. In the classical method the basic alkaline solution is added drop-wise to the solution mixture of iron salts then the pH increases gradually over time and after increasing to pH 3, Fe^{3+} ions are immediately precipitated as ferrihydrite, which then reacts with the existing Fe^{2+} ions in the solution to form magnetite (Kazemzadeh et. al., 2012). The electron transfer between Fe^{2+} and Fe^{3+} plays an

important role in the crystallization process and more than 10 % (mol) of Fe^{2+} ions persuade the crystallization of all the iron into spinel (Gnanaprakash et al., 2007).

For co-precipitation method, Aono et al. (2005) reported that with the gradual increase in pH value, it would cause an increase in the mean crystallite and particle size. In contrast, for the reverse co-precipitation method, the mixture of iron salts solution is added drop-wise into an alkaline solution and causes a small pH value changes in the alkaline solution and it allows a short and rapid nucleation of magnetite. Thus, the pH of the solution can be maintained during the precipitation process and it is also suggested that the magnetic nanoparticles do not grow in the reverse method (Aono et al., 2005) which is good for producing particles with monodisperse distribution. Since the pH of the alkaline solution plays an important role in controlling the growth and size of the synthesized nanoparticles (Tang et al., 2009), the reverse co-precipitation method was found to be preferable over the normal method.

Furthermore, a study reported that water dispersible carboxylate-functionalized superparamagnetic magnetite nanoparticles had been synthesized with the aid of biocompatible sodium citrate salt (Jing et al., 2012). It used commercially available, inexpensive, and environmentally acceptable raw reaction materials (water is the solvent), and represents an economic and green approach for the controlled synthesis of magnetite nanoparticles. More importantly, the as-prepared magnetite nanoparticles exhibit high water-dispersible stability and a superparamagnetic property with relatively high saturation magnetization at room temperature.

Many studies have been adapted using this method for example, ultrasonic assisted reverse co-precipitation of ferrous sulfate ($FeSO_4 \cdot 7H_2O$) in NaOH solution with the addition of surfactant in various types of atmospheres (Mizukoshi et al., 2009) and a study of reverse co-precipitation in ambient atmosphere (Mahmed et al., 2011). In addition, this method also allows

utilization of a single source of salt ion which is ferrous salt (Fe^{2+}) to synthesize magnetite nanoparticles (Alibeigi and Vaezi, 2008). The microwave- assisted method to synthesize magnetic iron oxides was utilized by applying heating to the co-precipitation process and is based on the microwave treatment of a mixture Fe^{3+} and Fe^{2+} salts at high pH (Hong et al., 2008). In comparison with conventional heating methods, reactions under microwave irradiation usually have higher reaction rates and the product can be obtained in a shorter period of time. In general, microwave irradiation can accelerate many chemical reactions in organic and inorganic syntheses.

2.1.2 pH-dependent surface charge of magnetic nanoparticles

In theory, metal ions such as Fe^{3+} occur at the top layer of the oxides surface and react with water molecules to form hydroxyl (OH) groups in an attempt to complete their coordination sphere. Due to the formation of chemically reactive surface hydroxyl (S-OH sites) groups, charge development could occur by direct proton transfer in surface protonation and deprotonation processes (Tombácz, 2009). Generally, this process is associated with chemical reactions with H^+ or OH^- ions. Surface protonation and deprotonation reaction for the amphoteric solid such as magnetite, show as follows:

$$Fe\text{-}OH + H^+ \longleftrightarrow Fe\text{-}OH_2^+ \text{ (protonation)} \qquad \text{Eqns. (1)}$$

$$Fe\text{-}OH \longleftrightarrow Fe\text{-}OH^- + H^+ \text{ (deprotonation)} \quad \text{Eqns. (2)}$$
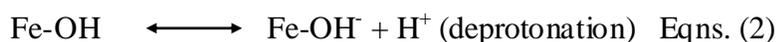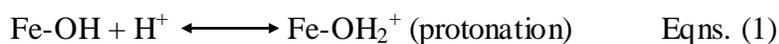
An experimental work to determine the magnetite nanoparticles point of zero charge (PZC) by potentiometric acid-base titration was conducted and presented as in Figure 2.2 (Illés and Tombácz, 2003). Herein, the PZS of magnetite was measured to be pH 7.0 ± 0.1 and

show that at pHs lower than the PZC, the surface charge is positive due to the accumulation of the H^+-ions on the surface, while oxide particles are negatively charged above the pH of PZC.
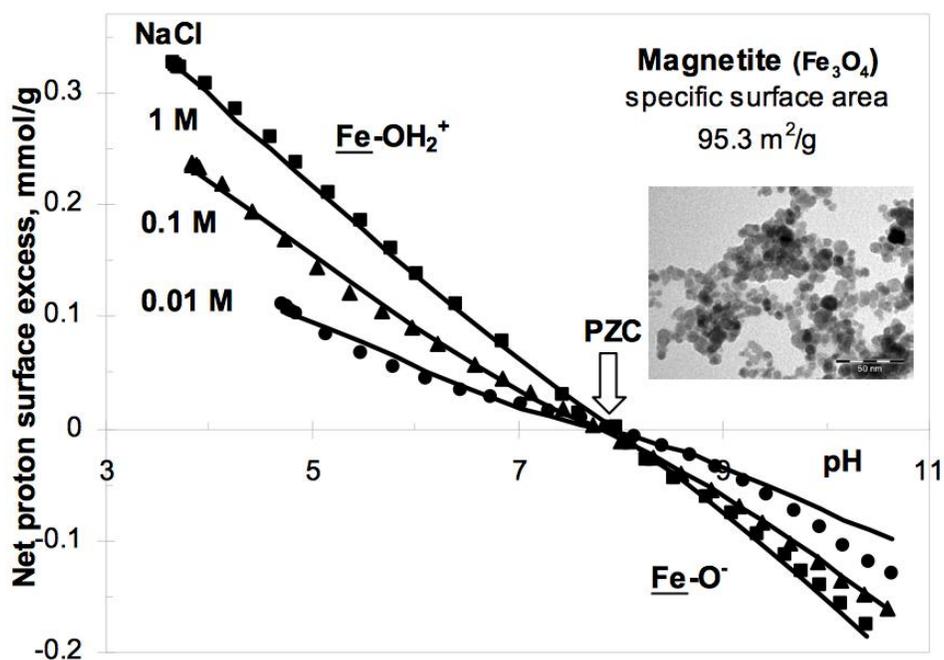
Figure 2.2   **Experimental charge potential curves of magnetite dispersed in different ionic strengths, the points of zero charge (PZC) was identified at the pH values of common intersection points (from Illés and Tombácz, 2003)**

The newly synthesized magnetic nanoparticles, particularly IONPs, have unstable colloidal and physical properties. With this pH-dependent characteristic, adhesion of colliding particles can be controlled by covering particles with an adsorption layer to avoid particles aggregation and a stable nanoparticles can be achieved. The surface is extremely reactive toward oxidizing agents and in the presence of water or humid air. Thus, protection of magnetic nanoparticles is of prime importance for obtaining physically and chemically stable colloidal

14

systems (Reddy et. al., 2012). Such protection can be achieved by surface coating of the magnetic nanoparticles.

In addition, this property had been manipulated to fabricate superparamagnetic multilayer hybrid hollow microspheres using a layer-by-layer technique (Mu et al., 2010). Their work demonstrated that the polyelectrolyte cation chitosan (CS) and the hybrid anion citrate modified ferroferric oxide nanoparticles (Fe_3O_4-CA) onto polystyrene sulfonate microspheres templates were assembled using electrostatic interaction. The layer-by-layer technique or known as LbL was adapted from the concept of the Langmuir or Langmuir-Blodgett deposition method (Bishop and Nuzzo, 1996). It consists of the transfer of amphiphilic molecules from the water-air interface, to a solid-air interface allowing for the transfer of multiple layers.

Polyelectrolytes (ionic polymers) have been introduced in the LbL assembly technique as an alternating adsorption of oppositely charged polymers. It modifies surfaces and colloids by exploiting electrostatic attraction for their deposition. This approach, in its simplest form, uses two solutions of oppositely charged polymers into which the substrate can be dipped (surface) (Hammond, 2000; Decher, 1997) or particles mixed (colloids) (Caruso, 2001). Once deposited, the layer of polyelectrolyte inverts the surface charge of the material it is adsorbed to, enabling a subsequent layer of polymer to be deposited from the second solution (Gittins and Caruso, 2001). This process is versatile as it can be deposited repeatedly and is able to generate a multilayered coating. In addition, one of the polyelectrolyte solutions can be replaced with a similarly charged species such as proteins, dyes, clays and nanoparticles to form composite multilayers (Hammond, 2000; Caruso, 2000; Decher, 1997).

2.2   Fabrication of bimetallic nanoparticles

Bimetallic nanoparticles consist of magnetic metals and noble metals and show a promising potential in fields such as magnetic sensors, catalysts, optical detection and biomedical applications (Duan and Wang, 2013). Generally, bimetallic nanoparticles are composed of two distinct metal elements by a certain mixing pattern and geometry architecture.

Iron oxide nanoparticles (IONPs) that contain magnetic metal elements, are frequently used for fabrication of a bimetallic structure with other noble metal due to their difficulty for bioanalytical purposes as bare magnetic nanoparticles tend to easily aggregate (Lia et al., 2009) and have limited available groups for surface functionalization. Gold nanoparticles (AuNps) is a noble metal that contains 5d metals (Duan and Wang, 2013). It is also known as an adequate shell coating for magnetic nanoparticles because it adds functionality to magnetic nanoparticles as well as to improve their stability in aqueous dispersions (Laurent et. al., 2008). Furthermore, AuNPs can be prepared with a high degree of monodispersity using the well-known citrate reduction technique or the Turkevich method. A study by Kimling et al. (2006) shows that gold particles can be produced in a wide range of sizes, from 9 to 120 nm, with defined size distribution, following the earlier work of Turkevich and Frens (the Turkevich method).

The bimetallic nanoparticles of magnetic and gold nanoparticles help to reduce particle agglomeration by steric or electronic repulsion and improve biocompatibility (Daniel and Astruc, 2004). Gold-coating are generally stable under acidic and neutral pH in aqueous media (Reddy et. al., 2012). Additionally, gold-coating also provides the opportunity for surface functionalization with a wide variety of ligands of interest (Sapsford et al., 2013; Netto et al 2013).

2.2.1 Synthesis of magnetic/gold nanoparticles and their morphologies

There are several strategies to fabricate magnetic/gold nanoparticles for example, gamma ray radiation, laser ablation, sonochemical reaction, layer-by-layer electrostatic deposition, chemical reduction, and micelle methods (Zhang et al., 2006; Kinoshita et al., 2005; Caruntu et. al., 2005; Spasova et al., 2005; Stoeva et al., 2005; Lyon et al., 2004; Mandal et al., 2005).

Water-soluble Au-coated magnetite nanoparticles with diameters of about 60 nm were synthesized by the reduction of Au III onto the surface via iterative hydroxylamine seeding (Lyon et al., 2004). Magnetite nanoparticles stabilized by oleic acid and 2-bromo-2-propionic acid and gold seed nanoparticles were covalently attached to amino-modified silica particles, and then, the growth of a complete gold shell provided superparamagnetic gold nanoshells (Kim et al., 2006).

Chemical reduction and deposition of AuNPs onto IONPs surfaces coupled with thermal processing is a favourable approach because it offers simple and effective size controllability. For example, a study reported a sequential synthesis method to produce gold-coated iron oxide core-shell nanoparticles by the reduction and deposition of gold onto pre-synthesized iron oxide nanoparticles and applied thermal processing strategy for the fabrication of Fe_2O_3/AuNPs (Park et al., 2007). Based on this study, the synthesized Fe_2O_3 nanoparticles were first capped with oleic acid (OA) then the Fe_2O_3/AuNPs assembled using a modified thermally activated processing strategy (Park et al., 2007). As a result, they showed that this method could produce highly monodisperse Fe_2O_3/AuNps with controllable sizes ranging from 5 to 100 nm. The thermal processing treatment of AuNps involved molecular desorption, nanocrystal core coalescence, and molecular re-encapsulation processes in the evolution of nanoparticle precursors at elevated temperatures (149 °C). The thermal processing of small monolayer-protected nanoparticles as precursors (Schadt et al., 2006; Maye et al., 2000; Zhong et al., 1999)

showed an ability to produce uniform particles. The inverse micelles were formed with cetyltrimethylammonium bromide as the surfactant, 1-butanol as a co-surfactant and octane as the continuous oil phase. $FeSO_4$ was then reduced using $NaBH_4$, followed by the addition of $HAuCl_4$ to coat the iron particles (Liu et al., 1998) but it is undesirable to use such organic solvents and strong reducing agents, for safety and environmental reasons.

In situ growth of AuNPs on the surface of IONPs also offers an interesting strategy for reusability purposes. In a recent study, a simple and green method for the *in situ* growth of AuNPs on the surface of polydopamine (PDA)-encapsulated iron oxide nanoparticles have been developed (Zeng et al., 2013). The iron oxide core with 400 nm diameter was enveloped with PDA/AuNPs shell layer. In this study PDA serves as a reductant as well as stabilizer, thus no additional reagent and thermal treatment are needed. Thus, the formation of IONPs/PDA/AuNPs facilitates an excellent nanocatalysts activity that shows an excellent recyclability for reduction of nitrobenzene.

Bimetallic nanoparticles morphologies can be categorized into three main types which are core-shell nanoparticles, dumbbell nanoparticles and alloyed nanoparticles. These three different morphologies are illustrated in Figure 2.3. According to Duan and Wang (2013), the formation of these different morphologies is based on the mixing pattern in wet-chemical synthesis. Core-shell nanoparticles are formed when one type of metal forms a core and then is fully coated by another kind of metal, thus, the core layer is protected from the environment. For dumbbell shape, two parts of the bimetallic nanoparticles only share a mixed interface. In this type, both metal parts are exposed to the environment. Different from core–shell or dumbbell structures, the elements of the alloyed nanoparticles are homogeneously mixed randomly or in an ordered manner.
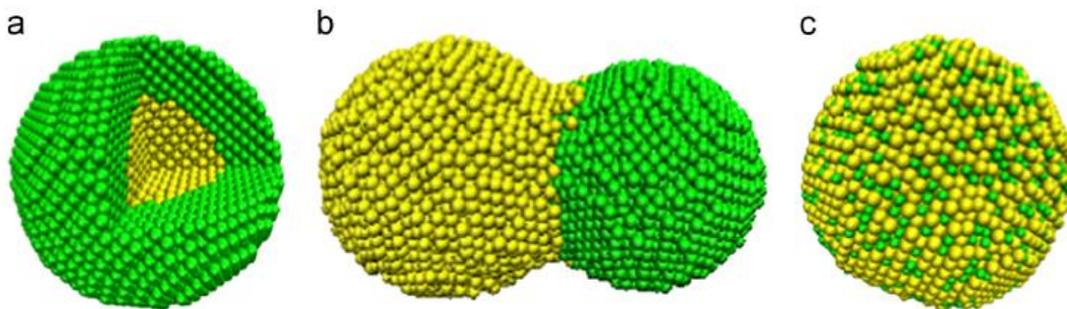
Figure 2.3 **Three types of bimetallic nanoparticles a) core-shell nanoparticles, b) dumbbell nanoparticles and c) alloyed nanoparticles (from Duan and Wang, 2013).**

2.2.2 Bimetallic nanoparticles physicochemical property

The fabrication of magnetic-noble multifunctional nanostructures could lead to the formation of a new physiochemical property. For examples, bimetallic nanoparticles have been demonstrated to exhibit improved catalytic performance, better selectivity and stability for the synergistic effect (Duan and Wang, 2013; Ferrando et al., 2008). This might be due to magnetic and noble metals have complex electron structures, thus, exhibiting promising potential in the field of catalysis containing electrochemical catalysis, heterogeneous catalysis, and photochemical catalysis.

In recent years, researchers have reported that bimetallic nanoparticles exhibit intrinsic peroxidase-like activity for examples Fe/Co (Chen et al., 2013), Fe_3O_4-Au (Sun et al., 2013), Au/Pt nanoparticles (He et al., 2011), Au/PdPt -nanorods(Zhang et al., 2011), CuPt nanorods (Kwon et al., 2011) and $Au_{core}Pd_{shell}$–graphene hybrids (Chen et al., 2011). Based on the strong metal–metal interactions and the extra stabilization of the transition state on the alloy -catalysts, their catalytic performance is different from a monometallic catalyst (Chen et al., 2013).

In general, the nanoparticles that show peroxidase-like activity are linked with reactive oxygen species (ROS)-related redox process. Reactive oxygen species (ROS), resulting from the

transfer of energy or electrons to oxygen, such as singlet oxygen, superoxide, hydrogen peroxide, and hydroxyl radical, are essential intermediates in certain physiological processes (e.g., photosynthesis, respiration, and cell signaling), and their levels within cells are tightly controlled via enzymes (e.g., superoxide dismutase, glutathione peroxidase, and catalase) or antioxidants (e.g., ascorbic acid, cysteine, glutathione, bilirubin, carotenoids, and bilirubin) (Wu et al., 2014). For example, the peroxidase-like activity for magnetic iron oxide nanoparticles originates from ferrous ions at the surface of nanoparticles. The mechanism follows the Fenton reaction which involves one-electron reduction of hydrogen peroxide by soluble ferrous iron species, generates hydroxyl radicals as follows (Zhang et al., 2010):

$$Fe^{2+} + H_2O_2 \longrightarrow Fe^{3+} + \cdot OH + OH^- \quad (1)$$

$$Fe^{3+} + H_2O_2 \longrightarrow Fe^{2+} + \cdot OOH + H^+ \quad (2)$$
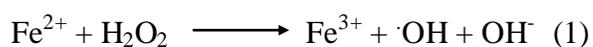
The formed hydroxyl radical is important in oxidation of chromogenic substrate such as 2,2-azino-bis (3-ethylbenzothiazoline-6-sulfonic acid) (ABTS) and 3,3,5,5-tetramethylbenzidine (TMB). In addition, the formation of multiple enzyme-mimetic properties have been reported can catalyze the rapid decomposition of H_2O_2 for instance Ag and Au nanoparticles (Li et al., 2015).

Many studies have been conducted for application of enzyme mimetic properties for analytical tools. A study by Guo et al. (2011) demonstrated that hemin-graphene hybrid nanosheets (H-GNs) have intrinsic peroxidase-like activity, which can catalyze the reaction of peroxidase substrate, due to the existence of hemin on the graphene surface. H-GNs exhibit the ability to differentiate ss- and ds-DNA in optimum electrolyte concentration, owing to the different affinities of ss- and ds-DNA to the H-GNs. Guo group have successfully developed a label-free colorimetric detection system for single-nucleotide polymorphisms (SNPs) in disease-

associated DNA. A recent study shows that incorporation of graphene oxide (GO) and gold nanoclusters shows high peroxidase-like activity over a broad pH range, even at neutral pH (Tao et al., 2013). In this study, the folic acid conjugated GO-AuNPs hybrid was used to design and develop a simple, cheap and highly selective and sensitive colorimetric assay to detect cancer cells.

2.3   Endocrine disrupting chemicals

The endocrine system is a complex system consisting of many interacting tissues connected by hormones. The hormones produced by endocrine glands are responsible for controlling a large number of processes in the body and it regulates a diverse set of physiological responses which are involved in early development and throughout adulthood. Hence, endocrine disruptors can be defined as a compound that can alter the normal functioning of the endocrine system, thereby having the potential to affect growth, development, and reproductive potential of both aquatic biota and humans (Frye et al., 2011). Endocrine disrupting chemicals (EDCs) can act by several mechanisms such as by inhibiting enzymes related to hormone synthesis, altering free concentrations of hormones by interaction with plasmatic globulins, altering expression of hormone metabolism enzymes, interacting with hormone receptors, acting as agonists or antagonists and altering signal transduction resulting from hormone action (Salgado et al., 2011).

2.3.1 Source, transportation and fate of contaminant

Identifying the chemicals with endocrine activity is a major challenge due to the fact that EDCs have heterogeneous structures and are distributed from varied sources. But with an extensive study, hundreds of chemicals, as well as persistent organic pollutants, have been identified as EDCs (Birnbaum, 2013). EDCs can be found in the natural or synthetic chemicals ranging from industrial processing effluents to the household product. Natural chemicals found

in human and animal food can also act as endocrine hormones (Diamanti-Kandarakis et al., 2009). Phytoestrogen, daidzein (Dai) and genistein (Gen) are soy-derived isoflavones found in a number of plants, including lupin, fava beans, soybeans, kudzu, and psoralea (Dang, 2009). A pilot study to examine children's exposure to isoflavones from different feeding methods showed that urinary concentrations of the phytoestrogens, genistein and daidzein were about 500-fold higher in infants fed soy formula compared with those fed cow's milk formula (Cao et al., 2009). According to Patisaul and Jefferson (2010), the effects of phytoestrogens-rich formula that might impact the infant's future reproductive health remain unknown. Therefore, the potential for endocrine disruption activity needs to be considered. Estrogenic compounds, for example estrone (E1), 17β-estradiol (E2) and estriol (E3), have been reported mainly in river water and sediments due to the inevitable link to WWTP effluents discharging into the receiving waters. The occurrence of 17β-estradiol (E2) in high concentration can have adverse health effects (renal failure, necrosis, and liver damage) in fish, even at very low concentrations (Gustavo et al., 2014) since low concentrations (e.g., a few ng L^{-1}) of this estrogenic compounds in the environment may have adverse effects on the endocrine system in wildlife and humans (Wang et al., 2011).

It is not surprising that most of the hazardous effects of EDCs are from synthetic chemicals where high production volume is found in a myriad of industrial processing activity and household products. For example, bisphenol A (BPA) is used as the monomer for the production of polycarbonate plastics and is a major component of epoxy resins (Julinová and Slavík, 2012). HPTE (2,2-bis(*p*-Hydroxyphenyl)-1,1,1-trichloroethane), an estrogenic metabolite of the pesticide methoxychlor, has estrogenic effects similar to that of BPA (Li et al., 2013). Phthalates or phthalic acid esters (PAEs) are used as plasticizers for polyvinyl chloride (PVC) resins,

cellulose film coatings, styrene, adhesives, cosmetics, as well as in pulp and paper manufacturing (Julinová and Slavík, 2012) and the by-products polychlorinated biphenyls (PCBs), polybrominated biphenyls (PBBs), and dioxins from synthetic chemicals of industrial solvents/lubricants (Diamanti-Kandarakis et al., 2009). In addition, alkylphenolethoxylates (APEOs) which are non-ionic surfactants are extensively used for detergent production comprising a hydrophobic part, usually an alkyl or alkylaryl chain, and a hydrophilic part, which can vary greatly. Both the surfactants and their metabolites, octylphenol (OP) and nonylphenol (NP) are relatively persistent and have been shown to cause endocrine disruption (Wille et al., 2012). A further source of EDCs is from agricultural activity, for example the pesticides methoxychlor, chlorpyrifos, dichlorodiphenyltrichloroethane (DDT), organophosphorous insecticides (OPs) (Frye et al., 2011) and the fungicide vinclozolin (Diamanti-Kandarakis et al., 2009). The chemical structures of several environmentally important EDCs are shown in Figure 2.4.
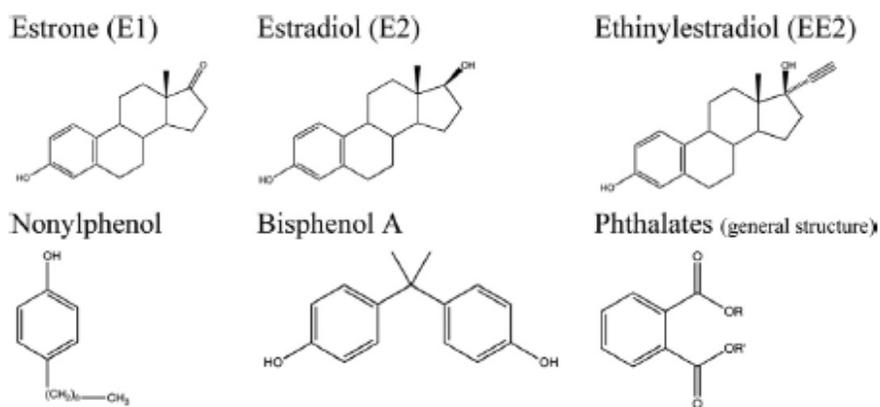
Figure 2.4 **Chemical structures of environmentally important endocrine disrupting compounds (EDCs) (from Wille et. al., 2012).**

It is known that the highest occurrence of EDCs in the environment is mostly from natural water courses and in fish (Poiger et al., 2004). For humans, exposure to EDCs can occur through air, contaminated water or food intake, dermal contact and even through medical consumables and devices such as catheters, breathing and respiratory equipment and blood bag (Ponzo et al., 2013). The mechanism by which they end up in the environment is uncertain and a better understanding of the transportation and fate mechanism. Advances in analytical capabilities have contributed to recent increases in the understanding of the routes of exposure for pharmaceuticals in wastewater and their fate and behaviour in the environment. However, there are currently no guidelines for acceptable concentrations for most of these emerging contaminants (Holeton et al., 2011).

The most common route of nonylphenol ethoxylate (APnEOs) entry into the environment is through municipal wastewater treatment plants (WWTP). Although advanced oxidation steps are often used in the drinking water treatment process, these technologies are no guarantee for the complete removal of such compounds. It was estimated that 60-65% of all nonylphenolic compounds introduced into WWTPs are discharged into the environment (Eric, 2007). It can move up to the food chain, but does not bio magnify to any great degree (Carlisle et al., 2009). Based on a pilot study on estrogenic compound conducted in Queensland, Australian Capital Territory and South Australia, the survey showed that BPA and OP had the lowest levels with median concentrations of 21.5 and 39.5 ng/L, respectively. NP ranged from 514 to 2991 ng/L with a median value of 1113 ng/L., NP1EO and NP2EO were within the same order of magnitude with median concentrations of 1484 and 782 ng/L. The steroidal estrogens were found at low ngL^{-1} concentrations, with E1 consistently found at higher concentrations (ranging from 3.1-39.3 ngL^{-1} with a median concentration of 23.9 ngL^{-1}) than E2 (ranging from 0.05-6.3 ngL^{-1}

with a median concentration of 3.8 ngL^{-1}), and EE2 (ranging from 0.01-1.30 ngL^{-1} with a median

concentration of 0.45 ngL^{-1}) (Williams et al., 2007). Regardless, it does not exclude negative

impacts because of a lack of bioaccumulation due to the fact that it act more like hormones

instead of toxicants. Thus its occurrence at low amounts can possibly give an impact to the

endocrine system and surprisingly, at low doses EDCs may even exert more potent effects than

higher doses (Diamanti-Kandarakis et al. 2009).

2.3.2 Effect of contaminants

The endocrine society has presented some evidence that EDCs are associated with the

effect of male and female reproduction, breast development and cancer, prostate cancer,

neuroendocrinology, thyroid, metabolism and obesity, and cardiovascular endocrinology

(Diamanti-Kandarakis et al. 2009). An overview by Frye et al. (2011) addresses the concern that

EDCs may alter reproductively-relevant or non-reproductive, sexually-dimorphic behaviours and

may also have significant effects on neurodevelopmental processes, influencing the morphology

of sexually-dimorphic cerebral circuits. In addition, exposure to EDCs can effect adulthood and

during specific 'critical periods' of life such as intrauterine, perinatal, juvenile or puberty

periods. Table 2.1 lists the common EDCs with their effects and possible mechanisms.

Table 2.1   Some of the common chemicals that show health effects with the possible mechanism.

EDCs	Effects	Possible mechanism	Reference
17β-estradiol	fishes inhabiting waters that receive untreated municipal wastewaters or effluents from municipal wastewater treatment plants (MWTPs) are exposed to chemicals that affect reproductive endocrine function	male fish downstream of some wastewater outfalls produce vitellogenin (VTG) mRNA and protein, associated with oocyte maturation in females, and early-stage eggs in their testes	Kidd et al., 2007
Phthalates	exposure at early development can cause birth defects in male reproductive tract	act as an anti-androgen at high dose exposure	Andrade et al., 2006
	exposure to diethyl phthalate may be associated with increased risk of breast cancer	potentially induce DNA damage and increase cancer risk human breast cells	López-Carrillo et al., 2010
Nonylphenol (NP)	observed in the fetal serum after administration at the last stage of gestation and present in the central nervous system and accumulates in the brain	alterations in the hypothalamic regulation of the excitatory/inhibitory amino acids–GnRH–gonadotropins of the reproductive system	Doerge et al., 2002 Ponzo and Silvia, 2013
Bisphenol A (BPA)	interferes with thyroid hormone pathways	binds to thyroid hormone receptor and can act as an antagonist to inhibit transcriptional activity stimulated by thyroid hormone	Moriyama et al., 2002 Zoeller, 2005

2.4   Application of magnetic/gold nanoparticles

For environmental application, a rapid processing of multiple samples and real-time detection with possibility for portability is desired. Thus, biosensors appear as a reliable and efficient method to occupy this requirement. Biosensors are usually classified according to the bioreceptor element involved in the biological recognition process such as enzymes, immunoaffinity recognition elements, whole cells of microorganism, plants or animals or DNA fragment (Salgado et al., 2011).

Biosensors, as defined by IUPAC, are an integrated device that is capable of providing specific quantitative or semi-quantitative analytical information using a biological recognition element such as enzymes, immunoaffinity recognition molecules, whole cells of microorganisms, plants or animals or DNA fragments (Salgado et al., 2011). The utilization of nanoparticles for monitoring systems is extensively adapted to biosensor applications.

The fascinating discovery of nano-interfacial phenomena had a huge impact on biosensors technology since it enables manipulation of the biophysical interface between nanomaterials and biomolecules, thus paving the way for the bioconjugation process. Subsequently, a nanoparticle that poses a good bioconjugation property make a great match for biosensing purposes.

2.4.1 Nanoparticle bioconjugates strategy

Nanoparticle bioconjugates are a conjugation between the modified nanoparticles' surface with the specific target biomolecules, for example biorecognition motifs (i.e. antibodies, or aptamers). They may also give the composite a bioderived activity such as catalysis (i.e. enzymes, DNAzymes). Biomolecules can be conjugated directly to the surface of some

27

nanoparticles and to surface-bound stabilizing ligands or coatings, either directly or using small cross-linking molecules and other intermediaries (Sapsford et al., 2013). Within the nano-bio interface, conjugation strategies are important in order to generate nanoparticle bioconjugates and achieve the desired final application. These strategies include nanoparticles size, shape, surface chemistry, and structure, the intrinsic nanoparticle itself, the nature of the nanoparticles surface ligands and their available functional groups, the type of biological molecules, its size and its chemical composition (Sapsford et al., 2013).

The main key to binding an enzyme or antibody to a gold surface is the ability to covalently attach it to the surface particles. The most common and simple conjugation strategy is to utilize specific chemical handles introduced by the coating of stabilizing ligands or polymer. The choice of conjugation strategy is dictated from the selection of AuNPs coated on magnetic nanoparticle surfaces. Gold nanoparticles, in particular, are excellent candidates for bioconjugation with proteins because amine groups and cysteine residues in the proteins are known to bind strongly with gold colloids (Gole, et. al., 2002; Gole et al., 2001a; Gole et. al., 2001b). This chemistry is almost always enabled by the formation of an intermediate monolayer coating of bifunctional thiol ligands on the surface of the Au (Sapsford et al., 2013). Mainly, chemisorption occurs between thiols and Au with reductive elimination of the thiol hydrogen as either H_2 or, with subsequent oxidation, as H_2O.

For example, antibodies have been immobilized on IONP/AuNps after an initial funtionalization step with the heterobifunctional linker -dithiobis(succinimidylpropionate) which

introduced amine-reactive succinimidyl moieties via thiolation of the Au surface (Lim et. al., 2008). In particular, the gold surface facilitates the attachment of biological molecules with inherent self-assembly properties onto the surface of NPs. This opens up new ways for assembling magnetic NPs rationally into well-organized and functional complexes through the lock-and-key functionality provided by the biological molecules on the surface (Robinson et al., 2010). According to Al-Aribe et al. (2011), during the biochemical immobilization process, the biotinylated alkylthiols modify the Au surface using HS terminals of the thiols and affix the labeled bacteriorhodopsin (bR) to the functionalized surface and a dry ultrathin photoelectric layer was successfully fabricated. The self-assembled monolayer of oriented purple membrane (PM) patches from bR is created on a bio-functionalized gold (Au) surface using a biotin molecular recognition technique. A study by Masereel et al. (2010) showed that the gold nanoparticle was coated covalently with anti-bovine serum antibody using a layer-by-layer technique. This study contributes to a simple and reliable method for cancer treatment and imaging.

In addition, N-hydroxysuccinimide (NHS) ester modification of amines along with carbodiimide-mediated condensation (EDC-linker) of carboxyls with amines and cross-linkers can be used to bioconjugate AuNPs with multifunctional ligands. Kim et al. (2011) used SMCC to couple cRDGyC (c = cyclic) peptides to AuNPs coated with an amino-PEG−thiolate ligand. They have proven that the AuNP−cRDGyC conjugates were stable from pH 2 to 8 and at salt concentrations ≤1 M, selectively targeted and were taken up by tumor cells through integrin $\alpha v\beta 3$ receptor-mediated endocytosis without appreciable cytotoxicity.

Another possible strategy that can be applied is to modify enzymes and antibodies for conjugation purposes. It is now very common to modify the bioconjugate to display a unique functional group such as thiol. Furthermore, the thiolated enzyme or antibody will allow a direct adsorption to the AuNPs surface. Alternatively, a site specific immobilization strategy can be explored where it provides a favorable orientation for biorecognition events while avoiding conformational changes (Stanciu et al., 2009). This method allows a site specific attachment at a pre-determined position for selected enzymes which eliminates the diffusion barriers or chemical bond formation that could affect the biological activity and therefore a lower detection limit and a fast response time could be expected. Johnson et al., (2008) used clone dehalogenase (Dh1A) fusion proteins with an affinity for either silica or iron oxide surfaces (Naik et al., 2002; Brown, 1992) and suggested that three different Dh1A recombinant enzyme were able to specifically bind to either iron oxide or silica.

Several conjugation strategies for nanoparticles-bioconjugates particularly to detect endocrine disrupting chemicals (EDCs) are listed in Table 2.1.

Table 2.2 **List of several bioconjugation strategies for nanoparticle-based biosensor application to detect EDCs.**

Nanoparticle-bioconjugate	Bioconjugation strategy	Target chemical compounds	References
MgFe$_2$O$_4$–SiO$_2$.Tyr	glutaraldehyde cross-linking	phenolic compound	Liu et al., 2005
Magnetic particles-secondary antibody	commercial RIA kit for E2	17β-estradiol	Xin et al., 2008
Rabbit polyclonal anti EE2-magnetic microbeads	glutaraldehyde cross-linking	ethinylestradiol (EE2)	Martinez et al., 2010
SWCNTs-AuNPs-Tyr	glutaraldehyde cross-linking	phenolic compound	Li et al., 2012
Goat anti rabbit IgG-	thiol-capped DNA and antibody thiol-tagged	3,4,3',4'-tetrachlorobiphenyl (PCB77)	Yang et al., 2014
AuNPs-DNA aptamer-CoS/AuNPs	17β-estradiol aptamer	17β-estradiol	Huang et al., 2014

2.4.2 Magnetic/gold nanoparticles in nanosensor

The development of various nanosensor schemes can be classified by conjugation of nanoparticles with different types of specific target biomolecules such as enzyme, immuno- and aptamer.

2.4.2.1 Enzyme-based nanosensor

Enzymes are known as highly efficient catalysts that are useful for bioremediation processes and also the detection of targeted pollutants. There is an extensive study for development of enzyme-based nanosensors which utilize enzyme immobilization on the nanoparticle surface. Many types of nanosensor have been explored and electrocatalysis shows a significant promise as many researchers use nanoparticles to enhance the conventional electrochemical method.

An electrochemical sensor is commonly comprised of two major components; (i) a chemical or biorecognition element; and (ii) a physical transducer (electrode) that transduces the analytical signal of the sensing event to an electronic circuit. They are known for their self-contained, compact and low cost with minimal power requirement (Govindhan et al., 2014). Advanced nanoparticle-based electrocatalysis methodologies employ the nanoparticle's unique chemical and physical properties by improving the electrode surfaces. For example a study on modified sulfite oxide/ $Fe_3O_{4@}Au$ nanoparticle electrocatalyst proved that it is a good nanoparticle bioconjugate for sulfite determination (Rawal et al., 2012). They concluded that this modification improved analytical performance with low response time, lower detection limit, higher storage stability, wider linear range and lack of interferences. The presence of gold coated

magnetite is of special interest, since the gold nanoparticle helps to improve their stability in aqueous dispersions (Laurent et al., 2008).

Furthermore, a study on the immobilization of tyrosinase on the surface of modified magnetic $MgFe_2O_4$ nanoparticles was developed. It is important to note that tyrosinase is known to catalyze the oxidation of phenolic compounds typically monophenols and *ortho*-diphenols to *ortho*-quinones (Gamella et al., 2006). The tyrosinase was first covalently immobilized on core–shell ($MgFe_2O_4$–SiO_2) magnetic nanoparticles, which were modified with an amino group on the surface. The resulting magnetic bio-nanoparticles were attached to the surface of a carbon paste electrode with the use of an external magnetic field (Liu et al., 2005). With this advancement, the recognition element can be renewed and provides an in-situ biosensing surface (Xu and Wang, 2012). Li et al. (2012) successfully fabricated a disposable biosensor using single-walled carbon nanotubes (SWCNTs), gold nanoparticles and tyrosinase and obtained a rapid determination of phenolic contaminants within 15 min with excellent repeatability and stability. This study revealed that SWCNTs lead to a high loading of tyrosinase and gold nanoparticles retained the bioactivity of tyrosinase and enhanced the sensitivity. The schematic and configuration of this electrochemical analysis can be seen in Figure 2.5. Based on extensive studies, the integration of a nanoparticle greatly enhances enzyme based nanosensor performance. For instance, the adding of superparamagnetic nanoparticles in electrocatalysis increases the enzyme concentration at the electrode surfaces, improving the electrochemical response and the efficiency of the electrocatalytic processes (Netto et al., 2013). It also demonstrates that nanoparticles are feasible

for many chemical contaminants detection and have the potential to be integrated into portable and rapid detection tools with quick response that show more economical value.
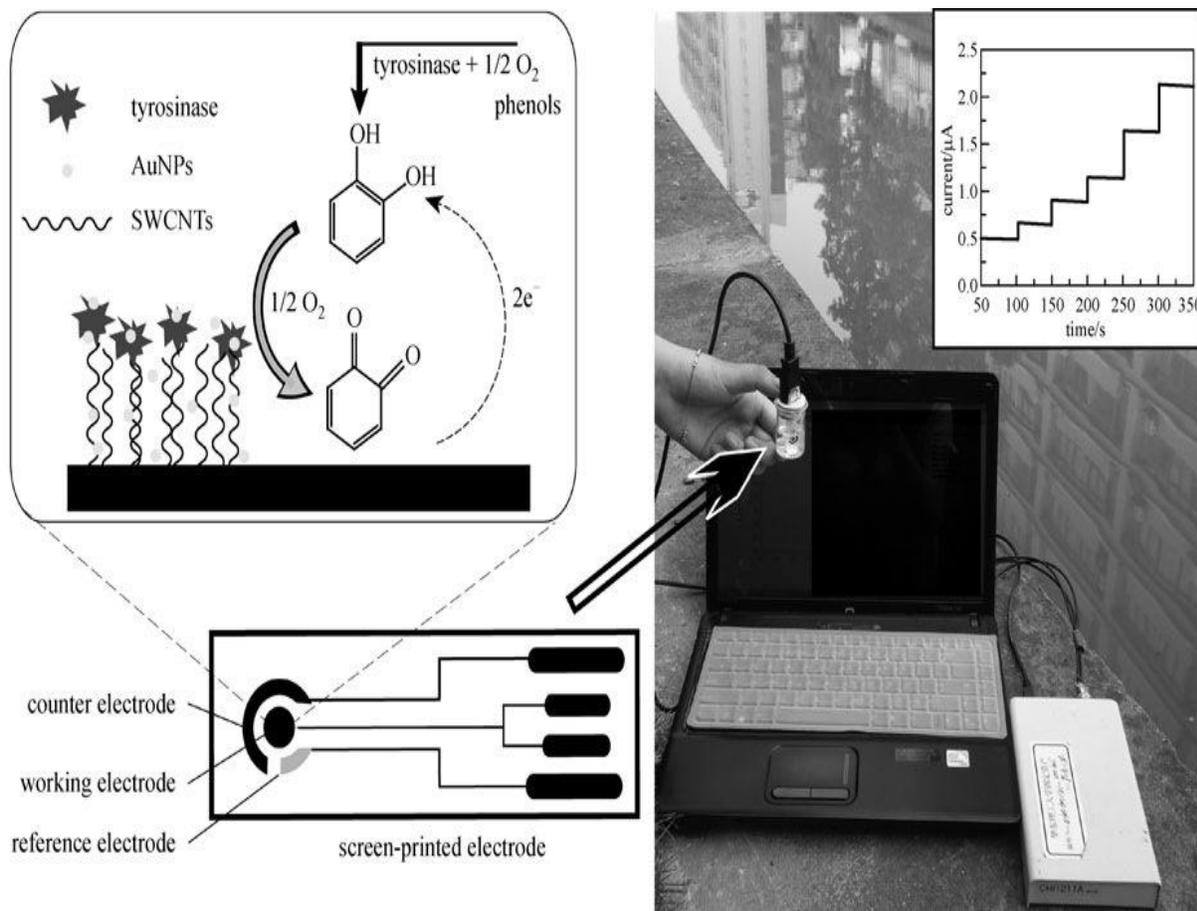
Figure 2.5   Diagram and configuration of the disposable biosensor using single-walled carbon nanotubes (SWCNTs), AuNPs and tyrosinase for determination of phenolic contaminant (from Li et al., 2012).

2.4.2.2 Immuno-based nanosensors

Since the early 1970s, many researchers have proposed the possibility of using immunosensors for environmental study and analysis because of their sensitivity towards specific analytes. This method emphasizes both screening and analytical purposes and it has proven to be a reliable, sensitive and selective method (Safarik et al., 2012). For instance, different types of EDCs were successfully detected using this method. A study by Zacco et al. 2006, successfully detected Arochlor 1248 (PCB) with detection limits of 0.4 ng/mL as well as atrazine with detection limits of 0.027 nmol L^{-1} by using anti-atrazine-specific antibody. In another study, Hu et al. (2003) reported that paraoxon was measured at a low detection limit at 12 μg/L and with a linear range within 24–1920 μg/L, which was achieved with an electrochemical immunosensor based on antibody-labeled gold nanoparticles on a glassy carbon electrode. Immuno-based nanosensors can be classified into immunosensors and immunoassays. "Immunosensor" is usually employed to describe the whole instrument, i.e an electrochemical devise, while "immunoassay" is commonly used to describe tests based immunoreaction e.g ELISA (Pei et al., 2013).

Similar to enzyme-based nanosensors, immuno- based nanosensor approaches also concentrate on the enhancement of the electrode surface. Antibody or antigen molecules are directly immobilized at the sensor surface (transducer) and the signal change is measured before and after the antigen-antibody interaction (Centi et al., 2007). An interesting study by this group used an estrogen receptor immobilized on a bilayer lipid membrane (s-BLM) modified with gold nanoparticles to selectively detect 17β-estradiol, bisphenol A (BPA) and nonylphenol (NP) (Xia et al., 2010). An estrogen receptor (ER) is used to detect estrogenic substances, which can be

found widely in EDCs and can interfere with endocrine system function (Kerdivel et al., 2013). The presence of gold nanoparticles produced a better microenvironment for s-BLM since it absorbs larger amounts of ER, contributing to increased sensitivity and longer time stability of the biosensor.

Although electrochemical analysis has been widely studied and used, immunoassays have receivesd a great amount of attention and a variety of analysis methods are currently available. The classical immunoassays exhibit a conversion to the new immunomagnetic assay where an appropriate antibody is immobilized on a magnetic carrier. Safarik et al. (2012) defines immunomagnetic separation (IMS) as the immobilization of antibodies specific against the target (micro) organism or virus to the magnetic particles. IMS has been used widely in environmental analysis for detection of bacteria (Bushon et al., 2009; Lee and Deininger 2004). Due to its competency, it also has been adapted for detection of EDCs. A study by Xin et al. (2009) presents a simple, fast and highly sensitive chemiluminescence enzyme immunoassay (CLEIA) for 17β-estradiol using magnetic particle labeled antibodies, which exhibited high performance with a detection limit of 2.0 pg/mL, linear range of 20–1,200 pg/mL, and total assay time of 45 min. Interestingly, they discovered that the mass transfer distance of analytes and reagents to the immobilized antibody is greatly reduced and antigen-binding equilibrium can be achieved rapidly with easy handling of samples since the immunocomplex was efficiently separated from a complex mixture under the influence of a magnetic field. A study by Gao et al. (2008) developed a magnetic nanoparticle-linked immunosorbent assay. In this study, the as-synthesized chitosan (CS)-MNPs had amine groups on their surface which provided good dispersibility in aqueous

solutions and convenient sites for covalent linking of antibodies with the MNPs. This assay showed the capability to catalyze color reactions in immunoassays and the magnetic properties could be used to capture, separate, and enrich antigens prior to the assay procedure. By employing both the catalytic and magnetic properties of the CS-MNPs, a capture-detection immunoassay was developed, where antigens can be captured, separated, and enriched prior to the assay procedure.

The unique properties of magnetic nanoparticles have also been utilized in microfluidic devices. A study to selectively quantify ethinylestradiol (EE2) using modified paramagnetic beads in a microfluidic system was successfully performed (Martinez et al., 2010). The increased reactive surface area and the reduced diffusion distance permitted a faster time of analysis and less sample consumption. Through this invention, the miniaturization of magnetic immunosensors is possible. In addition, other strategies such as immuno-polymerase chain reaction (IPCR) have been studied. Bu's group successfully fabricated a functionalized gold-nanoparticle bio-barcode assay, based on a real time IPCR system (Yang et al., 2014). This modified IPCR was designed to determine 3,4,3',4'-tetrachlorobiphenyl (PCB77) from water samples and showed an enhanced analyte signal since the gold nanoparticles in this immunoassay conferred a high ratio of signal DNA to the goat anti-rabbit IgG. Figure 2.6 shows the concept for this immunoassay.
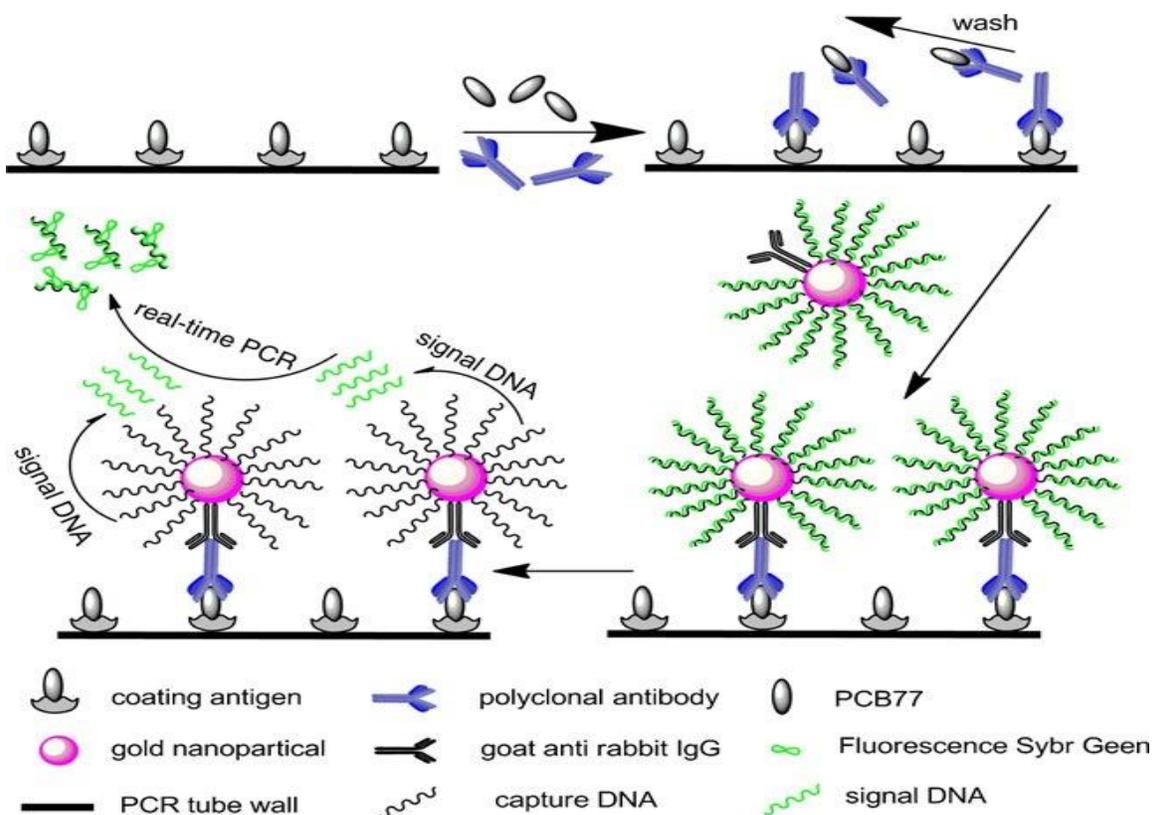
Figure 2.6 **Illustration of real time immuno-PCR based nanosensor to determine 3,4,3',4'-tetrachlorobiphenyl (PCB77). Initially, the antibody was captured by PCB77 hapten–OVA (coating antigen) coated on PCR tubes and followed by the addition of gold-nanoparticle probes, which were modified by goat anti-rabbit IgG and thioldsDNA to form sandwich immunocomplexes. Signal DNA was released from the probes by the initial heating procedure of realtime PCR. Signal DNA was used as the marker for PCB77, and was quantified by real-time PCR (from Yang et al., 2014).**

2.4.2.3 Aptamer-based nanosensor

In recent years, aptamer-based biosensors, particularly for detection of EDC compounds, were successfully developed (Long et al., 2014; Yildirim et al., 2012; Lin et al 2012; Olowu et al., 2010; Kim et al., 2007). Aptamers are short synthetic oligonucleotides that could be produced for any targets such as proteins, peptides, amino acids, nucleotides, drugs, carbohydrates, and other small organic and inorganic compounds (Ellington and Szostak, 1990; Luzi, et al., 2003). Since the screening process for aptamers synthesis was simplified using Systematic Evolution of Ligands by Exponential Enrichment (SELEX), aptamers-related analytical research has experienced explosive growth (Guo and Dong, 2009). SELEX technique enabling selection of specific oligonucleotides from libraries of randomized molecules whereas aptamer species consist of a randomized region of 30–50 nucleotides flanked by constant sequences that enable PCR amplification (Radom et al., 2013). As compared to antibodies, aptamers can be chemically synthesized, have a strong affinity for the target molecules, are easy to modify and show high stability (Sun and Zu, 2015). Furthermore, chemically synthesized aptamers are cost-effective and generally do not require complicated and expensive purification steps (Yildirim et al., 2012). Because of these advantages, aptamers have been used widely as a biorecognition element in biosensor applications.

However, there are still a very limited number of publications on the integration of nanoparticle to this biosensor. Huang's group is currently doing a progressive work on the detection of 17β-estradiol using aptamer-based nanosensor. In their studies, they utilized two-dimensional (2D) transition-metal chalcogenides, aptamer and AuNPs. Two-dimensional transition-metal chalcogenides such as cobalt sulfide (CoS), tungsten disulfide (WS_2) and copper

sulfide (CuS); are the material composed of the metal layer and sulfur layer and stacked together by weak Van der Waals interactions and is expected to act as an excellent functional material because the 2D electron–electron correlations among metal atoms would be helpful in enhancing planar electric transportation (Huang et al., 2014a; 2014b).

As discussed before, the addition of AuNPs are mostly recommended owing to the fact that they show a great hybridization property with biomolecules, as well as the possibility that they can greatly increase the current response of the modified sensor with good conductivity (Hai et al., 2014). Their work includes the construction of electrochemical-based biosensor using CoS and AuNPs (Huang et al., 2014a) and layered WS_2 nanosheets and AuNPs amplification (Huang et al., 2014b). The thiol group tagged 17β-estradiol aptamer was covalently bound on CoS and AuNPs modified electrodes. Besides exhibiting good selectivity, the CoS/AuNPs formed on the biosensor surface appeared to be a good conductor which is important for accelerating the electron transfer. In the most recent publication, they reported that combining CuS and AuNPs in the construction of modified electrodes efficiently accelerated the electron transfer and enhanced the detection signal with a detection limit of 60 fM (Huang et al., 2015). Based on their findings, this approach greatly enhanced the electrochemical assays by improving its sensitivity and signal amplification.

Therefore, the development and characterization of the aptamer-based nanosensor could lead to a more sophisticated analytical chemistry with the capacity to improve qualitative and quantitative measurements, with high sensitivity, speedy analysis, and importantly shows good stability.

References

Al-Aribe KM, Knopf GK, and Bassi AS. (2011) Photoelectric monolayers based on self-assembled and oriented purple membrane patches. *J Microelectromechl Syst* 20(4): 800-810

Alibeigi S, and Vaezi MR. (2008) Phase transformation of iron oxide nanoparticles by varying the molar ratio of Fe^{2+}:Fe^{3+}. *Chem Eng Technol* (31): 1591

Andrade AJM, Grande SW, Talsness CE, Grote K, and Chahoud I. (2006) A dose–response study following *in utero* and lactational exposure to di-(2-ethylhexyl)-phthalate (DEHP): Non-monotonic dose–response and low dose effects on rat brain aromatase activity. *Toxicol* 227(3): 185-192

Aono H, Hirazawa H, Naohara T, Maehara T, Kikkawa H and Watanabe Y. (2005) Synthesis of fine magnetite powder using reverse coprecipitation method and its heating properties by applying AC magnetic field. *Mater Res Bull* 40(7): 1126

Arruebo M, Fernandez-Pacheco R, Ibarra MR, and Santamaria J. (2007) Magnetic nanoparticles for drug delivery. *Nano Today* (2): 22–32

Babes L, Denizot B, Tanguy G, Le Jeune JJ, Jallet PJ. (1999) Synthesis of iron oxide nanoparticles used as MRI contrast agents: A parametric study. *Colloid Interface Sci* 212(2): 474

Batlle X, and Labarta A. (2002) Finite -size effects in fine particles: magnetic and transport properties. *J Phys D: Appl Phys* (35)

Berger P, Adelman NB, Beckman KJ, Campbell DJ, Ellis AB, and Lisensky GC. (1999) Preparation and properties of an aqueous ferrofluid. *J Chem Educ* (76): 943–948

Beveridge JS, Stephens JR, and Williams ME. (2011) The use of magnetic nanoparticles in analytical chemistry. *Ann Rev of Anal Chem* (4): 251-273

Bishop AR, and Nuzzo RG. (2008) Self-assembled monolayers: recent developments and applications. *Curr Opin in Coll & Inter Sci* 1(1): 127–136

Brown S. (1992) Engineered iron-oxide-adhesion mutants of the Escherichia coli phage lambda receptor. *Proc Nat Acad Sci USA* (89): 8651-8655

Bushon RN, Likirdopulos CA, and Brady AMG. (2009) Comparison of immunomagnetic separation/adenosine triphosphate rapid method to traditional culture-based method for E. coli and enterococci enumeration in wastewater. *Water Res*

Caruso F. (2001) Nanoengineering of particle surfaces. *Adv Mater* 13(11)

Caruntu D, Cushing BL, Caruntu G, and O'Connor CJ. *(*2005) Attachment of gold nanograins onto colloidal magnetite nanocrystals. *Chem Mater* 17(13): 3398

Carlisle J, Chan D, Painter P, and Wu L, (2009) Toxicological profile for nonylphenol. *Integrated Risk Assessment Branch Office of Environmental Health Hazard Assessment California EPA*

Cao Y, Calafat AM, Doerge DR, Umbach DM, Bernbaum JC, Twaddle NC, Ye X, and Rogan WJ. (2009) Isoflavones in urine, saliva and blood of infants—data from a pilot study on the estrogenic activity of soy formula. *J Expo Sci Environ Epidemiol* (19): 223–234

Centi S, Laschi S, Franek M, and Mascini M. (2005) A disposable immunomagnetic electrochemical sensor based on functionalised magnetic beads and carbon-based screen-printed electrodes (SPCEs) for the detection of polychlorinated biphenyls (PCBs). *Anal Chim Acta* 538(1–2): 205–212

Chen H, Li Y, Zhang F, Zhang G., and Fan X. (2011) Graphene supported Au-Pd bimetallic nanoparticles with core-shell structures and superior peroxidase-like activities. *J Mater Chem* 21(44): 17658–17661

Chen L, Feng T, Wang P, and Xiang Y. (2013) Transition metal (Fe, Co) and organic silanol modified mesoporous titanium phosphates as catalysts for the oxidation of benzyl alcohol in water. *React Kin, Mech & Catal* (110:2): 485-496

Cho SJ, Idrobo JC, Olamit J, Liu K, Browning ND, and Kauzlarich SM. (2005) Growth mechanisms and oxidation resistance of gold-coated iron nanoparticles. *Chem Mater* (17): 3181-3186

Daniel MC, and Astruc D. (2004) Gold nanoparticles: assembly, supramolecular chemistry, quantumsize-related properties, and applications toward biology, catalysis, and nanotechnology. *Chem Rev* (104): 293–346

Dang ZC. (2009) Dose-dependent effects of soy phyto-oestrogen genistein on adipocytes: mechanisms of action. *Obes Rev* 10(3): 342-349

Decher G. (1997) Fuzzy nanoassemblies: Toward layered polymeric muticomposites. *Sci* (277): 1232

Diamanti-Kandarakis E, Bourguignon JP, Giudice LC, Hauser R, Prins GS, Soto AM, Zoeller RT, and Gore AC, (2009) Endocrine-Disrupting Chemicals. *Endocrine Rev* 30(4): 293–342

Duan S, and Wang R. (2013) Bimetallic nanostructures with magnetic and noble metals and their physicochemical applications. *Prog In Nat Sci-Mater Intl* 23(2): 113-126

Doerge DR, Twaddle NC, Churchwell MI, Chang HC, Newbold RR, Delclos KB. (2002) Mass spectrometric determination of *p*-nonylphenol metabolism and disposition following oral administration to Sprague-Dawley rats. *Reprod Toxicol* 16(1): 45-56

Ellington AD, and Szostak J. (1990) *In vitro* selection of RNA molecules that bind specific ligands. *Nature* (346): 818–822

Eric SE. van Beelen. (2007) Municipal Waste Water Treatment Plant (WWTP) Effluents: a Concise Overview of the Occurrence of Organic Substances. *Assoc of River Waterworks – RIWA* ISBN: 978-90-6683-124-7

Ferrando R, Jellinek J, and Johnston RL. (2008) Nanoalloys: from theory to applications of alloy clusters and nanoparticles. *Chem Rev* 108(3): 845-910

Frye C, Bo E, Calamandrei G, Calzà L, Dessì-Fulgheri F, Fernández M, Fusani L, Kah O, Kajta M, Le Page Y, Patisaul HB, Venerosi A, Wojtowicz AK, and Panzica GC. (2011) Endocrine Disrupters: A Review of Some Sources, Effects, and Mechanisms of Actions on Behaviour and Neuroendocrine Systems. *J of Neuroendoc* 24(1): 144-159

Gamella M, Campuzano S, Reviejo AJ, and Pingarron JM. (2006) Electrochemical estimation of polyphenol index in wines using a laccase biosensor. *J Agric Food Chem* (54): 7960-7967

Gao LZ, Wu JM, Lyle S, Zehr K, Cao LL, and Gao D. (2008) Magnetite nanoparticle-linked immunosorbent assay. *J Phys Chem C* (112): 17357−17361

Gittins DI, and Caruso F. (2001) Tailoring the polyelectrolyte coating of metal nanoparticles. *J Phys Chem B* (105): 6846-6852

Gnanaprakash G, Philip J, Jayakumar T, Raj B. (2007) Effect of digestion time and alkali addition rate on the physical properties of magnetite nanoparticles. *J Phys Chem B* (111): 7978–7986

Guo Y, Deng L, Li J, Guo S, Wang E, and Dong S. (2011) Hemin−Graphene Hybrid Nanosheets with Intrinsic Peroxidase-like Activity for Label-free Colorimetric Detection of Single-Nucleotide Polymorphism. *ACS Nano 5* (2): 1282–1290

Gustavo Gallardo, Ferral Alberto, Alaniz Eugenia, Ferral Anabella, Sarmiento Tagle Martin, Vanesa Crissi Aloranti Comprehensive Assessment Of Estrogenic Contamination Of Surface Waters Of The River Basin Suquia. *Eur J of Sci*

Gole A, Dash C, Ramakrishnan V, Sainkar SR, Mandle AB, Rao M, Sastry M. (2001[a]) Pepsin– gold colloidal conjugates: Preparation, characterization and enzymatic activity. *Langmuir* (17): 1674– 1679

Gole A, Dash C, Soman C, Sainkar SR, Rao M, Sastry M. (2001[b]) On the preparation, characterization, and enzymatic activity of the fungal protease– gold colloid bioconjugate. *Bioconj Chem* (12): 684– 690

Gole A, Vyas S, Phadtare S, Lachke A, Sastry M. (2002) Studies on the formation of bioconjugate of endoglucanase with colloidal gold. *Coll Surf B Biointerf* (25): 129–138

Govindhan M., Adhikari B-R., and Chen A., (2014) Nanomaterials-based electrochemical detection of chemical contaminants. *RSC Adv* 4: 63741–63760

Guo S, and Dong S. (2009) Biomolecule-nanoparticle hybrids for electrochemical biosensors. *Trends in Anal Chem* 28(1): 96-109

Hai H, Yang F, Li JP (2014) Highly sensitive electrochemiluminescence "turn-on" aptamer sensor for lead(II) ion based on the formation of a G-quadruplex on a graphene and gold nanoparticles modified electrode. *Microchim Acta* (181): 893

He W, Liu Y, Yuan J, Yin JJ, Wu X, Hu X, Zhang K, Liu J, Chen C, Ji Y, and Guo Y. (2011) Au@ Pt nanostructures as Oxidase and Peroxidase Mimetics for Use in Immunoassays. *Biomater* (32): 1139–1147

Holeton C., Chambers PA., and Grace L. (2011) Wastewater release and its impacts on Canadian waters. *Can J Fish Aquat Sci* (68): 1836–1859

Huang KJ, Liu YJ, Wang HB, Gan T, Liu YM, Wang LL. (2014a) A novel aptamer sensor based on layered tungsten disulfide nanosheets and Au nanoparticles amplification for 17β-estradiol detection. *Anal. Methods* (6): 8011–8017

Huang KJ, Liu YJ, Wang HB, Wang YY, Liu YM. (2014b) Aptamer/Au nanoparticles/ cobalt sulfide nanosheets biosensor for 17β-estradiol detection using a guanine-rich complementary DNA sequence for signal amplification. *Biosens Bioelectron* (67): 184-191

Huang KJ, Liu YJ, and Zhang JZ. (2015) Aptamer-based electrochemical assay of 17β-estradiol using a glassy carbon electrode modified with copper sulfide nanosheets and gold

anoparticles, and applying enzyme-based signal amplification. *Microchim Acta* (182): 409–417

Julinová M, and Slavík R. (2012) Removal of Phthalates from Aqueous Solution by Different Adsorbents: A Short Review. *J Environ Manag* (94): 13–24

Hammond PT. (2000) Recent explorations in electrostatic multilayer thin film assembly. *Curr Opinion in Coll & Inter Sci* (4):430-442

Haun JB, Yoon T, Lee H, and Weissleder R. (2010) Magnetic nanoparticle biosensors. *Nanomed Nanobiotechnol* (2): 291–304

Hong RY, Li JH, Li HZ, Ding J, Zheng Y, and Wei DG. (2008) Synthesis of nanoparticles without inert gas protection used as precursors of magnetic fluids. *J Magn Magn Mater* (320): 1605–1614

Hu SQ, Xie JW, Xu QH, Rong KT, Shen GL, Yu RQ. (2003) A label-free electrochemical immunosensor based on gold nanoparticles for detection of paraoxon. *Talanta* (61): 769–777

Illés E, and Tombácz E. (2003) The role of variable surface charge and surface complexation in the adsorption of humic acid on magnetite. *Coll Surf. A: Physicochem. Eng. Aspects* (230): 99–109

Jeng HT, and Guo GY. (2002) First-principles investigations of the electronic structure and magnetocrystalline anisotropy in strained magnetite Fe3O4. *Phys. Rev. B*, (65): 094429

Jing J, Zhang Y, Liang J, Zhang Q, Bryant E, Avendano C, Colvin VL, Wang Y, Li W, Yu WW. (2012) One-step reverse precipitation synthesis of water-dispersible superparamagnetic magnetite nanoparticles. *J Nanopart Res* 14: 827

Johnson AK, Zawadzka AM, Deobald LA, Crawford RL, Paszcynski AJ. (2008) Novel method for immobilization of enzyme to magnetic nanoparticles. *J Nanopart Res* 10: 1009-1025

Kazemzadeh H, Ataie A, and Rashchi F. (2012) Synthesis of magnetite nano-particles by reverse co-precipitation. *Int. J Mod Phys Conf Ser* (5): 160-167

Kerdivel G, Habauzit D, and Pakdel F. (2013) Assessment and Molecular Actions of Endocrine-Disrupting Chemicals That Interfere with Estrogen Receptor Pathways. *Intl J of Endoc* 1-14

Kidd KA, Blanchfield PJ, Mills KH, Palace VP, Evans RE, Lazorchak JM, and Flick RW. (2007) Collapse of a fish population after exposure to a synthetic estrogen. *PNAS* 104(21): 8897–8901

Kim J, Park S, Lee JE, Jin SM, Lee JH, Lee IS, Yang I, Kim JS, Kim SK, Cho MH, and Hyeon T. (2006) Designed fabrication of multifunctional magnetic gold nanoshells and their application to magnetic resonance imaging and photothermal therapy. *Angew Chem Int Ed* (46): 7754

Kim YS, Jung HS, Matsuura T, Lee HY, Kawai T, Gu MB. (2007) Electrochemical detection of 17β-estradiol using DNA aptamer immobilized gold electrode chip. *Biosens and Bioelect* (22): 2525–2531

Kim YH, Jeon J, Hong SH, Rhim WK, Lee YS, Youn H, Chung JK, Lee MC, Lee DS, Kang KW, and Nam JM. (2011) Tumor targeting and imaging using cyclic RGD-PEGylated gold nanoparticle probes with directly conjugated iodine-125. *Small* (7): 2052

Kimling J, Maier M, Okenve B, Kotaidis V, Ballot H, and Plech A. (2006) Turkevich method for gold nanoparticle synthesis revisited. *J of Phy Chem B* (110:32):15700-7

Kinoshita T, Seino S, Otome Y, Mizukoshi Y, Nakagawa T, Okitsu K, and Yamamoto TA. (2005) Magnetic separation of amino acids by gold/iron-oxide composite nanoparticles synthesized by gamma-ray. *J Magn Magn Mater* (293): 106-110

Kwon T, Min M, Lee H, and Kim BJ. (2011) Facile preparation of water soluble CuPt nanorods with controlled aspect ratio and study on their catalytic properties in water. *J Mater Chem* 21(32): 11956–11960

LaMer VK, and Dinegar RH. (1950) Theory, production and mechanism of formation of monodispersed hydrosols. *J Am Chem Soc* 72(11): 4847–4854

Laurent S, Forge D, Port M, Roch A, Robic C, Vander Elst L, and Muller RN. (2008) Magnetic iron oxide nanoparticles: synthesis, stabilization, vectorization, physicochemical characterizations, and biological applications. *Chem Rev* (108): 2064–2110

Lee J, and Deininger R. (2004) Detection of E. coli in beach water within 1 hour using immunomagnetic separation and ATP bioluminescence. *Luminescence* (19): 31–36

Li Y, Liu J, Zhong Y, Zhang J, Wang Z, Wang L, An Y, Lin M, Gao Z, and Zhang D. (2011) Biocompatibility of Fe_3O_4@Au composite magnetic nanoparticles *in vitro* and *in vivo*. *Intl J Nanomed* (6): 2805–2819

Li Y, Li D, Song W, Li M, Zou J, and Long Y. (2012) Rapid method for on-site determination of phenolic contaminants in water using a disposable biosensor. *Front of Env Sci & Eng* 6(6): 831-838

Li Yi, Luh CJ, Burns KA, Arao Y, Jiang Z, Teng CT, Tice RR, and Korach KS. (2013) Endocrine-Disrupting Chemicals (EDCs): *In Vitro* Mechanism of Estrogenic Activation and Differential Effects on ER Target Genes. *Env Health Persp* (121): 459-466

Li J, Liu W, Wu X, and Gao X. (2015) Mechanism of pH-switchable peroxidase and catalase-like activities of gold, silver, platinum and palladium. *Biomaterials* (48): 37-44

Lia S, Yu-Ho W, Mallikarjunarao G, and Silvana A. (2009) Magnetic Particle-Based Hybrid Platforms for Bioanalytical Sensors. *Sensors* 9(4): 2976-2999

Lim IIS, Njoki PN, Park HY, Wang X, Wang LY, Mott D, and Zhong CJ. (2008) Gold and magnetic oxide/gold core/shell nanoparticles as bio-functional nanoprobes. *Nanotechnol* 19(305102)

Lin ZY, Chen LF, Zhang GY, Liu QD, Qiu B, Cai ZW, Chen GN (2012) Label-free aptamer-based electrochemical impedance biosensor for 17β-estradiol. *Analyst* 137: 819

Liu QX, Xu ZH, Finch JA, and Egerton R. (1998) A novel two-step silica-coating process for engineering magnetic nanocomposites. *Chem of Mater* 10(12): 3936-3940

Liu ZM, Liu YL, Yang HF, Yang Y, Shen GL, and Yu RQ. (2005) A phenol biosensor based on immobilizing tyrosinase to modified core-shell magnetic nanoparticles supported at a carbon paste electrode. *Anal Chim Acta* 533(1): 3-9

Lopez-Carillo L, Hernandez-Ramirez RU, Calafat AM, TorresSanchez L, Galvan-Portillo M, Needham LL, Ruiz-Ramos R, and Cebrian ME. (2010) Exposure to Phthalates and Breast Cancer Risk in Northern Mexico. *Env Health Persp* 118(4): 539-544

Long F, Shib H, and Wanga H. (2014) Fluorescence resonance energy transfer based aptasensor for the sensitive and selective detection of 17β-estradiol using a quantum dot-bioconjugate as a nano-bioprobe. *RSC Adv* 4: 2935–2941

Luzi E, Minunni M, Tombelli S, Mascini M. (2003) New trends in affinity sensing: Aptamers for ligand binding. *Trends Anal Chem* 22(11): 810–818

Lyon JL, Fleming DA, Stone MB, Schiffer P, and Williams ME. (2004) Synthesis of Fe Oxide Core/Au shell nanoparticles by iterative hydroxylamine seeding. *Nano Lett* 4(4): 719-723

Mahmed N, Heczko O, Söderberg O, and Hannula SP. (2011) Room temperature synthesis of magnetite ($Fe_{3-\delta}O_4$) nanoparticles by a simple reverse co-precipitation method. *IOP Conf. Series: Materials Sci and Eng* 18

Mandal M, Kundu S, Ghosh SK, Panigrahi S, Sau TK, Yusuf SM, and Pal T. (2005) Magnetite nanoparticles with tunable gold or silver shell. *J Coll Inter Sci* 286: 187

Martínez NA, Schneider RJ, Messina GA, and Raba J. (2010) Modified paramagnetic beads in a microfluidic system for the determination of ethinylestradiol (EE2) in river water samples. *Biosens and Bioelect* 25(6): 1376-1381

Masereel B, Dinguizli M, Bouzin C, Moniotte N, Feron O, Gallez B, Borght V, Michiels C, and Lucas S. (2010) Antibody immobilization on gold nanoparticles coated layer-by-layer with polyelectrolytes. *J Nanopart Res*

Maye MM, Lou Y, and Zhong CJ. (2000) Core-shell gold nanoparticle assembly as novel electrocatalyst of CO oxidation. *Langmuir* (16): 7520 -7523

Mizukoshi Y, Shuto T, Masahashi N, and Tanabe S (2009) Preparation of superparamagnetic magnetite nanoparticles by reverse precipitation method: Contribution of sonochemically generated oxidants. *Ultrasonics Sonochem* 16(4): 525-531

Moriyama K, Tagami T, Akamizu T, Usui T, Saijo M, Kanamoto N, Hataya Y, Shimatsu A, Kuzuya H, and Nakao K. (2002) Thyroid hormone action is disrupted by bisphenol A as an antagonist. *J Clin Endocrinol Metab* 87: 5185–5190.

Mu B, Liu P, Dong Y, Lu C, and Wu X. (2010) Superparamagnetic pH- sensitive multilayer hybrid hollow microspheres for targeted controlled release. *J of Poly Sc* 48(14): 3135-3144

Naik RR, Brott LL, Clarson SJ, Stone MO. (2002) Silica-precipitating peptides isolated from a combinatorial phage display peptide library. *J NanoSci Nanotechno* 2: 95-100

Netto CGCM, Toma HE, and Andrade LH. (2013) Superparamagnetic nanoparticles as versatile carriers and supporting materials for enzymes. *J of Mol Catal* (85-86): 71-92

Nunes AC, and Yu ZC. (1987) Fractionation of a water-based ferrofluid. *J Magn Magn Mater* 1(65): 265

Olowu RA, Arotiba O, Mailu SN, Waryo TT, Baker P, Iwuoha E. (2010) Electrochemical aptasensor for endocrine disrupting 17β-estradiol based on a poly(3,4-ethylenedioxylthiopene)-gold nanocomposite platform. *Sensors* 10: 9872

Park HY, Schadt MJ, Wang L, Lim IIS, Njoki PN, Kim SH, Jang MY, Luo J, and Zhong CJ. (2007)Fabrication of magnetic core@shell Fe oxide@Au nanoparticles for interfacial bioactivity and bio-separation. *Langmuir* (23): 9050-9056

Patisaul HB, and Jefferson W. (2010) The pros and cons of phytoestrogens. *Front in Neuroendocrin* 31(4): 400-419

Pei X., Zhang B., Tang J., Liu B., Lai W., Tang D. (2013) Sandwich-type immunosensors and immunoassays exploiting nanostructure labels: A review. Analytica Chimica Acta 758: 1-18

Poiger T, Busar HR, Balmer ME, Bergquist PA, and Muller MD, (2004) Occurrence of UV filter compounds from sunscreens in surface waters: regional mass balance in two Swiss lakes. *Chemosphere* (55): 951– 963

Ponzo OJ, and Silvia C. (2013) Evidence of reproductive disruption associated with neuroendocrine changes induced by UV–B filters, phtalates and nonylphenol during sexual maturation in rats of both gender. *Toxicol* 311: 41–51

Radom F, Przemysław M. Jurek, Maciej P. Mazurek, Jacek Otlewski, Filip Jeleń (2013) Aptamers: Molecules of great potential. *Biotech Adv* (31): 1260–1274

Racuciu M, Creanga DE, Apetroaie N, and Birsan E, (2008) Dimensional comparative study of magnetic nanoparticles dispersed in water or kerosene. *J Optoelectron Adv Mater* 10(2), 280

Rawal R, Chawla S, and Pundir CS. (2012) An electrochemical sulfite biosensor based on gold coated magnetic nanoparticles modified gold electrode. *Biosens and Bioelectron* (31):144-150

Reddy H, Arias JL, Nicolas J, and Couvreur P. (2012) Magnetic nanoparticles: Design and characterization, toxicity and biocompatibility, pharmaceutical and biomedical applications. *Chem Rev* (112): 5818−5878

Robinson I, Tung LD, Maenosono S, Wálti C, and Thanh NTK. (2010) Synthesis of core-shell gold coated magnetic nanoparticles and their interaction with thiolated DNA. *Nanoscale* (2): 2624–2630

Rodriguez-Mozaz S, Marco MP, J. Lopez de Alda M, and Barceló D. (2004) Biosensors for environmental applications: Future development trends. *Pure Appl Chem* 76(4): 723–752

Safarik I, Horska K, Pospiskova K, and Safarikova M. (2012) Magnetic techniques for the detection and determination of xenobiotics and cells in water. *Anal Bioanal Chem* (404): 1257–1273

Safarik I, Horska K, and Safarikova M. (2011) Magnetic Nanoparticles for Biomedicine. *Fundamental Biomed Tech* (5): 363-372

Safarik I, and Safarikova M. (2009) Magnetic nano- and microparticles in biotechnology. *Chem Papers* (63):497–505

Salgado AM, Silva LM and Melo AF. (2011) Biosensor for environmental applications, environmental biosensors. *InTech* DOI: 10.5772/20154

Sapsford KE, Algar WR, Berti L, Gemmill KB, Casey BJ, Oh E, Stewart MH, and Medintz IL. (2013) Functionalizing nanoparticles with biological molecules: Developing chemistries that facilitate nanotechnology. *Chem Rev* 113(3): 1904–2074

Schadt MJ, Cheung W, Luo J, and Zhong CJ. (2006) Molecularly-tuned size selectivity in thermal processing of gold nanoparticles. *Chem Mater* (18): 5147-5148

Sjogren CE, Johansson C, Naevestad A, Sontum PC, BrileySaebo K, and Fahlvik AK. (1997) Crystal size and properties of superparamagnetic iron oxide (SPIO) particles. *Magn Reson Imaging* (15): 55

Spasova M, Salgueirino-Maceira V, Schlachter A, Hilgendorff M, Giersig M, Liz-Marzan LM, and Farle M. (2005) Magnetic and optical tunable microspheres with a magnetite/gold nanoparticle shell. *J Mater Chem* 15: 2095-2098

Stanciu L, Won YH, Ganesana M, and Andreescu S. (2009) Magnetic particle-based hybrid platforms for bioanalytical sensors. *Sensors* 9: 2976-2999

Stoeva SI, Huo F, Lee JS, and Mirkin CA. (2005) Three-layer composite magnetic nanoparticle probes for DNA. *J Am Chem Soc* (127): 15362

Sun H, Jiao X, Han Y, Jiang Z, and Chen D. (2013) Synthesis of Fe_3O_4-Au Nanocomposites with Enhanced Peroxidase-Like Activity. *Eur J Inorg Chem* 109–114

Sun H, and Zu Y. (2015) A Highlight of Recent Advances in Aptamer Technology and Its Application. *Molecules* (20): 11959-11980

Tang B., Yuan L., Shi T., Yu L., and Zhu Y. (2009) Preparation of nano-sized magnetic particles from spent pickling liquors by ultrasonic-assisted chemical co-precipitation. *J of Hazrd Mater* (163): 1173–1178

Tartaj P, Morales MP, Veintemillas-Verdaguer S, González-Carreño T and Serna CJ. (2003) The preparation of magnetic nanoparticles for applications in biomedicine. *J Phys D: Appl Phys* 36

Tao Y, Lin Y, Huang Z, Ren J, and Qu X. (2013) Incorporating graphene oxide and gold nanoclusters: A synergistic catalyst with surprisingly high peroxidase-like activity over a broad pH range and its application for cancer cell detection. *Adv Mater* (25): 2594–2599

Teraoka Y, Taura Y, Moriguchi I, and Kagawa S. (1995) Preparation and catalytic activity for me thane oxidation of perovskite-type La(0.8)Sr(0.2)Mo(3) (M=CO, MN) with high-surface-area. *Kagaku Kogaku Ronbunshu* (29): 1202–1203

Thurm S, and Odenbach S. (2002) Magnetic separation of ferrofluids. *J Magn Magn Mater* 252: 247

Tombácz E. (2009) pH-dependent surface charging of metal oxides. *Periodica Polytec-Chem Eng* 53(2): 77-86

Wang S, Li Y, Ding M, Wu X, Xu J, Wang R, Wen T, Huang W, Zhou P, Ma K, Zhou X, and Du S. (2011) Self-assembly molecularly imprinted polymers of 17β-estradiol on the surface of magnetic nanoparticles for selective separation and detection of estrogenic hormones in feeds. *J of Chrom B* (879): 2595-2600

Wille K, De Brabander HF, De Wulf E, Caeter PV, Janssen CR, Vanhaecke L. (2012) Coupled chromatographic and mass-spectrometric techniques for the analysis of emerging pollutants in the aquatic environment. *Trends in Anal Chem* 35

Williams M., Woods M., Kumar A., Ying G.G., Shareef A., Karkkainen M., and Kookana R. (2007) Endocrine Disrupting Chemicals in the Australian Riverine Environment: A pilot study on estrogenic compounds. *Land & Water Aus*

Wu H, Yin JJ, Wamer WG, Zend M, and Lo YM. (2014) Reactive oxygen species-related activities of nano-iron metal and nano-iron oxides. *J Food and Drug Anal* (22): 86-94

Xia W, Li .Y., Wan Y., Chen T., Wei J., Lin Y., and Xu S. (2010) Electrochemical biosensor for estrogenic substance using lipid bilayers modified by Au nanoparticles. *Biosens and Bioelect* (25): 2253–2258

Xin TB, Liang SX, Wang X, Li H, and Lin JM. (2008) Determination of estradiol in human serum using magnetic particles-based chemiluminescence immunoassay. *Analy Chim Acta* 627(10): 277-284

Xu Y, and Wang E. (2012) Electrochemical biosensors based on magnetic micro/nano particles. *Electrochim Acta* (84): 62-73

Yang GX, Zhuang HS, Chen HY, Ping XY, and Bu D. (2014) A sensitive immunosorbent bio-barcode assay based on real-time immuno-PCR for detecting 3,4,3',4'-tetrachlorobiphenyl. *Analy and Bioanaly Chem* 406(6): 1693-1700

Yildirim N., Long F., Gao C., He M., Shi H. and Gu A. (2012) Aptamer-based optical biosensor for rapid and sensitive detection of 17beta-estradiol in water samples. *Environ Sci Technol* (46): 3288–3294

Zacco E, Pividori MI, Alegret S, Galve R, and Marco M-P. (2006) Electrochemical magnetoimmunosensing strategy for the detection of pesticides residues. *Anal Chem* 78(6): 1780–1788

Zeng T, Zhang XL, Niu HY, Ma YR, Li WH, and Cai YQ. (2013) *In situ* growth of gold nanoparticles onto polydopamine-encapsulated magnetic microspheres for catalytic reduction of nitrobenzene. *Appl Catal B: Env* (134-135): 26-33

Zhang J, Post M, Veres T, Jakubek ZJ, Guan J, Wang D, Normandin F, Deslandes Y, and Simard B. (2006) Laser-assisted synthesis of superparamagnetic Fe@Au core-shell nanoparticles. *J Phys Chem B* 110: 7122

Zhang XQ, Gong SW, Zhang Y, Yang T, Wang CY, and Gu N. (2010) Prussian blue modified iron oxide magnetic nanoparticles and their high peroxidase-like activity. *J Matter Chem* (20): 5110-5116

Zhang K, Hu X, Liu J, Yin JJ, Hou S, Wen T, He W, Ji Y, Guo Y, Wang Q, and Wu X. (2011) Formation of PdPt Alloy Nanodots on Gold Nanorods: Tuning Oxidase-like Activities via Composition. *Langmuir* 27(6): 2796–2803

Zhao G, Feng JJ, Zhang QL, Li SP, and Chen HY. (2005) Synthesis and characterization of Prussian blue modified magnetite nanoparticles and its application to the electrocatalytic reduction of H_2O_2. *Chem Mater (*17): 3154-3159

Zhong CJ, Zheng WX, Leibowitz FL, and Eichelberger HH. (1999) Size and shape evolutions for thiolate-encapsulated gold nanocrystals. *Chem Commun* (13): 1211-1212

Zoeller RT. (2005) Environmental chemicals as thyroid hormone analogues: new studies indicate that thyroid hormone receptors are targets of industrial chemicals? *Mol. Cell. Endocrinol* (242): 10–15

Chapter 3

Analysis of the heterogeneous structure of iron oxide/gold nanoparticles and their application in a nanosensor

3.1 Summary

Purpose: The aim of this study was to investigate the formation of iron oxide nanoparticles-gold nanoparticles (IONPs-AuNPs) with heterogeneous structure using a simple electrostatic -self - assembly technique, and the application of these nanoparticles in a nanosensor system for an analyte in aqueous solution.

Methods: IONPs and AuNPs were synthesized separately, where IONPs were synthesized using a reverse co-precipitation method and then treated with HNO_3 while AuNPs were synthesized using the Turkevish method followed by microwave-assisted irradiation. Then, both nanoparticles were allowed to interact to form IONPs-AuNPs heterogeneous structure. This interaction is based on the manipulation of the opposite interfacial charges exhibited between them. For a nanosensor application, a colorimetric assay to detect glucose was studied as a model system. Glucose oxidase (GOx) was immobilized on IONPs-AuNPs using a carbodiimide-coupling technique and the bioactivity of the nanoparticles-GOx for glucose detection was measured using an ABTS assay. For characterization, UV-Vis spectrophotometer, DLS, zeta potential, TEM, EDX, XPS and FTIR techniques were used.

Results: A simple analytical signal using a UV-Vis spectrophotometer successfully determined the formation of IONPs-AuNPs, and this was further verified by other characterization methods. The particle diameter obtained from TEM was 16.1± 11.1 nm and EDX confirmed the presence of Au and Fe elements. It is suggested that the IONPs nanostructure species is maghemite (γ-Fe_2O_3) and that alloy-like morphology (Fe/Au) was formed, as was observed in HRTEM and XPS analysis. In addition, FTIR results exhibited strong vibrational modes around 1655, 1545 and 3290 cm^{-1} that appeared to be primarily due to immobilization of GOx onto Fe/Au. The colorimetric assay also showed a significant increase in green color intensity (due to oxidation of ABTS) with increasing glucose concentrations ranging from 20 μM to 100 μM.

Conclusions: The direct deposition technique used in this study suggested the formation of a metastable alloy-like morphology, Fe/Au. Moreover, these nanoparticles also showed a good potential for application in a colorimetric assay to detect glucose in aqueous solution, thus suggesting an excellent basis for a nanosensor system using these particles.

3.2 Introduction

In recent years, a large number of studies have focused on the construction of magnetic nanoparticles coated with gold nanoparticles as it provides an excellent platform for multifunctionality. In the nanosized scale, both nanoparticles develop into a new material where the surface effect dominates and contributes to a superparamagnetism phenomenon for the magnetite phase (Batlle and Labarta, 2002) and a high plasmon field and surface functionalization for the gold nanoparticle portion (Sapsford et al., 2012). Based on these special characteristics, the selective separation or removal of magnetic nano- and micro- particles and composites from the complex samples is easily performed. This process is very important for bio-application and environmental technology because most of the biological materials and contaminants have no magnetic properties. When this biological material or contaminant is magnetically modified, an efficient selective separation is enabled from the complex mixture (Safarik and Safarikova, 2009; Arruebo et al., 2007).

Gold nanoparticles (AuNPs), a nanosized metal particle that have a high plasmon field upon receiving optical energy (Kang et al., 2011), are used widely for analytical signals. The AuNPs capability for surface functionalization receives a great attention as it exhibits a strong interaction with thiolated linkers or biomolecules. Amine groups and cysteine residues in proteins are known to bind strongly with gold colloids (Gole et al., 2001a; Gole et al., 2001b; Gole, et al., 2002) due to chemisorptions occur between thiol group and AuNPs.

It is known that iron oxide nanoparticles (IONPs) coated with AuNPs is a versatile approach particularly for biodiagnostic applications. Since IONPs are not stable, easily oxidized and have limited options for bio-functionalization, hence, further chemical functionalization

needs to be made to form biocompatible nanoparticles. AuNPs are known as an adequate shell coating for magnetite as it adds functionality to magnetite as well as improves its stability in aqueous dispersions (Laurent et. al., 2008). The composition of the core, shell and interface structure exhibits a unique physiochemical property and makes them suitable in many nano-biotechnology research applications.

However, the formation of core-shell nanoparticles is quite challenging as the Au shell forms a poor diffusion barrier against the core layer and there are significant difficulties in controlling the uniformity and thickness of the metal coating (Dahal et al., 2008). Therefore, some researchers have suggested the formation of alloy nanoparticles or nanoalloys. A few studies have reported the preparation of nanoalloys using pulsed laser deposition (Chang et al., 2006), carbon film deposition at very high temperature (1600 K) in the presence of helium flow (Saha et al., 1999) and electrodeposition (Lu et al., 2002). A study by George and coworkers used high-temperature colloidal synthesis to decompose iron pentacarbonyl in the presence of gold nanocrystals (George et al., 2011). In addition, dumbbell-like Au–Fe_3O_4 exhibit bifunctional properties with high magnetization and excellent catalytic activity toward nitrophenol reduction (Lin and Doong, 2011). They fabricated Au–Fe_3O_4 using thermal decomposition of the iron-oleate complexin the presence of Au seeds.

Some studies have provided information on the interfacial reactivity, the structural and electronic properties of various morphologies of Au–Fe_3O_4 heterostructures and an understanding of the interaction between the magnetite and the gold (III) nanoparticle surfaces (Odio et al., 2014; Lin and Doong 2013; Wang et al., 2005). However, the information on

IONPs-AuNPs fine heterostructure, charge transfer and their interfacial relationship are still limited and ongoing investigation needs to be done. In addition, it is also of interest to investigate this heterogeneous nanoparticles application as a supporting material for biomolecules such as enzymes. Several enzymes and biomolecules have been successfully immobilized onto IONPs-AuNPs nanoparticles for examples glucose oxidase (Samphao et al., 2015), sulfite oxidase (Rawal et al., 2012) and tyrosinase (Li et al., 2012).

In our work, the heterogeneous structure of hybrid iron oxide nanoparticles- gold nanoparticles (IONPs-AuNPs) was investigated, as well as their potential application in nanosensors. The IONPs surface allowed for interaction with AuNPs using a simple and easy electrostatic -self -assembly technique. This strategy was adapted from the layer-by-layer deposition technique which exploits the surface layer electrostatic attractions for a quick and easy deposition of heterogeneous nanoparticles. Instead of using polyelectrolyte, we manipulated the interfacial charge exhibited between IONPs and AuNPs since IONPs surface charge can easily be tuned to positive charge or negative charge by a simple pH adjustment. For this study, we used acidic solution to gain positively charged IONPs. Then, these nanoparticles were used to immobilize glucose oxidase on the surface, and these were then used for the colorimetric detection of glucose in aqueous solution using an ABTS assay.

3.3 Materials and methods

3.3.1 Chemicals

The chemical reagents used in this work were ferrous sulfate heptahydrate ($FeSO_4.7H_2$, ReagentPlus®, > 99%), hydrogen tetrachloro-aurate (III) ($HAuCl_4.3H_2O$, ≥ 99.9%), sodium hydroxide (NaOH, ACS Reagent, ≥ 97%), trisodium citrate ($Na_3C_6H_5O_7$, anhydrous, ≥ 98%, GC), nitric acid (HNO_3, ACS Reagent 70%) diluted to 65%, 2,2'-azino-bis(3-ethylbenzthiazoline-6-sulfonic acid) diammonium salt (ABTS, 10 mg/tablet), N-ethyl-N'- (3-dimethylaminoprophyl) carbodiimide hydrochloride linker (EDC-linker, commercial grade, powder), N-hydroxysuccinimide (NHS, 98%), D-glucose (≥ 99.5%, GC), glucose oxidase Type VII from *Aspergillus Niger* (GOx), horseradish peroxidase lyophilized powder (HRP), 11-Mercaptoundecanoic acid (11-MUDA, M_w : 218.36 g/mol), PBS buffer (tablet), Tween 20 (viscous liquid), 2-(*N*-morpholino)ethanesulfonic acid buffer (MES buffer, ≥ 99.5%) and sodium acetate anhydrous buffer (NaAc). All reagents were purchased from Sigma Aldrich and were used as received without further purification.

3.3.2 Synthesis of IONPs

IONPs were synthesized using a reverse co-precipitation method. This method was adapted from Mahmed et al. (2011) with slight modification. Firstly, 50 mL NaOH (1 M) and 1 mL $Na_3C_6H_5O_7$ (1 mM) were mixed in 50 mL deionized water. Then, ±55.6 mg of $FeSO_4.7H_2O$ was added into the mixture with vigorous stirring for 10 min at room temperature. After adding the salts into the alkaline solution, black precipitates were observed, suggesting the formation of IONPs. The resulting precipitate was then immediately microwave irradiated for up to 30 s and

58

then was readily collected by a permanent magnet when the solution cooled down to room temperature. After that, the black precipitates were air-dried overnight. 12 mg of this black precipitates were treated with 10 mL HNO_3 (6 M) by stirring vigorously for 10 min and the color immediately changed to brown-reddish. IONPs were resuspended in deionized water, were centrifuged for 10 min at 6.5x1000 rpm, and separated using a permanent magnet. The separated IONPs were then added to 1 mL deionized water with the IONPs final concentration of 12 mg/mL and were stored at room temperature until use.

3.3.3 Synthesis of AuNPs

AuNPs were synthesized using the Turkevish method by mixing 500 μL $HAuCl_4.3H_2O$ (10 mM) in a solution containing 300 μL $Na_3C_6H_5O_7$ (100 mM) and 10 mL deionized water. The solution was microwave irradiated for 45 s with 10 s interval mixing and the formation of AuNPs was observed as the solution color changed to dark red.

3.3.4 Synthesis of IONPs-AuNPs

AuNPs were coated on the IONPs surface using a layer-by-layer deposition technique. A preliminary study to construct IONPs-AuNPs using polyelectrolytes (ionic polymer) was explained in Appendix A. For electrostatic-self assembly methodology, 12 mg/mL of IONPs treated with HNO_3 were mixed with 2.5 mL citrate-capped AuNPs for 1 hr. Then, the nanoparticles were separated by a permanent magnet overnight. The separated IONPs-AuNPs were stabilized with 3.5 mL of PBS-T (10mM, pH 4) by vigorous mixing for 1 hr. Subsequently, the solution was centrifuged for 10 min at 6.5x 1000 rpm and the IONPs-AuNPs were separated

using a permanent magnet and washed several times with PBS-T and were stored at 4°C until use.

3.3.5 Detection of glucose

3.3.5.1 Carbodiimide-coupling strategy

IONPs -AuNPs were weighed out to approximately 29 mg and added to 950 μL MES buffer, (10 mM, pH 4). In a separated falcon tube, 28.85 mg of 11-MUDA was dissolved in 10 mL methanol. 50 μL of this freshly prepared solution was then added to the IONPs-AuNPs solution and this was mixed at room temperature for 1 hr. In order to remove the unbound 11-MUDA, the solution was washed several times and IONPs-AuNPs were separated using a permanent magnet. Finally, 1mL of MES buffer (10mM, pH 4) was added to the nanoparticles. In a separate tube, 0.312 mg of EDC-linker and 1.24 mg of NHS were mixed in 1 mL MES buffer (10 mM, pH 4). Subsequently, this solution was added to the carboxylate-modified nanoparticles (IONPs-AuNP-COOH) and this was incubated at 4°C for 30 min without mixing. To remove excess EDC-linker and NHS, the solution was centrifuged for 10 min at 6.5x1000 rpm and washed several times with PBS-T (10 mM, pH 4). The nanoparticles were separated using a permanent magnet and 1 mL MES buffer (10 mM, pH 4) was added to the nanoparticles which were then stored at 4°C until use.

3.3.5.2 Immobilization of glucose oxidase (GOx)

180 μL of the carboxylate-modified nanoparticles was mixed with 20 μL of GOx (1 mg/mL) and was incubated at 4°C for 1 hr. Subsequently, the nanoparticles-bioconjugate (IONPs-AuNP-GOx) was centrifuged for 10 min at 6.5x1000 rpm and separated using a

permanent magnet. The unbound GOx was carefully pipetted from the separated nanoparticles-bioconjugate. Then, the nanoparticles-bioconjugate was added into 200 μL MES buffer (10 mM, pH 4) and this was stored at -20°C until use.

3.3.5.3 Colorimetric detection

In order to detect glucose using immobilized GOx on IONPs-AuNP, the ABTS assay was used. 100 μL of each sample, including a positive control, negative control and the nanoparticles-bioconjugate (IONPs-AuNP-GOx), were mixed in 1650 μL NaAc buffer, (10 mM, pH 5). Then, to the mixture was added 100 μL of various glucose concentrations (20 μM, 40 μM, 60 μM, 80 μM and 100 μM) and this was incubated for 15 min. At the end of incubation, 50 μL of horseradish peroxidase (HRP) enzyme was added and the mixture was subsequently measured using UV-vis spectrophotometer. Then, 100 μL of ABTS reagent was added and incubated for another 15 min. The reaction solution was adjusted by 2 fold dilution using dH$_2$O and measured using UV-Vis spectrophotometer.

3.3.6 Characterization

For morphology and heterostructural analysis, the nanoparticle samples were sent to the Canadian Centre for Electron Microscopy (CCEM), McMaster University, where high-resolution transmission electron microscopy (HRTEM, JEOL) was used at an accelerating voltage of 200 kV, and the Energy Dispersive X-Ray Analysis (EDX) technique was used to identify the elemental composition of the materials. Dynamic light scattering (DLS) and zeta potential was employed using a Malvern Zetasizer to obtain information on the hydrodynamic size of nanoparticles and the nanoparticles surface charge. A UV-Vis spectrophotometer using a 1 cm

path length quartz cuvette was used to determine the surface plasmon resonance shifted bands. X-ray photoelectron spectroscopy (XPS) analysis was performed at the Waterloo Advanced Technology Lab (WATLab) using a multi-technique ultra-high vacuum Imaging XPS Microprobe system (Thermo VG Scientific ESCA Lab 250). Fourier transform infrared spectroscopy (FTIR) was performed using FTIR equipment (Tensor 27). The samples were previously prepared by grinding the dry nanoparticles and KBr into a fine powder using pestle and mortar. Then this powder was pressed to form a pellet and further investigate with FTIR.

3.4 Results and discussion

3.4.1 Investigation of magnetic and plasmonic properties of IONP-AuNPs

IONP-AuNPs shows both magnetic and plasmonic properties since they are fabricated from heterodimers structures. Interestingly, both properties can easily be detected using simple analysis methods. For a simple detection of magnetic property, the prepared IONPs-AuNPs was observed by separating the nanoparticles from the solution using a permanent magnet as shown in Figure 3.1. It illustrates the non-magnetic effect of AuNPs and the movement of IONPs-AuNPs towards the external magnet field. As shown in Figure 3.1 (a), the synthesized AuNPs did not show any magnetic property since it did not showing any response towards the permanent magnet. After the IONPs were allowed to interact with the AuNPs, the color of the solution changed from bright red to purplish color and they were well dispersed in PBS buffer at pH 4 as shown in Figure 3.1 (b). When a magnetic field was applied, the suspended IONPs-AuNPs gradually moved toward the wall near the permanent magnet, eventually leaving a clear solution. This is the first indicator that the prepared IONPs-AuNPs exhibited superparamagnetic properties where they aggregates towards the applied magnetic field and remained well dispersed in the buffer solution when the permanent magnet was removed.

(a)   (b)
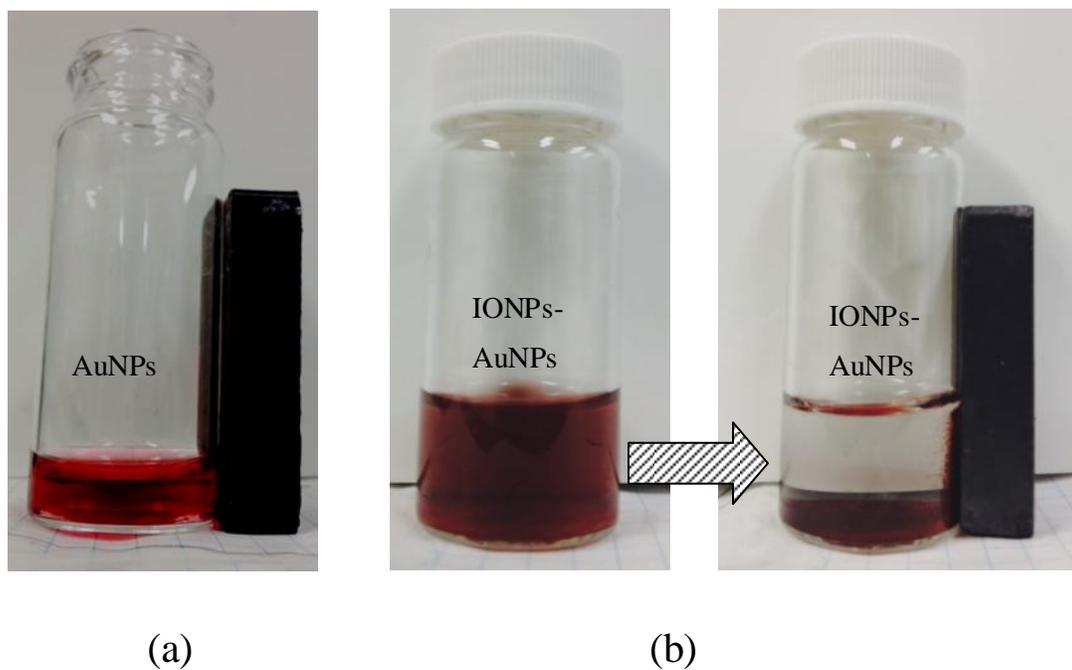
Figure 3.1   **Illustration of (a) the lack of effect of a magnetic field on AuNPs and (b) the movement of IONPs-AuNPs towards the external magnetic field after approximately 1 hr of mixture separation.**

With the presence of the AuNPs plasmonic property, a simple analytical signal to observe the interaction between IONPs and AuNPs can be used. Small changes in the local refractive index that converts into spectral shifts in the extinction and scattering spectra can give an indication of the interaction that occur between IONPs and AuNPs. Measurements of the surface plasmon resonance band of the nanoparticles provided an indirect piece of evidence supporting the formation of IONPs-AuNPs. Furthermore, identification of plasmon resonance is important for sensing applications such as colorimetric or fluorescence detection. This localized surface plasmon resonance can be utilized for AuNP size and shape determination as well as the dielectric properties of the medium surrounding the nanoparticle (Sapsford et al., 2013). For example, spherical AuNPs are often characterized by a bright red or purple color and an absorption maximum between 517 nm and 575 nm for particle diameters between ~9 and 99 nm (Daniel and Astruc, 2004).

Figure 3.2 (a) shows UV-Vis spectrophotometer absorbance measurements comparing the control, pure AuNP, pure IONPs, and IONPs-AuNPs dispersed in aqueous solution at 60 min. For IONPs-AuNPs, different interaction times from 1 min to 60 min were observed. The absorbance measurement for pure AuNPs showed a sharp peak at 520 nm, which is a peculiar characteristic of the gold surface plasmon band, whereas for pure IONPs, there was no obvious peak observed in the visible region. IONPs showed magneto-optical (MO) effects which are typically small in most media and these effects provide physical information on electronic and spin structure of the materials (Jain et al., 2009) and can be enhanced by integration with phototonic crystal (Diwekar et al., 2004; Kahl and Grishin, 2004) and metal films (Khanikaev et

al., 2007; Belotelov et al., 2007). As reported by Jain group, the MO effects of IONPs are greatly enhanced by coating with AuNPs and are known as surface plasmon resonance-enhanced magneto-optical (SuPREMO) effects (Jain et al., 2009).

Measurement by UV-Vis spectrophotometry of the heterogeneous nanoparticles (IONPs-AuNPs) demonstrated blue shift phenomenon after allowing interaction for 60 min. As shown in Figure 3.2 (b), the initial maximum wavelength of AuNPs, 520 nm shifted towards a lower wavelength after 10 min of interaction and were consistent at 516 nm from 40 to 60 min. Several factors could contribute to this phenomenon, such as changes of materials to a more spherical shape and filling the initial hollow shell (Lyon et al., 2004), an increment of shell thickness due to further deposition of AuNPs coating (Jain et al., 2009) and the core dielectric permittivity that controlled the core-shell plasmon resonance (Levin et al., 2009).

(a)

(b
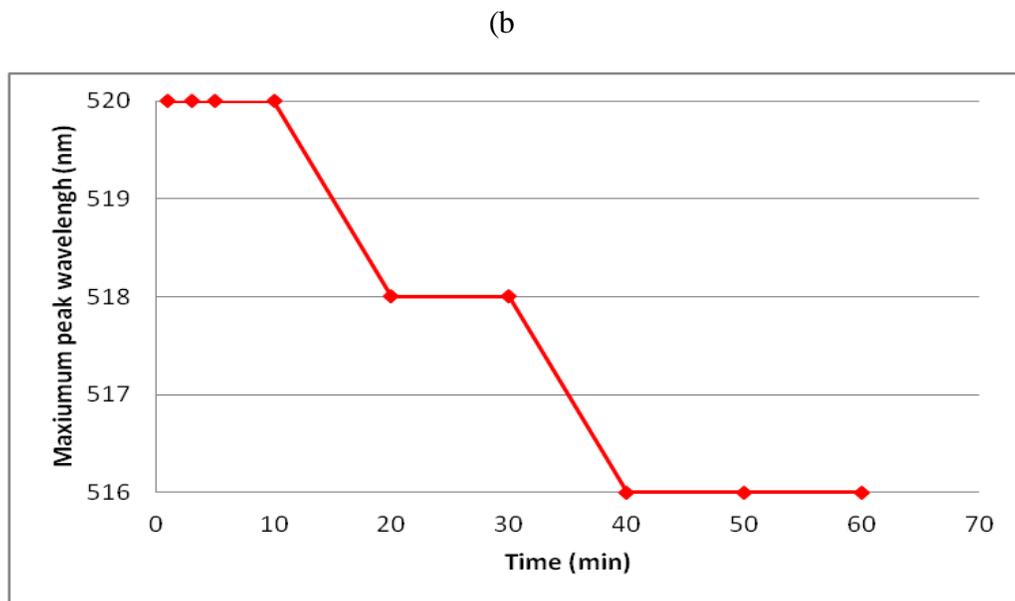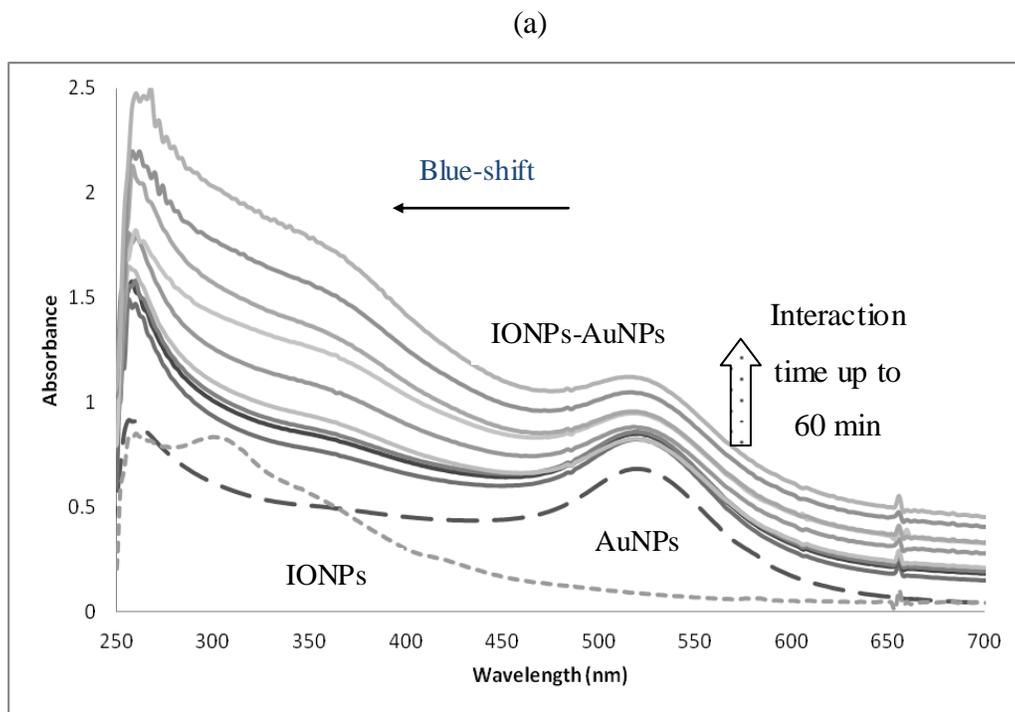
Figure 3.2   **UV-Vis spectra of (a) pure IONPs (small dashed line) at 1 hr, pure AuNPs (big dashed line) at 1 hr and IONPs-AuNPs from 1 min to 60 min (b) IONP-AuNPs wavelength of the peak maximus versus the different interaction times.**

3.4.2 Size and morphological characterization of IONPs.AuNPs

In this subsection, information on the size, morphology, surface charge and elemental composition of the prepared nanoparticles is discussed. Based on the DLS measurement in Table 3.1, significant changes in nanoparticle size were obtained. The IONPs treated with HNO_3 showed a smaller hydrodynamic diameter (d_h) as compared to as-synthesis IONPs. A study by Nurdin et al. (2014) revealed that by increasing the HNO_3 concentration, the nanoparticles were produced as smaller size particles, with lower magnetization, better thermal stability and a more stable nanoparticle suspension. Since the IONPs were dissolved in acidic solution, they went through a dissolution processes that caused nanoparticle size reduction. HNO_3 also acts as an oxidizing agent to produce maghemite (γ-Fe_2O_3) nanoparticles as presented in the chemical reaction of the precipitation process below:

$$Fe^{2+} + 2\,Fe^{3+} + 8OH^- \rightarrow Fe_3O_4 + 4H_2O \qquad (1)$$

$$2Fe_3O_4 + HNO_3 \rightarrow \gamma\text{-}3Fe_2O_3 + HNO_2 \qquad (2)$$
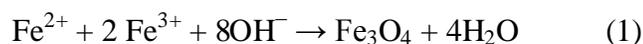
Thus, IONPs produced using this precipitation method mainly produced maghemite (γ-Fe_2O_3) since Fe_3O_4 colloid undergoes oxidation via Fe cation diffusion (Joliviet et al., 1988 and Swaddle et al., 1980 as cited in Lyon et al., 2004). Alibeigi and coworkers suggested that reverse co-precipitation of ferrous or ferric mixed salts in sodium hydroxide (NaOH) solution in an oxidizing environment resulted in the formation of maghemite instead of magnetite particles due to the oxidation of Fe^{2+} to Fe^{3+} (Alibeigi et al., 2008). Supporting data from XPS analysis to verify the iron oxide nanoparticles speciation will be described in a later subsection (3.4.3). Results from the zeta potential analysis of the as-synthesized IONPs shifted from negative charge

to positive charge due to changes of solution environment after the sample was treated with HNO$_3$. This phenomenon confirms the amphoteric nature of IONPs that can develop charges in the protonation and deprotonation reaction of Fe.OH sites on the surface (Illés and Tombácz, 2006). A detail explanation of this phenomenon is discussed in Chapter 2.0 (subsection 2.1.2).

Characterization with DLS also indicated that the heterostructured nanoparticles, IONPs-AuNPs, achieved colloidal stability and become more uniform as the nanoparticles size and polydispersity index (PDI) value decreased. In addition, we can also assume that the formation of IONPs-AuNPs become moderately polydisperse (PDI values between 0.1- 0.4). PDI is a number calculated from a simple two parameter fit to the correlation data (the cumulants analysis). In the Cumulants analysis, a single particle size mode is assumed and a single exponential fit is applied to the autocorrelation function and the polydispersity describes the width of the assumed Gaussian distribution (Malvern Instruments Limited, 2011).

Furthermore, zeta potential measurements revealed that the nanoparticles' net surface charge become negative due to the presence of citrate anions on the AuNPs surface and achieved incipient stability at -24.70 mV. It is generally held that nanoparticles suspension becomes stable with a zeta potential value greater than ± 30 mV (Nurdin et al., 2014).

Table 3.1 DLS measurement of the d_h size of nanoparticles' and their surface charge. PDI represent the nanoparticles' size distribution.

	Size d_h (nm)	PDI	Zeta potential (mV)
as-synthesized IONPs	409.10	0.68	-16.00
IONPs treated with HNO_3	223.60	0.42	17.80
AuNPs	221.50	0.53	-28.90
IONPs-AuNPs	93.62	0.38	-24.70

Transmission electron microscopy (TEM) is another analysis method that has been used to characterize particle size distribution and morphologies. The particle size distribution for IONPs, AuNPs and IONPs-AuNPs are presented in Figure 3.3 (a, b and c) as determined by taking approximately 90 particles for each sample and analyzing using *ImageJ* software. As compared to TEM measurement, particle sizes obtained from DLS results are expected to be larger due to the presence of surfactants and a hydration layer around IONPs and AuNPs. Another plausible factor is because the nanoparticles aggregation presence in the samples. The hydrodynamic diameter (d_h) from DLS analysis measures the nanoparticles sphere that has the same translational diffusion coefficient with their surrounding solvent layers while the diameter (*d*) obtained from TEM is based on the measurement of the nanoparticles' image area. Thus, the estimated size was smaller and more physically accurate when observed by TEM compared to the DLS technique.

Based on the image presented in Figure 3.3 (a), IONPs were formed with an irregular spherical shape and these nanoparticles were mostly aggregated which may be due to long-range magnetic dipole-dipole interactions (Nurdin et al., 2014). The average diameter for IONPs was 7.1 ± 5.1 nm and is slightly smaller as compared to a study conducted by the Nurdin group which synthesized IONPs with the same preparative route. In contrast to IONPs, AuNPs were formed with a spherical shape with average diameter 11.3 ± 5.5 nm (Figure 3.3 (b)). AuNPs were a stable colloid as they appeared well separated between each other, and this is in agreement with the zeta potential results as AuNPs achieved colloidal stability at -28.9 mV. The average diameter for heterostructured, IONPs-AuNPs was 16.1 ± 11.1 nm and this showed a slight change in particle size (Figure 3.3 (c)).
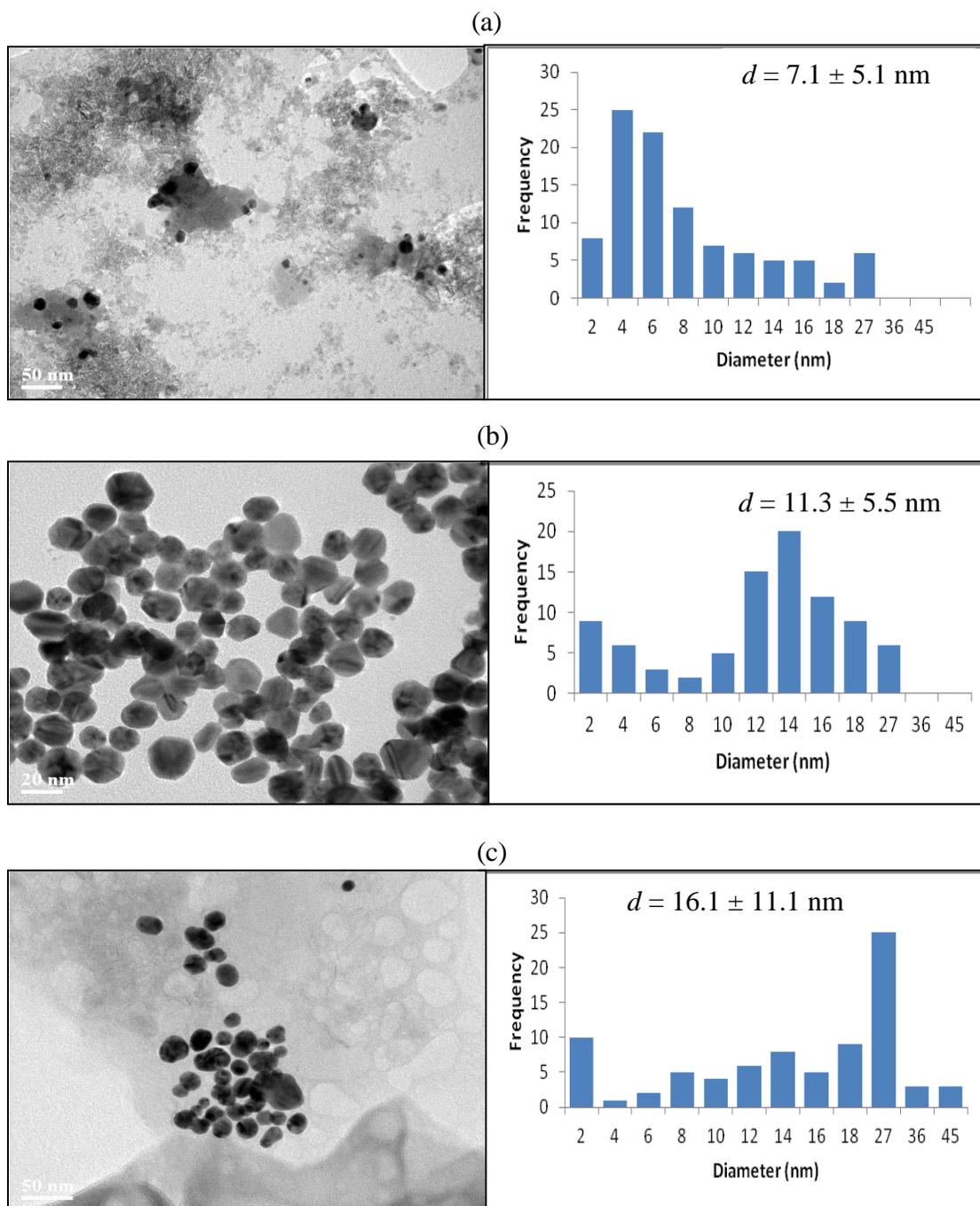
Figure 3.3   TEM images of sample (a) IONPs (b) AuNPs and (c) IONPs-AuNPs and the histograms representing the particle size distributions for each sample.

As reported by Lyon et al., (2004), they suggested that iterative addition of Au layers contributed to a constant average particle diameter but the particles become more uniform in size as Au^{3+} preferentially reduces onto γ-Fe_2O_3 surfaces, and this occurred at more oxidized sites. Thus, the surface coating thickness was difficult to detect and define clearly, suggesting the formation of morphologies such as dumbbell-like or alloy-like.

The Energy Dispersive X-Ray Analysis (EDX) technique was used to identify the elemental composition of the nanoparticles. As shown in the EDX analysis in Figure 3.4, the appearance of various prominent peaks for Au and Fe confirmed the presence of these elements. Furthermore, the presence of oxygen indicates that the iron particles were oxidized to iron oxide, and this result was further validated using XPS analysis. As presented in this result in Figure 3.4 (c), the Fe element relative intensity is higher compared to Au element. This finding indicates that the nanoparticles were dominated by the Fe character rather than Au.

HRTEM analysis was performed on an individual nanoparticle where the arrangement of atoms in the crystallographic planes can be observed. Thus, the epitaxial relationship between IONPs and AuNPs in heterostructured nanoparticles can be fully understood. The calculated Fast Fourier Transform (FFT) were taken from individual nanoparticles images and analyzed using *ImageJ* analytical software. Analysis of the FFT patterns allowed us to identify the nanocrystal structure and it is then similar to indexing an electron diffraction pattern. Insets in Figure 3.5 (a and b) show that the crystal lattice of IONPs is closely oriented to γ-Fe_2O_3 {211} with estimated interplanar spacing (*d*-spacing) value, 0.34 nm and has a similar value as reported in Liu et al., (2014). For AuNPs, the estimated *d*-spacing value is 0.24 nm and is well indexed to Au {111}

73

plane of face center cubic (fcc) as in Ban et al., (2005). All lattice planes can be describes by a set of indices (Miller indices *hkl*) and the distance *d* between two parallel planes is called interplanar spacing (Weidenthaler, 2011).

A distinct separation between heterostructure is presented by a large lattice mismatch at the nanoparticle boundary as observed in Figure 3.5 (c). The lattice mismatch was observed at different grains since Au is easily identified due to the formation of dark contrasts while Fe is recognized by the light contrast. Interestingly, a similar FFT pattern was observed at the boundary and might correspond to the formation of mixed Fe and Au atom at the interface, thus dumbbell shape is suggested for IONPS-AuNPs. Furthermore, the lattice value constant of γ-Fe_2O_3 {211} is reduced to 0.31 nm and Au {111} is increased to 0.27 nm. The reason for the changes of lattice value after formation of heterostructure is most likely the Fe filled into Au vacancy spaces at the interfaces and causes nanoparticle coalescence and recrystallization. However, the HRTEM technique was unable to provide a sufficiently precise *d*-spacing measurement in order to explain the Fe/Au morphology mechanism. More detailed information of this finding was carried out using XPS analysis.
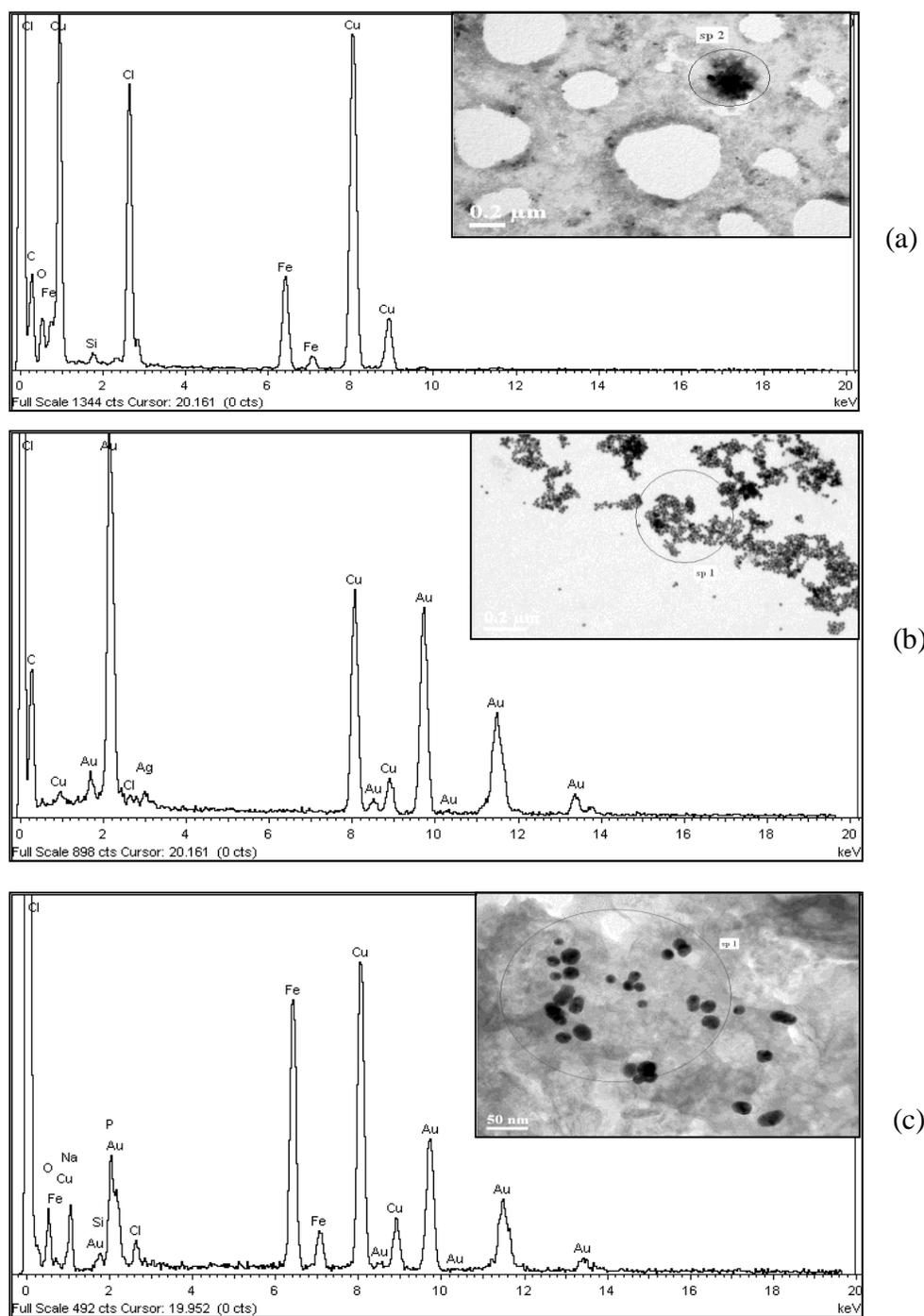
Figure 3.4 EDX analysis of (a) IONPs treated with HNO_3 (b) AuNPs and (c) IONPs-AuNPs. Insets are the TEM images of the analyzed sample.

75
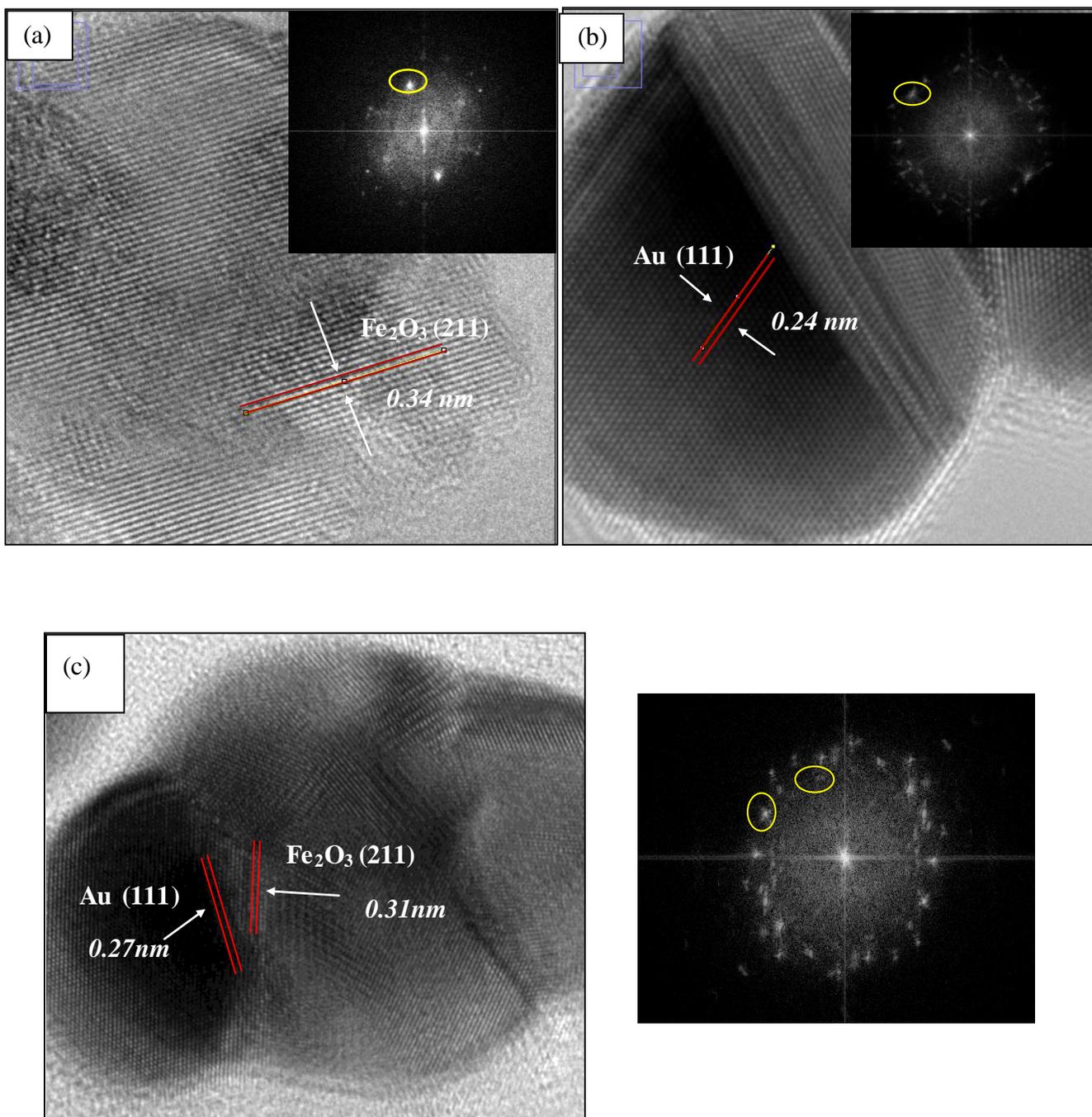
Figure 3.5   **HRTEM images of (a) IONPs, (b) AuNPs and (c) IONPs-AuNPs. Inset images show the FFT analysis to identify the nanocrystal structure.**

3.4.3 Quantitative measurement of IONPs-AuNPs surface

In this subsection, detailed information of the IONPs nanostructure, heterostructure change, and the surface functionalization effect on IONPs-AuNPs was investigated and explained using XPS analysis. Collected XPS spectra were analysed using *CasaXPS* software where all spectra were calibrated using the adventitious C1s peak with a fixed value of 284.5eV and the background from each spectrum was subtracted using a Shirley-type background to remove most of the extrinsic loss structure (Grosvenor et al., 2004).

In this study, IONPs were synthesized at ambient temperature where it is known that IONPs are sensitive to the oxidizing conditions. In addition, the IONPs were treated with HNO_3 resulting in reduction of Fe_3O_4 to γ-Fe_2O_3, and, thus the sample may contain a mixture of both IONPs species. XPS analysis was conducted in order to confirm the formation of IONPs nanostructured species and as supporting evidence for the production of maghemite (γ-Fe_2O_3) nanoparticles, as discussed previously in the chemical reaction of the precipitation process in Subsection 3.4.2. The XPS spectrum for pure IONPs in Figure 3.6 (a) shows a pair of peaks at 713.50eV and 725.5eV, which are attributed to the $Fe2p_{3/2}$ and $Fe2p_{1/2}$, spin-orbital coupling, respectively. For studies involving IONPs, only the region corresponding to the $2p_{3/2}$ peak are discussed. This peak is generally attributed to high spin Fe^{3+} and Fe^{2+} compounds and is broadened compared with $Fe^{(0)}$ metal or low spin Fe^{2+1} (Grosvenor et al., 2004).

The de-convoluted $2p_{3/2}$ peak in Figure 3.6 (b) shows two main spectra at 713 eV and 715.4 eV, assigned to the Fe^{3+} octahedral and Fe^{3+} tetrahedral, respectively, and one satellite peak at 721 eV. It is known that γ-Fe_2O_3 contain the Fe^{3+} ions that occupy both octahedral and tetrahedral sites with an unequal frequency of 5:3 (Fujii et al., 1999). The observed main peak in

this study is slightly higher compared to the reported values located at 710.6 and 713.4eV for Fe^{3+} octahedral and Fe^{3+} tetrahedral. The plausible reason for this phenomenon is the presence of excess oxygen on the metal oxide as oxygen act as electronegative adsorbents can induce positive binding energy shifts of approximately 1eV (Parkinson et al., 2003). This seems to be a reasonable interpretation since the precipitation process was done under oxidizing conditions. The absence of Fe^{2+} compound around 709.1eV further confirms the complete oxidation of Fe_3O_4 to γ-Fe_2O_3 as a result of the accelerating oxidation of Fe^{2+} to Fe^{3+}. Furthermore, the satellite peak obtained at 721 eV is clearly distinguishable and does not overlap either $Fe2p_{3/2}$ or $Fe2p_{1/2}$ and is located 8 eV higher than the main $Fe2p_{3/2}$. This result is in agreement with a study conducted by Fujii et al. (1999).

(a)

(b)
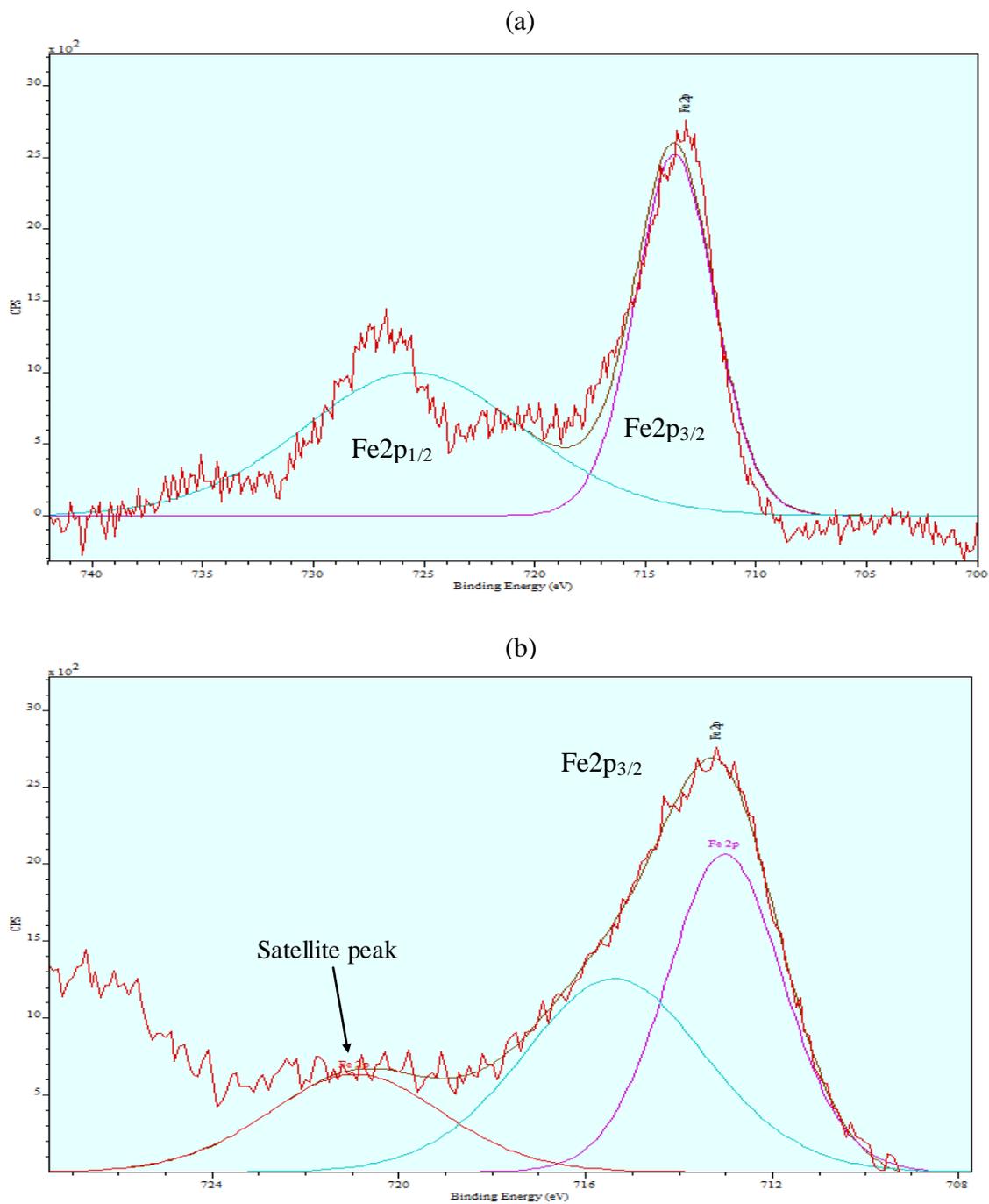
Figure 3.6 **(a) The XPS spectrum of Fe2p from the fractured surface of the γ-Fe₂O₃ sample and (b) the de-convoluted Fe2p₃/₂ region**

It is of interest to examine in detail the formation of the heterostructured nanoparticles. As mentioned beforehand, the EDX analysis shows that the particles are largely Fe in character and results from the XPS spectra also show that the average peak height intensities for Fe2p (Figure 3.7 (a)) are higher after the deposition process. This indicates that Fe dominates at the surface instead of Au, since the peak intensities measure the materials concentration at the surface. On the other hand, the average height intensities for Au4f decrease as shown in Figure 3.7 (b). The proposed mechanism for this finding may indicate the nanoparticles coalescence and recrystallization as reported by Dahal et al. (2010), where the clusters undergo a spontaneous shape deformation in order to lower their surface energy. This mechanism is also concomitant with the observations from TEM images in Figure 3.4, as the γ-Fe_2O_3 shape transformed from an irregular spherical shape to become more spherical and increased in stability as Fe atoms filled some of the Au vacancy lattice. This result further corroborates the formation of alloy-like morphology instead of pure core-shell nanoparticles.

A distinct spectral change is observed in the Fe2p$_{3/2}$ and Fe2p$_{1/2}$ regions in Figure 3.7 (a), which are shifted towards the lower binding energy signal at 712.1 eV and 724.2 eV, hence indicating the addition of Au atoms. The de-convoluted peak for Fe^{3+} octahedral and Fe^{3+} tetrahedral also shifted towards the reported values assigned at 711.3 and 713.5 eV and suggested the removal of excess oxygen with coating material, as supported by the difference in the intensity ratio after Au deposition. Both findings suggest the strong interaction between Au and γ-Fe_2O_3 and most likely Au helps to stabilize the iron oxide domains. This further supports the zeta potential results in Subsection 3.4.2, which showed an increase in the nanoparticle stability.

A similar finding was observed for AuNPs in Figure 3.7 (b), as the Au4f core level of pure AuNPs centred at 88.1 eV and 91.7 eV assigned as $Au4f_{7/2}$ and $Au4f_{5/2}$ respectively, and the position and difference between the two peaks (3.6 eV) almost exactly matched the value reported for Au^0 (Annadhasan et al., 2015). As can be seen, the Au4f peaks were located at comparatively higher binding energy and this could be attributed to the binding of a trisodium citrate ($Na_3C_6H_5O_7$) layer on the AuNPs surface that acted as capping agent. After Au deposition to the γ-Fe_2O_3 surface, the Au4f peaks decreased to 84.4 and 88.1 eV indicating metallic Au^0 as reported in many studies. For example, a study by Amendola et al. (2014) stated that the binding energy centered at 84.4 eV is the typical value of metal Au and is also expected for Fe/Au alloys. Interestingly, a new intense peak was observed for the Au4f spectra at 94 eV in Figure 3.7 (b). As proposed by Sohn et al. (2015), this peak might indicate the formation of a new cationic Au species, for example Au-O bonding, since the O atoms at the topmost layer of γ-Fe_2O_3 indeed react with deposited Au atoms, producing the Au-O bonding at the interface. A study by Khoudiakov et al. (2005) reported that they found a mixed metallic (major) and cationic (minor) Au species in their Au4f XPS study for Au prepared by a deposition-precipitation method. In contrast, our XPS analysis showed that the cationic Au species is the major and broad peak compared to metallic Au, hence, revealing a strong interaction between γ-Fe_2O_3 and Au atoms.

(a)

(b)
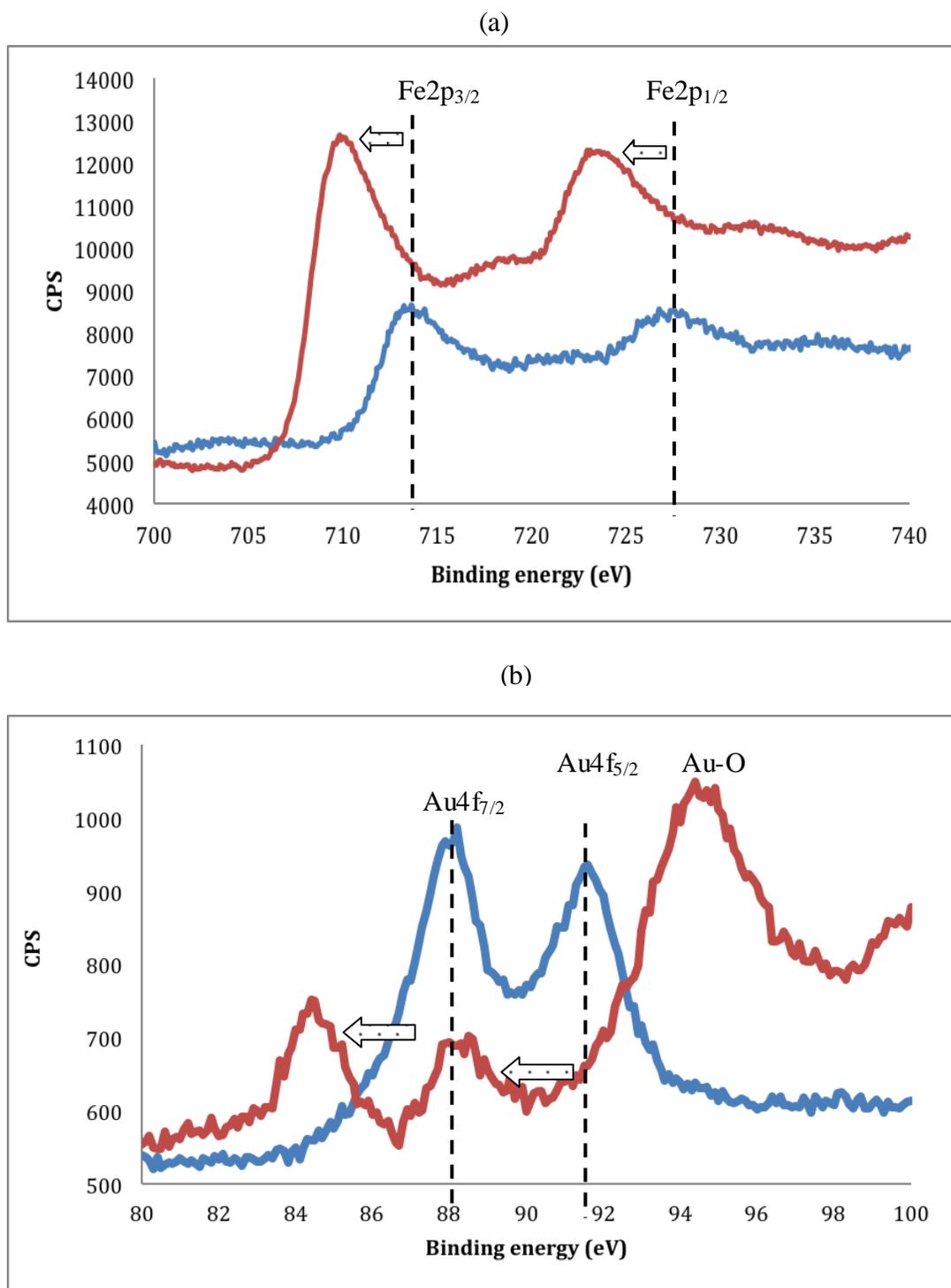
Figure 3.7   XPS spectrum of (a) Fe2p (blue line: γ-Fe₂O₃; red line: Fe/Au) and (b) Au4f for pure and coalesced nanoparticles (blue line: AuNPs; red line: Fe/Au).

Based on the heterogeneous nanoparticles characterization analysis, the formation of alloy-like morphology is suggested. A proposed mechanism for electrostatic -self -assembly performed in this study is illustrated in Figure 3.8. According to the literature, metal ions such as Fe^{3+} are reactive towards water molecules and subsequently form a chemically reactive surface hydroxyl (Fe-OH) group that easily been replaced (Tombácz, 2009). Therefore, the addition of nitric acid into the solution would develop a positively charge IONPs at the Fe-OH site supported by the result from zeta potential data. After the negatively charged citrated-capped AuNPs were mixed into IONPs solution, the inter-particles interaction was initiated by electrostatic driving force followed by magnetic interaction and subsequently formed a dumbbell-like morphology as observed in HRTEM image in Figure 3.8. However, the hybrid metallic nanoparticles further undergo coalescence and recrystallization and metastable alloy-like morphology was then observed. This fact is supported with the results analysis of the blue-shift phenomena, more spherical heterogeneous nanoparticles, increase in nanoparticles stability as well as a slight change in the nanoparticles' diameter.
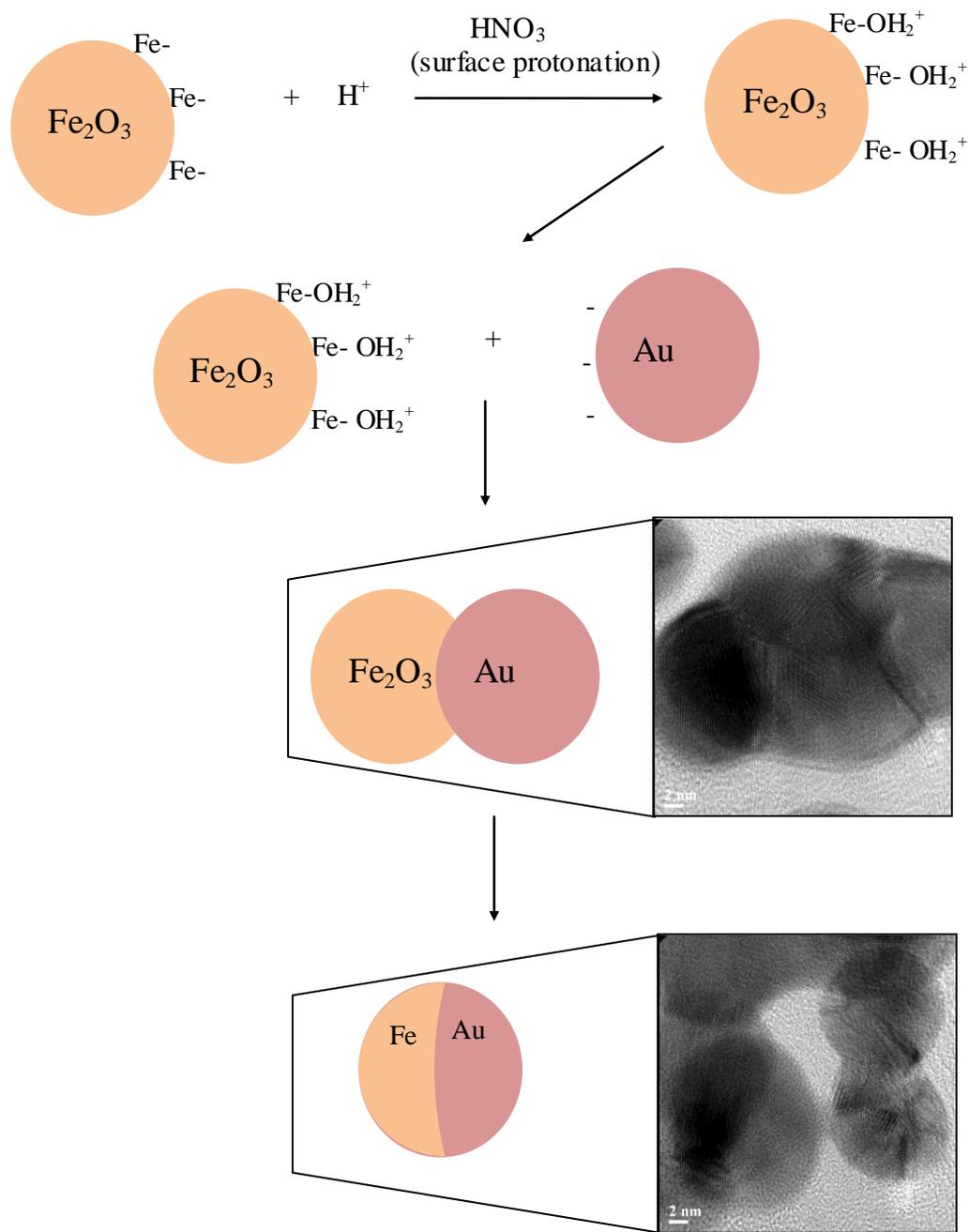
Figure 3.8 **Illustration of heterogeneous nanoprticles, Fe/Au formation using electrostatic –self -assembly technique.**

3.4.4 Colorimetric sensing for glucose detection

To investigate the application of Fe/Au nanoparticles in a nanosensor system, a colorimetric assay to detect glucose was studied, based on the use of the enzyme glucose oxidase (GOx). The fabrication of Fe/Au-GOx is shown in Figure 3.9, where the carbodiimide-coupling technique was utilized to covalently attach GOx onto the Fe/Au surface. An amide bond was formed from carboxylic acid by activation of N-ethyl-N'- (3-dimethylaminoprophyl) carbodiimide hydrochloride linker (EDC-linker) with the assistance of additives such as N-hydroxysuccinimide (NHS) and followed by the addition of an amine (i.e the enzyme) sequentially in one-pot or in stepwise reactions (Yan et al., 2015). Therefore, to functionalize Fe/Au surface with a carboxyl functional group to self-assemble with the enzyme, 11-Mercaptoundecanoic acid (11-MUDA), a ligand with thiolated-carboxylic functional groups was used in this study. Carboxyl-terminated Fe/Au was obtained by the attachment of the thiol group (-SH) in 11-MUDA based on the well-established Au-SH chemisorptions process. Subsequently, the carboxylate groups were activated by EDC-linker/NHS crosslinking and were reacted with GOx in solution. The side-chain amino groups on the GOx surfaces displaced the terminal NHS group of Fe/Au in phosphate buffer and thus formed Fe/Au-GOx.

3.4.4.1 Surface functionalization with 11-MUDA

The effect of surface functionalization with 11-MUDA on the alloy-like morphology was investigated. The XPS spectra for Au4f in Figure 3.8 (a) show many shake-up peaks and no intense peak can be observed. However, the de-convoluted peaks show that three main spectra assigned as metallic Au (Au4f$_{7/2}$ and Au4f$_{5/2}$) and cationic Au species (Au4f) were still present

after surface functionalization and were slightly shifted to a higher binding energy. Based on this analysis, 11-MUDA can still access to Au since the scattered peaks are attributed to charge transfer between Au and thiol groups. Xie et al., (2011) used the two-dimensional TEM image for flower-like Au-Fe$_3$O$_4$ morphology and identified that the gold core was accessible by SH-PEG$_{5000}$ even though Fe$_3$O$_4$ surrounded the Au.

Furthermore, the C1s shifted to a higher binding energy after carboxyl functionalization as seen in Figure 3.10 (b) where the main peak assigned to 285.5 shifted to 287.5 eV and is attributed to the C-S peak since differing binding energies of ~2 eV confirmed the addition of thiol groups to the surface as reported in Güzel et al. (2010). The increase in peak intensity of the shoulder peak at 289.4 eV which is assigned to O-C=O of carboxylate carbon indicates that the 11-MUDA was attached to the nanoparticles.

FTIR was utilized in order to analyze the immobilization of GOx onto Fe/Au nanoparticles surface. With this characterization method, the chemical bonds present on the nanoparticles surface can be determined. In Figure 3.11, the fabrication of Fe/Au-GOx is presented by several characteristic peaks, two peaks at ~1654 cm^{-1} and 1546 cm^{-1} corresponding to the secondary amide or amide I (red curve) (de Jesus et al., 2013). The peak at 3369 cm^{-1} is assigned to NH deformation (amide II band) (Pandey et al., 2007). As a comparison, these peaks were absent before GOx immobilization, as shown by unmodified Fe/Au (purple curve) and carboxylate-modified Fe/Au (blue curve). Therefore, this result confirmed that GOx was successfully immobilized on the Fe/Au surface.
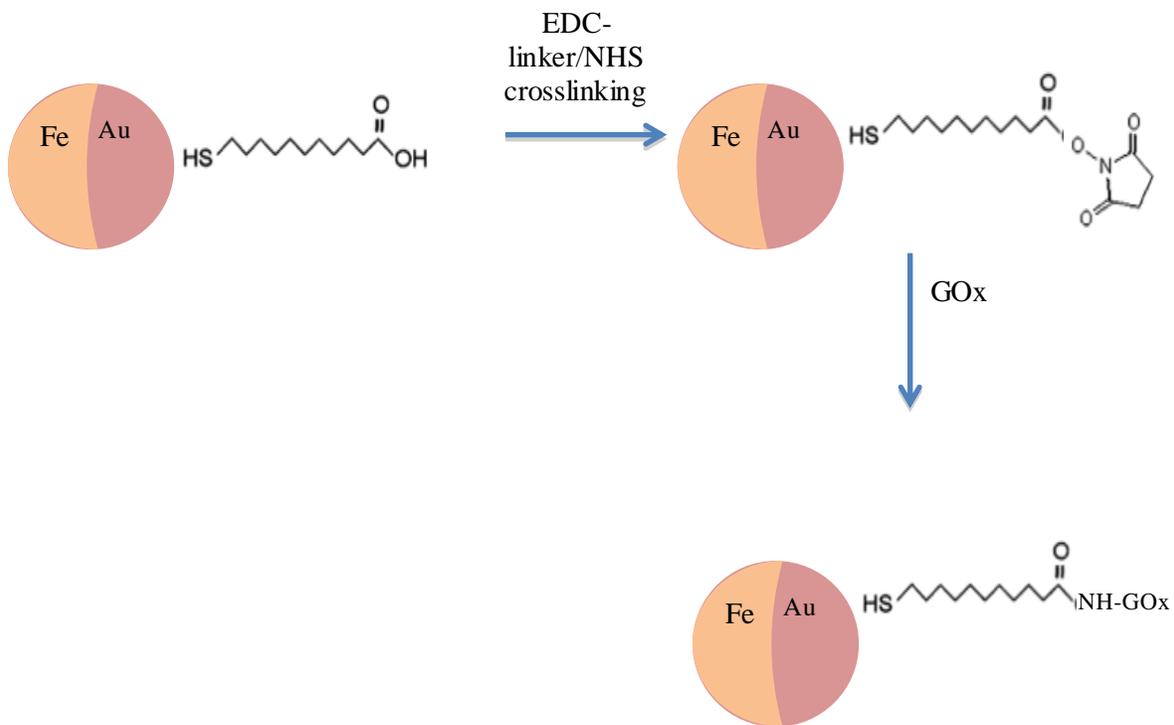
Figure 3.9   **(a) A schematic mechanism illustrates the fabrication of Fe/Au-GOx using the carbodiimide-coupling technique.**

(a)

(b)
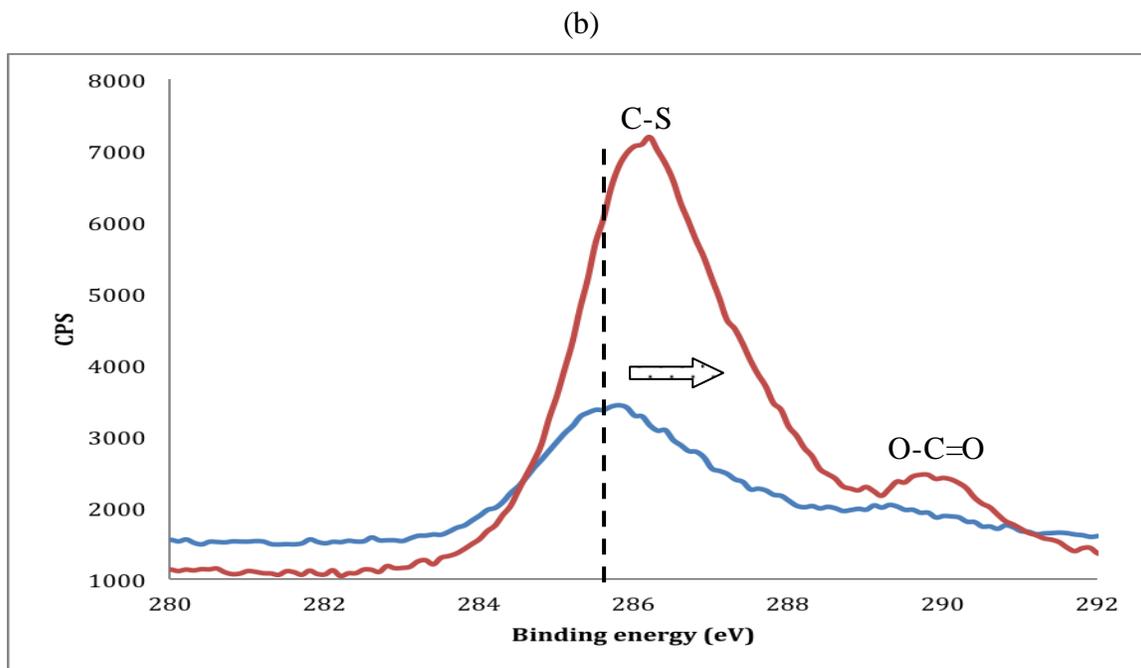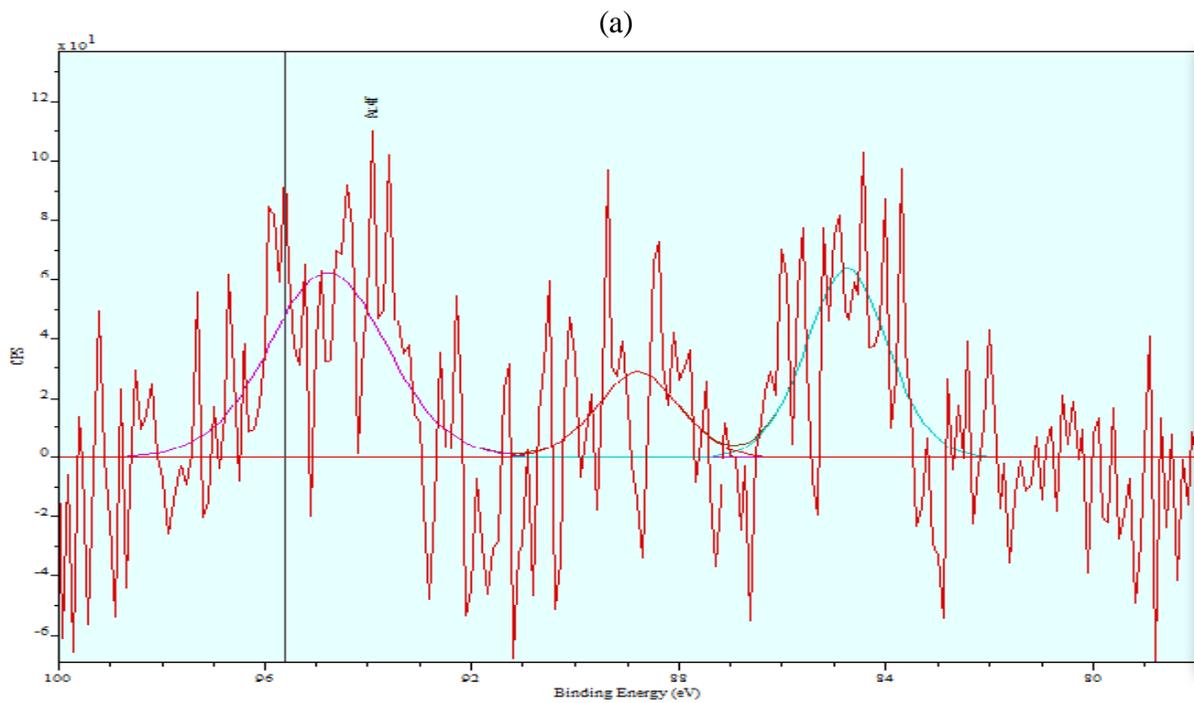
Figure 3.10   XPS spectra (a) Au4f and (b) C1s of Fe/Au functionalized with 11-MUDA (blue line: Fe/Au; red line: Fe/Au -11-MUDA).
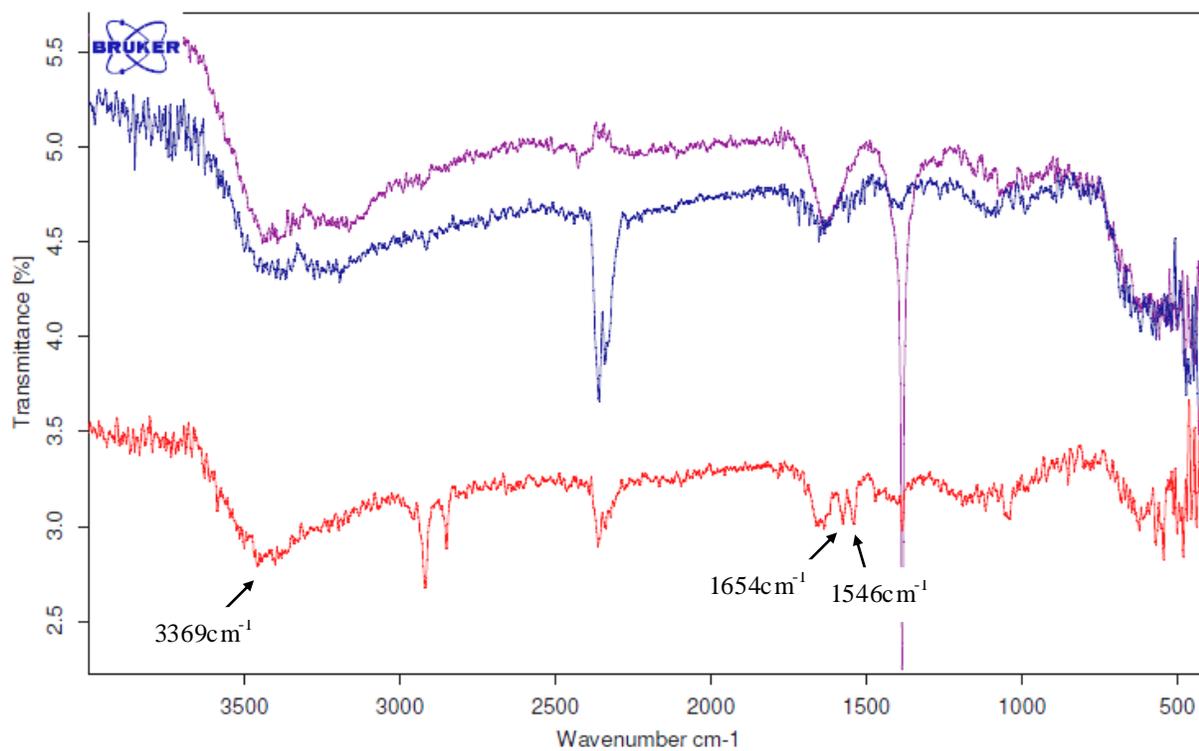
Figure 3.11 **FTIR spectra of Fe/Au (purple curve), Fe/Au-11-MUDA (blue curve) and Fe/Au-GOx (red curve).**

3.4.4.2 Glucose detection

After the Fe/Au-GOx was successfully prepared and confirmed by FTIR measurements, a colorimetric sensing system was prepared. As shown in Figure 3.12 (a), analysis with the UV-Vis spectrophotometer revealed increased absorbance at around 414 nm, corresponding to oxidized ABTS, thus confirming the catalytic activity of GOx immobilized on the Fe/Au nanoparticles. In principle, hydrogen peroxide (H_2O_2) evolved from GOx oxidation of glucose can directly oxidize ABTS in the presence of peroxidase, for example horseradish peroxidase or HRP (Yu et al., 2009). The solution color changed from colorless to green due to the oxidized ABTS and this can easily be measured using the spectrophotometer. The catalytic reaction of this ABTS assay is as follows:

$$\text{D-glucose} + H_2O + O_2 \xrightarrow{\text{GOx}} \text{Gluconic acid} + H_2O_2$$

$$H_2O_{2} + \text{reduced ABTS} \xrightarrow{\text{HRP}} H_2O + \text{oxidized ABTS}$$
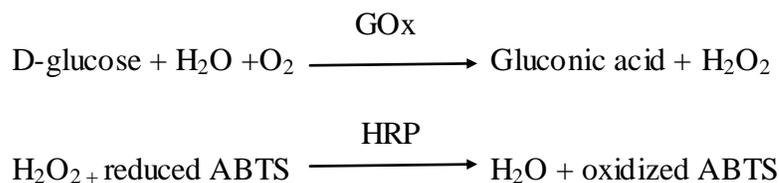
Based on this fact, the increase in absorbance correlates with the glucose concentration as shown in Figure 3.12 (a) inset with a linear range from 20 μM to 100 μM. These absorbance data indicate that GOx immobilized on Fe/Au retained its catalytic activity and suggesting the good stability of immobilized enzyme on the Fe/Au nanoparticles' surface. Furthermore, the increase of green color intensity with increasing amounts of glucose, shown in Figure 3.12 (b), shows a significant potential for application as a colorimetric sensing system.

(a)
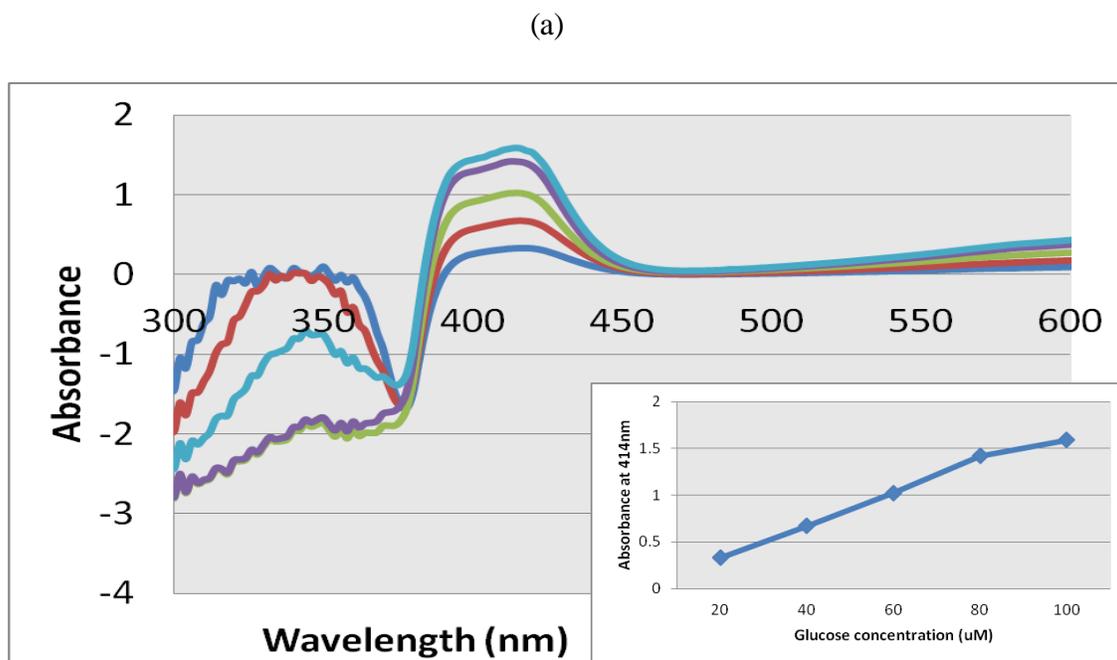
(b)
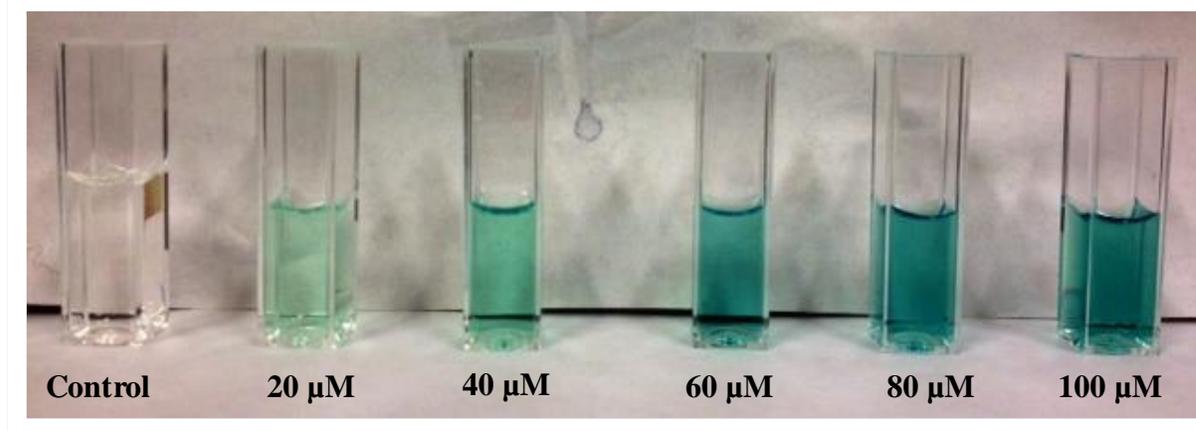
Figure 3.12 **(a) UV-Vis spectrophotometer analysis for detection of glucose using Fe/Au-GOx. Inset: A linear increase of absorbance at 414 nm as a function of glucose concentration (b) Image of solution color change with different concentrations of glucose (20 μM to 100 μM).**

3.5 Conclusions

In this study, we have demonstrated the feasibility of depositing AuNPs onto IONP surfaces by manipulation of the opposite interfacial charges exhibited between these two metallic nanoparticles and resulting in a strong interaction. The UV-Vis spectrophotometer absorbance for the formation of IONPs-AuNPs show a blue-shift in contrast with many reported studies due to the nanoparticles coalescence and recrystallization as the nanoparticles become more spherical with a low PDI, and shows a slight change in the nanoparticles' diameter. The XPS analysis also reveals the formation of maghemite (γ-Fe_2O_3) as the IONPs species. In addition, deposition of AuNPs onto γ-Fe_2O_3 formed alloy-like morphology instead of core-shell nanoparticles. This is supported by the HRTEM and XPS analysis, which also shows that there is a strong interaction between Au and Fe atoms at the interface. Moreover, results from zeta potential analysis also indicate that the heterogeneous nanoparticles increase in stability.

In conclusion, we can assume that the direct deposition technique used in this study formed metastable alloy-like morphology, Fe/Au, with lack of bimetallic nanoparticles synthesis controllability. However, it does not significantly affect the potential attachment of ligands (11-MUDA) and shows that Au still can be accessible for surface modification. Furthermore, Fe/Au nanoparticles also appear to be excellent candidates as a supporting material for biomolecules and this was further demonstrated by use in a potential nanosensor system based on glucose oxidase.

References

Alibeigi S, and Vaezi MR. (2008) Phase transformation of iron oxide nanoparticles by varying the molar ratio of Fe^{2+}: Fe^{3+} .*Chem Eng Technol* (31): 1591

Amendola V, Scaramuzza S, Agnoli S, Polizzib S, and Meneghetti M. (2014) Strong dependence of surface plasmon resonance and surface enhanced Raman scattering on the composition of Au–Fe nanoalloys. *Nanoscale* (6): 1423-1433

Annadhasan M, Kasthurib J, and Rajendiran N. (2015) Green synthesis of gold nanoparticles under sunlight irradiation and their colorimetric detection of Ni^{2+} and Co^{2+} ions. *RSC Adv* (5): 11458-11468

Arruebo M, Fernandez-Pacheco R, Ibarra MR, and Santamaria J. (2007) Magnetic nanoparticles for drug delivery. *Nano Today* (2): 22–32

Ban Z, Barnakov YA, Li F, Golub VO, and O'Connor CJ. (2005) The synthesis of core–shell iron@gold nanoparticles and their characterization. *J Mater Chem* (15): 4660–4662

Batlle X, and Labarta A. (2002) Finite -size effects in fine particles: magnetic and transport properties. *J Phys D: Appl Phys* (35)

Belotelov VI, Doskolovich LL, Zvezdin AK. (2007) Extraordinary Magneto-Optical Effects and Transmission through Metal-Dielectric Plasmonic Systems. *Phys ReV Lett* 98(077401)

Chang WS, Park JW, Rawat V, Sands TD, and Lee GU. (2006) Templated synthesis of gold-iron alloy nanoparticles using pulsed laser deposition. *Other Nanotech Publ* (35)

Dahal N, Chikan V, Jasinski J, and Leppert VJ. (2008) Synthesis of water-soluble iron gold alloy nanoparticles. *Chem Mater* 20(20): 6389–6395

Dahal N, Wright JT, Willey TM, Meulenberg RW, and Chikan V. (2010) Preparation of Iron and Gold Silicide Nanodomains on Silicon (111) by the Reaction of Gold, Iron-Gold Core-Shell, and Alloy Nanoparticles with Triethylsilane. *Appl Mat and Interf* 2(8): 2238–2247

Daniel MC, and Astruc D. (2004) Gold nanoparticles: assembly, supramolecular chemistry, quantumsize-related properties, and applications toward biology, catalysis, and nanotechnology. *Chem Rev* (104): 293–346

de Jesus CG, Lima D, dos Santos V, Wohnrath K, and Pessôa CA. (2013) Glucose biosensor based on the highly efficient immobilization of glucose oxidase on layer-by-layer films of silsesquioxane polyelectrolyte. *Sensors and Actu B* (186): 44– 51

Diwekar M, Kamaev V, Shi J, and Vardeny ZV. (2004) Optical and magneto-optical studies of two-dimensional metallodielectric photonic crystals on cobalt films. *App Phy Lett* 84(16): 3112

Fujii T, De Groot FMF, Sawatzky GA, Voogt FC, Hibma T, Okada K, and Fujii K. (1999) In situ XPS analysis of various iron oxide films grown by NO 2 -assisted molecular-beam epitaxy. *Phy Rev B* 59(4): 3195-3202

George C, Genovese A, Korobchevskaya K, Comin A, Falqui A, Marras S, Roig A, Zhang Y, Krahne R, and Manna L. (2011) Optical and electrical properties of colloidal (spherical Au)-(spinel ferrite nanorod) heterostructures. *Nanoscale* (3): 4647-4654

Grosvenor AP, Kobe BA, Biesinger MC, and McIntyre NS. (2004) Investigation of multiplet splitting of Fe 2p XPS spectra and bonding in iron compounds. *Surf Interface Anal* (36): 1564–1574

Gole A, Dash C, Ramakrishnan V, Sainkar SR, Mandle AB, Rao M, Sastry M. (2001a) Pepsin–gold colloidal conjugates: Preparation, characterization and enzymatic activity. *Langmuir* (17): 1674– 1679

Gole A, Dash C, Soman C, Sainkar SR, Rao M, Sastry M. (2001b) On the preparation, characterization, and enzymatic activity of the fungal protease– gold colloid bioconjugate. *Bioconj Chem* (12): 684– 690

Gole A, Vyas S, Phadtare S, Lachke A, Sastry M. (2002) Studies on the formation of bioconjugate of endoglucanase with colloidal gold. *Coll Surf B Biointerf* (25): 129–138

Güzel R, Üstündağ Z, Ekşi H, Keskin S, Taner B, Durgun ZG, Turan AA, Solak AO. (2010) Effect of Au and Au@Ag core-shell nanoparticles on the SERS of bridging organic molecules. *J of Coll and Inter Sci* (351): 35-42

Illés E, and Tombácz E. (2006) The effect of humic acid adsorption on pH-dependent surface charging and aggregation of magnetite nanoparticles. *J Coll and Inter Sci* 295(1): 115-123

Jain PK, Xiao Y, Walsworth R, and Cohen AE. (2009) Surface Plasmon Resonance Enhanced Magneto-Optics (SuPREMO): Faraday Rotation Enhancement in Gold-Coated Iron Oxide Nanocrystals. *Nano Lett* 9(4): 1644–1650

Kahl S, and Grishin AM. (2004) Enhanced Faraday rotation in all-garnet magneto-optical photonic crystal. *Appl Phy Lett* 84(9): 1438

Kang KA, Wang J, Jasinski JB, and Achilefu S. (2011) Fluorescence Manipulation by Gold Nanoparticles: From Complete Quenching to Extensive Enhancement. *J of Nanobiotech* 9(16): 1-13

Khanikaev AB, Baryshev AV, Fedyanin AA, Granovsky AB, Inoue M. (2007) Anomalous Faraday effect of a system with extraordinary optical transmittance. *Optics express* 15(11): 6612-22

Khoudiakov M., Gupa MC., and Deevi S. (2005) Au/Fe2O3 nanocatalysts for CO oxidation: A comparative study of deposition-precipitation and coprecipitation techniques. *Appl Catal A* 291: 151–161

Laurent S, Forge D, Port M, Roch A, Robic C, Vander Elst L, and Muller RN. (2008) Magnetic iron oxide nanoparticles: synthesis, stabilization, vectorization, physicochemical characterizations, and biological applications. *Chem Rev* (108): 2064–2110

Levin CS, Hofmann C, Ali TA, Kelly AT, Morosan E, Nordlander P, Whitmire KH, and Halas NJ. (2009) Magnetic−Plasmonic Core− Shell Nanoparticles. *ACS Nano* 3(6): 1379–1388

Lin F, and Doong R. (2011) Bifunctional Au−Fe_3O_4 Heterostructures for Magnetically Recyclable Catalysis of Nitrophenol Reduction. *J Phys Chem C* 115(14): 6591–6598

Liu X, Si W, Zhang J, Sun X, Deng J, Baunack S, Oswald S, Liu L, Yan C, and Schmidt OG. (2014) Free-standing Fe_2O_3 nanomembranes enabling ultra-long cycling life and high rate capability for Li-ion batteries. *Sci Rep* (4): 7452

Lu D, Domen K, and Tanaka K (2002) Electrodeposited Au−Fe, Au−Ni, and Au−Co Alloy Nanoparticles from Aqueous Electrolytes. *Langmuir* 18(8): 3226–3232

Lyon JL, Fleming DA, Stone MB, Schiffer P, and Williams ME. (2004) Synthesis of Fe Oxide Core/Au shell nanoparticles by iterative hydroxylamine seeding. *Nano Lett* 4(4): 719-723

Malvern Instruments Limited (2011) Dynamic Light Scattering Common Term Defined. *Inform White Paper*

Nurdin I, Johan MR, Yaacob II, and Ang BC. (2014) Effect of Nitric Acid Concentrations on Synthesis and Stability of Maghemite Nanoparticles Suspension. *The Sci World J* 589479: 1-6

Odio OF, Lartundo-Rojas L, Santiago-Jacinto P, R. Martínez R, and Reguera E. (2014) Sorption of Gold by Naked and Thiol-Capped Magnetite Nanoparticles: An XPS Approach. *J Phys Chem C* 118(5): 2776–2791

Pandey P, Singh SP, Arya SK, Gupta V, Datta M, Singh S, and Malhotra BD. (2003) Application of Thiolated Gold Nanoparticles for the Enhancement of Glucose Oxidase Activity. *Langmuir* (23): 3333-3337

Parkinson CR, Walker M, and McConville CF. (2003) Reaction of atomic oxygen with a Pt(111) surface: chemical and structural determination using XPS, CAICISS and LEED. *Surf Sci* (545): 19–33

Rawal R, Chawla S, and Pundir CS. (2012) An electrochemical sulfite biosensor based on gold coated magnetic nanoparticles modified gold electrode. *Biosens and Bioelectron* (31):144-150

Safarik I, and Safarikova M. (2009) Magnetic nano- and microparticles in biotechnology. *Chem Papers* (63):497–505

Saha DK, Koga K, and Takeo H. (1999) Stable icosahedral nanoparticles in an as-grown Au–Fe alloy. *The Eur Phy J D* 9(1): 539-542

Samphao A, Butmee P, Jitcharoen J, Švorc Ľ, Raber G, and Kalcher K. (2015) Flow-injection amperometric determination of glucose using a biosensor based on immobilization of glucose oxidase onto Au seeds decorated on core Fe_3O_4 nanoparticles. *Talanta* (142): 35-42

Sapsford KE, Algar WR, Berti L, Gemmill KB, Casey BJ, Oh E, Stewart MH, and Medintz IL. (2013) Functionalizing nanoparticles with biological molecules: Developing chemistries that facilitate nanotechnology. *Chem Rev* 113(3): 1904–2074

Sohn Y, Pradhan D, Kang JS, and Leung KT. (2015) Nanoscale architecture of bimetallic hybrid Fe–Au nanostructures with and without 1,4-phenylene diisocyanide pre-functionalization. *Royal Soc of Chem Adv* 5: 31472–31478

Tombácz E. (2009) pH-dependent surface charging of metal oxides. *Periodica Polytec-Chem Eng* 53(2): 77-86

Wang L, Luo J, Fan Q, Zhong CJ, Suzuki M, Suzuki IS, Kim N, Wang JQ, Engelhard MH, and Lin Y. (2005) Monodispersed Core−Shell Fe_3O_4@Au Nanoparticles. *J Phys Chem B* 109(46): 21593–21601

Weidenthaler C. (2011) Pitfalls in the characterization of nanoporous and nanosized materials. *Nanoscale* (3): 792–810

Xie J, Zhang F, Aronova M, Lin X, Quan Q, Liu G, Zhang G, Choi KY, Kim K, Sun X, Lee S, Sun S, Leapman R, and Chen X. (2011) Manipulating the power of an additional phase: A flower-like Au-Fe$_3$O$_4$ optical nanosensor for imaging protease expressions *in vivo*. *ACS Nano* (5): 3043- 3051

Yan Q, Zheng HN, Jiang C, Li K, and Xiao SJ. (2015) EDC/NHS activation mechanism of polymethacrylic acid: anhydride versus NHS-ester. *RSC Adv* (5): 69939–69947

Yu F, Huang Y, Cole AJ, and Yang VC. (2009) The artificial peroxidase activity of magnetic iron oxide nanoparticles and its application to glucose detection. *Biomater* 30(27): 4716

Chapter 4

Manipulation of Fe/Au peroxidase-like activity for development of a nanocatalytic-based assay

4.1 Summary

Purpose: The aim of this study is to investigate the synthesized Fe/Au nanoparticles's peroxidase-like activity and further evaluate them for development of a nanocatalytic-based assay particularly designed to detect 17β-estradiol.

Methods: The peroxidase-like activity of the synthesized Fe/Au nanoparticles was optimized using the H_2O_2-ABTS system and was analyzed using Michaelis-Menten kinetics. Initially, the nanoparticles surface was functionalized with aptamers in order to confer a specific conjugation with the target analyte, 17β-estradiol. Development of a nanocatalytic-based assay is based on two fundamental steps, which are the immobilization process and the catalytic reaction process. For the immobilization process, the analytes were conjugated at the aptamer-tagged nanoparticles and formed nanoparticles-analytes complexes (Fe/Au-17β-estradiol). Then the catalytic reaction of this complex was measured using the H_2O_2-ABTS colorimetric system. The feasibility of this assay was tested at different concentration of aptamer-tagged Fe/Au nanoparticles and 17β-estradiol. Also, a cross-reactivity study was conducted with potentially interfering materials for assessment of assay selectivity.

Results: Fe/Au nanoparticles showed a good peroxidase-like activity that followed Michaelis-Menten kinetics. Results obtained from absorbance data reveal that the Fe/Au-17β-estradiol complex significantly hampered the catalytic activity. The absorbance intensity declined drastically after aptamer-tagged nanoparticles (Fe/Au-fl-apt) "captured" the targets and formed nanoparticles-analytes complexes. Serial dilution of 17β-estradiol was tested using this assay and showed that the absorbance intensity was inversely proportional to the 17β-estradiol concentrations. It is suggested that steric effects are a plausible reason for this phenomenon. In addition, this assay shows considerably high accuracy and reproducibility for detection of 17β-estradiol concentration ranging from 0.01 nM to 1 nM when low concentration of aptamer-tagged nanoparticles is used. Furthermore, the aptamers used in this study are selective towards the target analyte, 17β-estradiol.

Conclusions: A simple, rapid and sensitive detection assay, specifically to detect 17β-estradiol was developed using a new detection strategy by manipulation of nanoparticles' peroxidase-like activity.

4.2 Introduction

Recently, nanoparticles that exhibit a peroxidase-like activity have attracted considerable attention since it shows a fascinating research discovery and potential for multiple applications. Many nanoparticles have been reported to show enzyme mimetic activity such as magnetite (Liang et al., 2013; Gao et al., 2007), Au nanoparticles (Jv et al., 2010), CuO (Chen et al., 2012), Fe_3O_4-Au (Sun et al., 2013) and Ag_3PO_4 (Liu et al., 2014a). This enzyme-like nanoparticles display a beneficial property as they could potentially replace peroxidase in various applications, including hydrogen peroxide dependent systems.

Besides the growing interest in nanoparticles' catalytic property, nanoparticles have long been known for their excellent ability to conjugate with biomolecules such as enzymes, DNAzymes, antibodies and aptamers. These biomolecules can be immobilized on the modified nanoparticle surfaces by direct conjugation to the surface of some nanoparticles and to surface-bound stabilizing ligands or coatings, either directly or using small cross-linking molecules and other intermediaries (Sapsford et al., 2013). Aptamers are short synthetic oligonucleotides that could be synthesized for any targets and show many advantages as discussed in Section 2.4.2.3. Therefore, in this study, the nanoparticles were conjugated with aptamers in order to confer a specific detection with the target analytes.

Analytical assays that utilize a hydrogen peroxide dependent system by catalyzing the oxidation of certain substrates have been extensively used for numerous applications. This analytical assay has become a powerful detection tool especially in immunoassay studies. Recently, replacement of horseradish peroxidase with nanoparticles as a peroxidase mimetic

has demonstrated improvement in biosensors. Zhang's group presented work with γ-Fe$_2$O$_3$ nanoparticles modified by Prussian blue (PBMNPs) that were further conjugated with staphylococcal protein A (SPA) and showed a potential application in bio-detection. Here, the PBMNPs served as an inexpensive horseradish peroxidase, HRP (Zhang et al., 2010). A recent study conducted by Liu et al., (2014b) reported an efficient colorimetric biosensor for glucose based on a peroxidase-like protein-Fe$_3$O$_4$ complex. The incorporation of casein on magnetic nanoparticles helped to improve the affinity towards both H$_2$O$_2$ and 3,3',5,5'-tetramethylbenzidine (TMB) thus resulting in a simple, inexpensive, highly sensitive and selective method for glucose detection. The peroxidase substrate, TMB commonly used for hydrogen peroxide dependent system. The observed oxidation product produced two colored products which is blue-charged-transfer complex of diamine and yellow diimine (Liu et al., 2014b).

While prior work has demonstrated the capability of nanoparticles to conjugate with the target analytes and has utilized nanoparticles' peroxidase-like activity for an analytical assay, we observed that a similar strategy could be adapted for development of a nanocatalytic-based assay. It has been reported that peroxidase-like activity of iron oxide nanoparticles is dependent on the surface attributes of the nanoparticles (Yu et al., 2009). Therefore, in this study we report on a detection strategy formulated by the nanoparticles capability to conjugate with analytes and then the surface modified-nanoparticles or nanoparticles-analytes catalytic activity was evaluated using a hydrogen peroxide dependent system. We envisaged that the conjugation of target analytes to the Fe/Au nanoparticles would hinder the peroxidase activity resulting in an assay

response that was inversely proportional to the analyte concentration. This is based on the fact that the formation of this complex would create a gap with substrate molecules and lower the nanoparticles catalytic activity by reducing the affinity of nanoparticles for substrate molecules.

To evaluate the feasibility of this assay, the synthesized nanoalloy, Fe/Au nanoparticles was initially assessed for its peroxidase-like activity using the hydrogen peroxide dependent system, H_2O_2-ABTS. A specifically modified aptamer was attached to the Fe/Au nanoparticles to confer specific conjugation abilities with the target analyte. For this study, 17β-estradiol is selected as our target analyte. It is known as an endocrine disrupting chemical (EDCs) that has the greatest estrogenic activity (Liu et al., 2014c). When 17β-estradiol was successfully "captured" by aptamer-tagged nanoparticles and formed Fe/Au-17β-estradiol complex, the catalytic activity of this complex was measured using the hydrogen peroxide dependent system.

This is the first work reported, to our knowledge, to use this approach for development of detection assay. Hence, it is hoped that this study would initiate a comprehensive research exploration of nanoparticles' peroxidase-like activity in nanosensor systems and further develop a simple, reliable and sensitive detection assay.

4.3 Materials and methods

4.3.1   Chemicals

Chemical reagents used in this experiment were 2,2'-azino-bis(3-ethylbenzthiazoline-6-sulfonic acid) diammonium salt (ABTS, 10 mg/tablet), 30% H_2O_2, PBS buffer (tablet), Tween 20 (viscous liquid), sodium acetate anhydrous (NaAc), MES buffer ($\geq$ 99.5%), 17β-estradiol (98%), estriol ($\geq$ 97%), nonylphenol (99.8%) and carbaryl (99.8%). These chemical reagents were purchased from Sigma Aldrich. Thiolated aptamer (SH-apt) was adapted from Wang et al., 2009 with slight modification and was synthesized at Alpha DNA (Montreal, Quebec) and the probe aptamer (fl-apt) was adapted from Kim et al., (2007) with slight modification and was synthesized from Eurofins MWG Operon LLC (Hunstville, AL). All reagents were analytical grade and were used as received without further purification.

4.3.2   Preparation of Fe/Au nanoparticles

AuNPs were coated on the γ-Fe_2O_3 surface using a simple deposition technique as presented previously in Chapter 3.2.4.

4.3.3   Measurement of Fe/Au peroxidase-like activity

To investigate the Fe/Au nanoparticles peroxidase-like activity, a hydrogen peroxide dependent system was used. The chromogenic substrate, $ABTS_{(red)}$ was oxidized in the presence of Fe/Au nanoparticles and H_2O_2. The prepared Fe/Au nanoparticles weighed to approximately 50 mg and were added into 1 mL PBS buffer (10 mM, pH 4). Then, the Fe/Au nanoparticles catalytic reaction was observed in different pH buffer (10 mM NaAc at pH 2, 3, 4, 5 and 6) and in different concentration of Fe/Au nanoparticles (0.5 mg/mL, 1.25 mg/mL, 2.5 mg/mL and 12.5

103

mg/mL). The extent of reaction was indicated by a green colour development and was measured by absorbance at 414 nm based on the presence of the oxidized ABTS (ABTS$_{ox}$) in the solution, using microplate reader (Multiskan Ascent, Labsystems). The catalytic reaction by Fe/Au is as follows:

$$H_2O_2 \; + \quad \text{[ABTS]} \quad \xrightarrow{\text{Fe/Au}} \quad H_2O + \quad \text{[ABTS}^{\cdot+}\text{]}$$
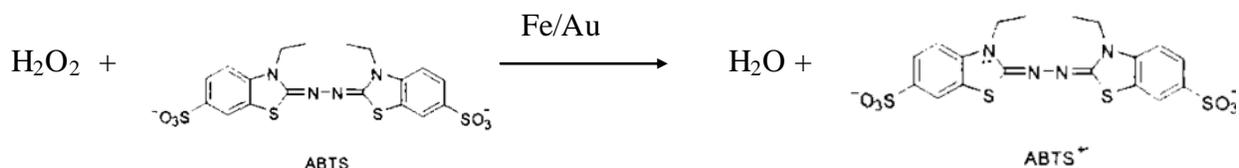
4.3.3.1 Steady-state kinetic analysis

The kinetic analysis of Fe/Au and γ-Fe$_2$O$_3$ nanoparticles with ABTS as the substrate was performed by adding 10 µL of nanoparticles aliquot, 10 µL of H$_2$O$_2$ (100 mM) and different concentrations (0.9 mM, 1.8 mM, 3.6 mM and 4.5 mM) of ABTS reagent. For kinetic analysis with H$_2$O$_2$ as the substrate, 10 µL of nanoparticles aliquot, 30 µL of ABTS (18.2 mM) and different concentrations (0.5 mM, 1.5 mM, 2.5 mM and 5.0 mM) of H$_2$O$_2$ were used. Both kinetic analyse were performed in 165 µL reaction buffer (10 mM NaAc, pH= 5). The green color developed as the reactions proceeded was monitored kinetically in a 96-well microplate at room temperature for 300 sec with 60 sec of time interval. The Michaelis-Menten constant was calculated based on a Hanes-Woolf plot:

$$\frac{[S]}{v} = \frac{[S]}{V_{\max}} + \frac{K_m}{V_{\max}}$$

where v is the initial velocity, V_{max} is the maximal reaction velocity, [S] is the concentration of substrate and K_m is Michaelis constant for the particular enzyme being investigated.

4.3.4   Development of nanocatalytic-based assay

In order to develop a nanocatalytic-based assay that can specifically detect 17β-estradiol, the Fe/Au nanoparticles' surface was functionalized with aptamers. Then, Fe/Au-17β-estradiol formation was evaluated using the peroxidase dependent system.

4.3.4.1 Surface functionalization with aptamer

Fe/Au nanoparticles were weighed to approximately 50 mg and were added to 1 mL MES buffer (10 mM, pH 4). Subsequently, 5 μM of the thiolated aptamer (SH-apt) was added to the solution and this was incubated by mixing at room temperature for 1 hr. To remove the unbound SH-apt, the solution was centrifuged for 5 min and was washed twice with PBS-T, pH 4 and was further separated using a permanent magnet. 1 mL MES buffer, pH 7 was added to the Fe/Au-SH-apt nanoparticles. The next step of this strategy was to attach the probe aptamer (fl-apt) to the Fe/Au-SH-apt nanoparticles, where 5 uM of fl-apt was added to the solution. The interaction was allowed at room temperature for 1hour. To remove the unbound fl-apt, the solution was centrifuged for 10min and was washed twice with PBS-T, pH 4 and was separated using permanent magnet.   Finally, 1 mL PBS buffer, pH 4 was added to the aptamer-tagged nanoparticles (Fe/Au-fl apt) and stored at 4°C until use. The presence of bound aptamers on the nanoparticles surface was evaluated using a UV-VIS spectrophotometer (Diode Array spectrophotometer, HP) based on the presence of fluorescent molecules, cyanine dye (Cy5.5). The two types of aptamers, that is SH-apt and fl-apt, used in this study are presented in Table 4.1.

Table 4.1   **The synthesized sequences for thiolated-aptamer (SH-apt) and probe aptamer (fl-apt) for functionalization and conjugation purpose.**

Aptamer	Sequences (3'-5')
SH-apt	SH-C6-<u>TCTCTTGGACCC</u>
fl-apt	<u>AGAGAACCTGGG</u>-GCT-TCC-AGC-TTA-TTG-AAT-TAC-ACG-CAG-AGG-GTA-GCG-GCT-CTG-CGCATT-CAA-TTG-CTG-CGC-GCT-GAA-GCG-CGG-AAG-C- (Cy5.5)

4.3.4.2 Assessment of nanocatalytic-based assay

The basic principle of the nanocatalytic-based assay is based on the evaluation of the complexed nanoparticles-analytes catalytic activity. Therefore, 10 μL of the prepared Fe/Au-fl-apt nanoparticles (approximately 50 mg) was incubated with 100 μL of 17β-estradiol (100 nM) and 890 μL PBS buffer (10 mM, pH 4) at room temperature for 1 hr to allow Fe/Au-17β-estradiol complex formation. To remove the unbound 17β-estradiol, the solution was centrifuged for 10 min and was washed twice with PBS-T, pH 4, and was further separated using a permanent magnet. Then, the nanoparticles-analytes catalytic activity was measured by adding 50 μL of Fe/Au-17β-estradiol aliquot, 10 μL of H_2O_2 (100 mM), 30μL of ABTS reagent (18.2 mM), and 110 μL reaction buffer (10 mM NaAc, pH 5) in 96-wells microplate. The absorbance signal at 414 nm was measured using the microplate reader after 5 min of interaction. High absorbance intensity (or green colour development) indicated that a strong catalytic activity was present.

Further assessment was done by testing a serial dilution of 17β-estradiol (0.01 nM, 0.1 nM, 1.0 nM and 10 nM) at different Fe/Au-fl-apt nanoparticles concentrations (33 mg/mL, 17 mg/L and 2.5 mg/mL) in PBS buffer (10 mM, pH 4) with total volume of 1 mL. To remove the unbound 17β-estradiol, the solution was centrifuged for 10 min and was washed twice with PBS-T, pH 4, and was further separated using a permanent magnet. Then, the nanoparticles-analytes catalytic activity was measured as discuss previously.

In this study, the experimental assay was measured in triplicate (n = 3) for inter- assay and two assays run (n = 2) for determination of intra-assay variability. The coefficient of variation (CV) for inter- and intra assay was determined by the following formulae:

Inter-assay CV (%) = Standard deviation of mean x 100/ Mean

Intra-assay CV (%) = Mean of standard deviation x100/ Mean

To assess the selectivity of this assay, a cross-reactivity study was conducted with potentially interfering materials such as estriol, nonylphenol (4NNP) and carbaryl and was evaluated at 100 nM concentrations for each EDCs.

To further test this assay in real water sample, different concentration of 17β-estradiol were detected in tap water samples using Fe/Au-fl-apt nanoparticles. This test was conducted by adding different concentration of 17β-estradiol (0.1 nM, 1 nM and 10 nM) into filtered tap water (F) and non-filtered tap water (NF). Then, 10 μL prepared Fe/Au-fl-apt nanoparticles (approximately 50 mg) was added into the contaminant aqueous solution (17β-estradiol in both tap water) with total solution volume is 1 mL. The detection was conducted at room temperature for 1 hr. To remove the unbound 17β-estradiol, the solution was centrifuged for 10 min and was

washed twice with PBS-T, pH 4, and was further separated using a permanent magnet. Then, the nanoparticles-analytes catalytic activity was measured as discussed previously and detection efficiency was calculated as follows:

$$Detection\ efficiency:\ (A_0 - A)/A_0$$

whereas A_0 and A are absorbance intensity at 414 nm before and after various concentration of 17β-estradiol are added in tap water samples.

4.4 Results and discussion

4.4.1 Analysis of Fe/Au peroxidase like activity

As presented in Chapter 3, Fe/Au nanoparticles are prepared by a strong electrostatic interaction between γ-Fe_2O_3 and AuNPs that subsequently formed a metastable heterogeneous structure. Due to the fact that both nanoparticles (γ-Fe_2O_3 and AuNPs) exhibit a good peroxidase-like activity, it is of interest to investigate the catalytic activity of the synthesized Fe/Au nanoparticles. The catalysis performance of the synthesized nanoparticles was examined using ABTS, which is a chromogenic substrate. ABTS has been proven to be a non-carcinogenic derivative and is oxidized in the presence of peroxidase and H_2O_2 to a green reaction product with maximum absorbance at approximately 414 nm. Figure 4.1 (a) shows the UV-VIS absorption spectra of the Fe/Au catalytic reaction systems upon 5 min of reaction and a single peak is observed around 414 nm, indicating that ABTS was successfully oxidized. We can also notice that ABTS is able to react with H_2O_2 alone due to the oxidative environment. Therefore, to identify the amount of absorption that is contributed by the Fe/Au catalytic reaction, the obtained absorbance needed to be subtracted from the control absorbance. The absorbance measurement at 414 nm at different time was observed as shown in Figure 4.1 (b) with high absorbance observed at 5 min of reaction and confirming that Fe/Au behaves as a catalyst.

Since Fe/Au exhibits intrinsic peroxidase-like activity, the effect of pH buffer on the catalytic properties was investigated. The catalytic experiment was observed in NaAc buffer with different pH values. In Figure 4.2 (a), the optimum pH value was found at pH 5 was selected for subsequent study. A study by Liu et al. (2014) suggested that the catalytic activity of the

109

modified magnetite particles (casein-MNPs) is faster in acidic solution than that in neutral or basic solutions and shows a similarity to many other peroxidase-like nanomaterials. They also ruled out the possibility that the observed activity is caused by leaching of iron ions into an acidic solution.

In addition, the effect of Fe/Au nanoparticle concentration on the catalytic activity was also investigated as the results show in Figure 4.2 (b). There was a linear absorbance increase with a correlation coefficient of 0.995 as a function of Fe/Au concentration. This finding strongly suggests that due to the high Fe/Au atoms presence in the solution and the nanoparticles' surface area increase, which is known as the source of catalytic activity or active site, the peroxidase-like activity would significantly increase. However, we also observed that increase of nanoparticles concentration also contribute to nanoparticles aggregation represent by high standard deviation (S.D) for 12.5mg/mL. We can speculate that due to the increase of nanoparticles-substrate interaction that lead to surface modification, the nanoparticle tends to aggregate since Fe/Au shows metastable structure.
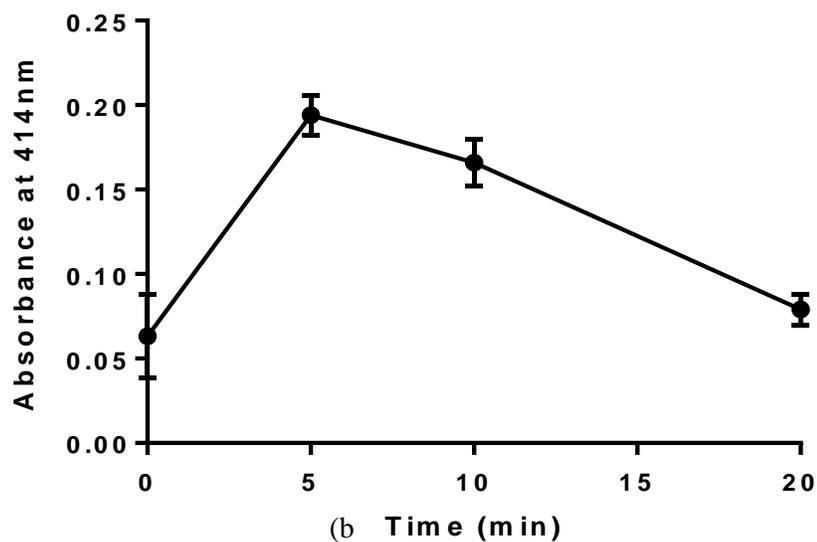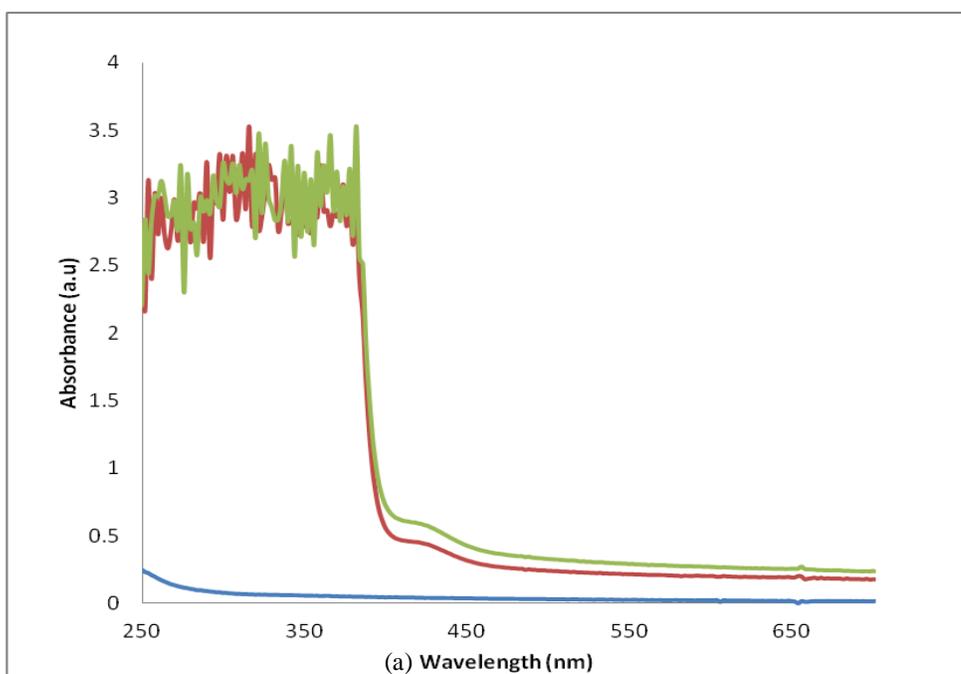
Figure 4.1 (a) UV-Vis spectrophotometer measurement of H_2O_2 (blue), ABTS + H_2O_2 (red) and ABTS + H_2O_2 + Fe/Au nanoparticles (green) (b) Absorbance measurement at 414 nm at different times for Fe/Au nanoparticle catalytic reaction. (Error bars represent S.D of the absorbance mean)
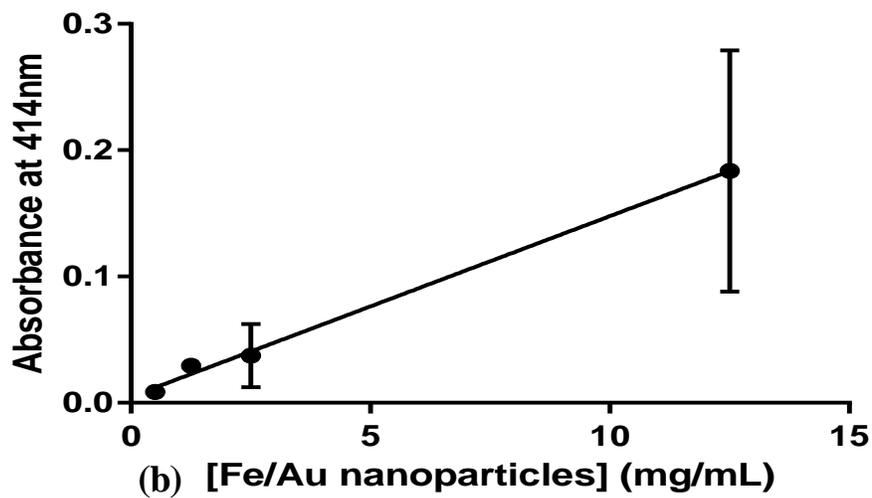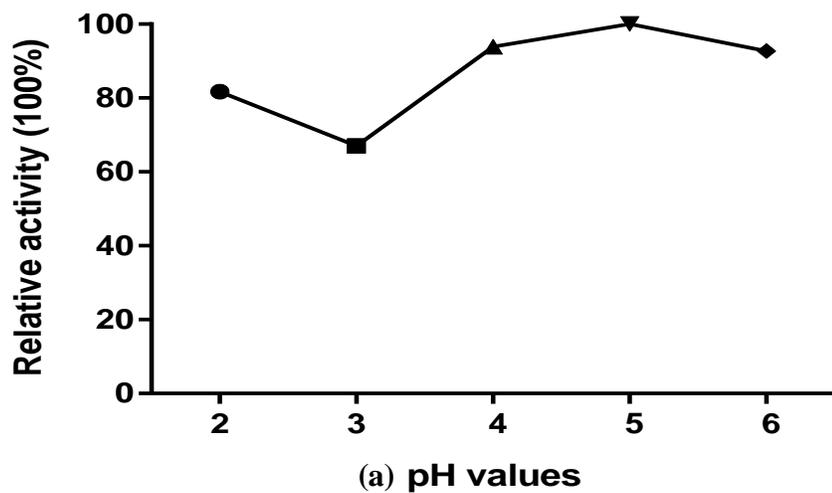
Figure 4.2   (a) **Effect of different pH value on Fe/Au peroxidase-like activity (b) Effect of different concentration of Fe/Au on peroxidase-like activity. (Error bars represent S.D of the absorbance mean)**

4.4.1.1 Steady-state kinetic analysis

To further investigate the peroxidase-like activity of Fe/Au nanoparticles, the steady-state kinetics were determined. The steady-state reaction rates at different concentrations of substrate and co-substrate (ABTS and H_2O_2) were obtained by calculating the slopes of initial absorbance changes with time. The reaction was determined in 10 mM NaAc buffer, pH 5 at room temperature for 300 sec. Absorbance data were back-calculated to concentration by the Beer–Lambert Law using a molar absorption coefficient of 36, 000 $M^{-1}cm^{-1}$ (Liu and Yu, 2011) for ABTS-derived oxidation products at 414 nm. As a comparison, the steady state kinetics for γ-Fe_2O_3 nanoparticles were also examined to investigate the surface modification impact on catalytic activity.

The curves shown in Figure 4.3 (a) and Figure 4.4 (a) indicate that the reaction catalyzed by Fe/Au and γ-Fe_2O_3 nanoparticles displayed Michaelis–Menten kinetics. The Michaelis constant (K_m) and maximal reaction velocity (V_{max}) were obtained from the slope and intercept of the extrapolated straight line with the horizontal axis in the Hanes-Woolf plot as shown in Figure 4.3 (b) and Figure 4.4 (b). The K_m value is an indicator of enzyme affinity for its substrate (Yu et al., 2009). A high K_m value represents a weak affinity whereas a low K_m value suggests high affinity (Liu et al, 2014d). As presented in Table 4.2, the K_m value of Fe/Au with H_2O_2 as the substrate was significantly lower than γ-Fe_2O_3. Thus, this finding shows that Fe/Au nanoparticles have a strong affinity towards H_2O_2. The corresponding K_m values of the Fe/Au nanoparticles also indicate that the catalytic reaction can reach the maximum rate at a lower concentration of H_2O_2. According to Voinov et al. (2011), Fe_3O_4 nanoparticles were significantly

more effective in producing hydroxyl radicals ($\cdot$OH) than the γ-Fe_2O_3 nanoparticles at the same ratio of the nanoparticle total surface and reaction volume. Since γ-Fe_2O_3 nanoparticles contain only ferric ions (Fe^{3+}) that occupy both octahedral and tetrahedral sites (Fujii et al., 1999), the peroxidase-like activity mostly originates from ferric ions which have a low rate constant and is thus a rate-limited reaction process (Zhang et al., 2010).

As confirmed by EDX and XPS data analysis shown in Chapter 3, the prepared Fe/Au nanoparticles contain both Fe and Au elements. Considering the limitation of Fe^{3+} ions from γ-Fe_2O_3, Au deposition on the nanoparticles surface helped to enhance Fe/Au affinity towards H_2O_2. He et al. (2010) reported that formation of bimetallic nanoparticles successfully improved the nanoparticles' catalytic performance. Another study conducted by Sun et al. (2013) demonstrated that Fe_3O_4-Au nanocomposites exhibited better catalytic activity than pure Fe_3O_4 resulting from the specific electronic structure at the nanoparticles interfaces. They proposed that the AuNPs changed the electron structure at the interface, which may accelerate the electron transfer. Moreover, the partial electron transfer from Fe_3O_4 to Au facilitates H_2O_2 adsorption and activation. Hence, it is most likely the synthesized γ-Fe_2O_3 catalytic activity in this study was enhanced upon surface modification with AuNPs as proven by the strong affinity of Fe/Au nanoparticles towards H_2O_2.

Conversely, the K_m value for Fe/Au nanoparticles with ABTS as the substrate was slightly higher than γ-Fe_2O_3 (Table 4.2), suggesting that the Fe/Au nanoparticles had a slightly lower affinity for ABTS. The plausible reason for this phenomenon is due to the difference in charges present on the Fe/Au and γ-Fe_2O_3 nanoparticles' surface. Results obtained from zeta

potential measurements in Chapter 3 showed that the γ-Fe$_2$O$_3$ nanoparticles have a positive surface charge (+17.80 mV) while Fe/Au nanoparticles have a negative surface charge (-24.70 mV) in an acidic environment. It is known that ABTS contains two negatively charged sulfonic groups, thus, exhibiting higher affinity toward a positively charged nanoparticles surface (Yu et al., 2009). Due to this reason, γ-Fe$_2$O$_3$ nanoparticles with a positive surface charge would show a stronger affinity towards ABTS through electrostatic interactions between the particle and substrate molecules. On the other hand, the Fe/Au nanoparticles would show an electrostatic repulsion with ABTS. However, the effect of charge difference was relatively small because of the slight difference in K$_m$ values, and suggested that the surface modification by Au deposition help to enhance the interaction between nanoparticles and ABTS. As an alternative, a positively charged chromogenic substrates such as 3,3',5,5'- tetramethylbenzidine (TMB) can be used. TMB is a polyamino compound and becomes protonated in acidic solution, so it has a stronger affinity towards negatively charge nanoparticles (Sun et al., 2013).

Based on the aforementioned findings, the intrinsic peroxidase-like activity of Fe/Au nanoparticles is largely influenced by surface modification. From this information, we could utilized the nanoparticles surface modification flexibility and manipulate the catalytic property to develop an analytical assay. Development of the detection assay is further discussed in the next subsection.
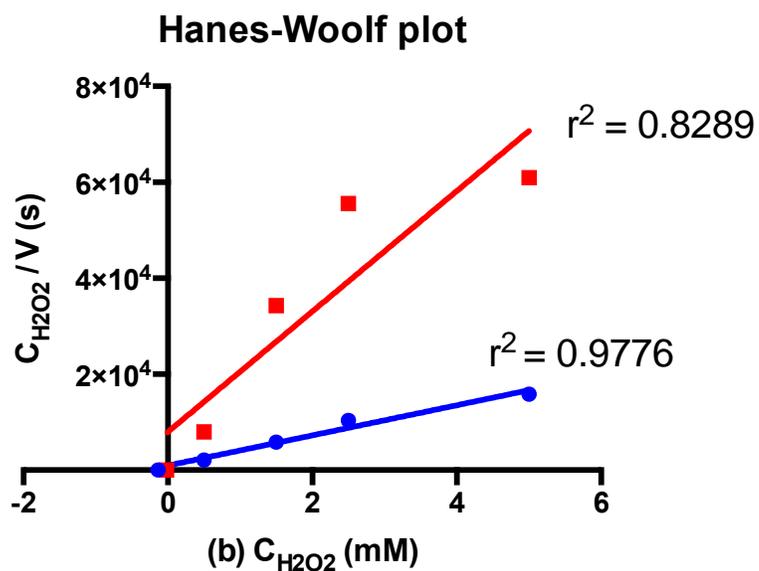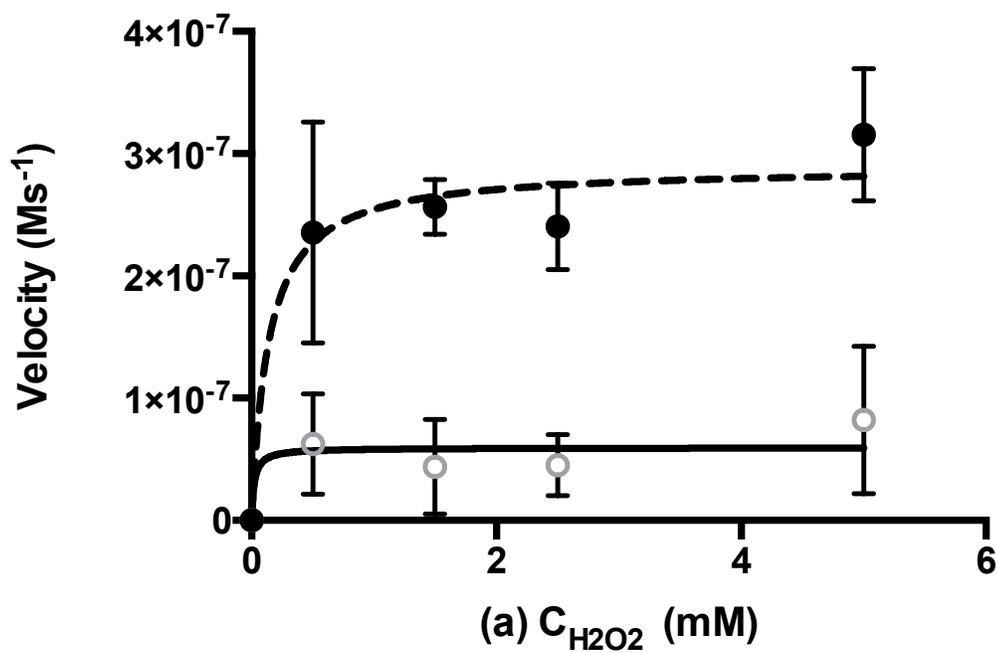
Figure 4.3 (a) Steady-state kinetics of γ-Fe$_2$O$_3$ (dashed line) and Fe-Au nanoparticles (black line) with ABTS concentration at 1.8 mM and varied H$_2$O$_2$ concentration. (b) Hanes-Woolf plot of γ-Fe$_2$O$_3$ (blue) and Fe/Au nanoparticles (red). (Error bars represent S.D of the velocity mean)

(a) C_{ABTS} (mM)

Hanes-Woolf plot

$r^2 = 0.9725$

$r^2 = 0.9724$

(b) C_{ABTS} (mM)
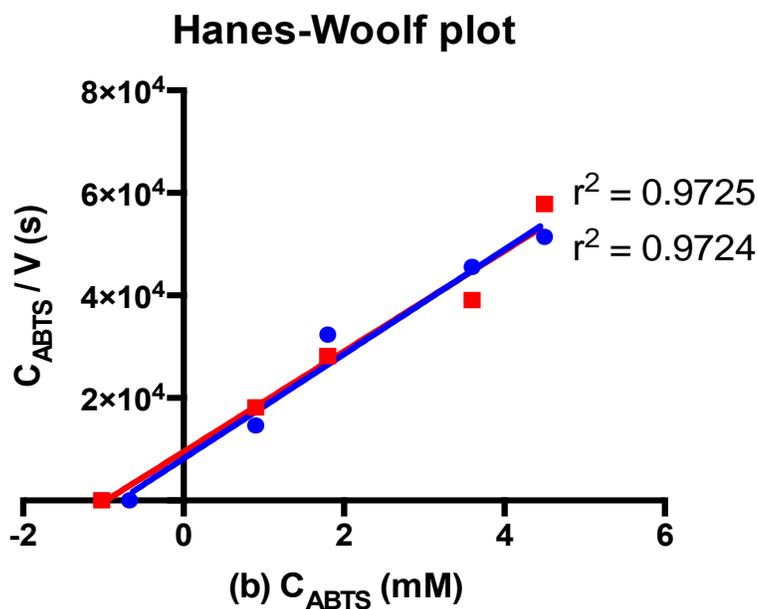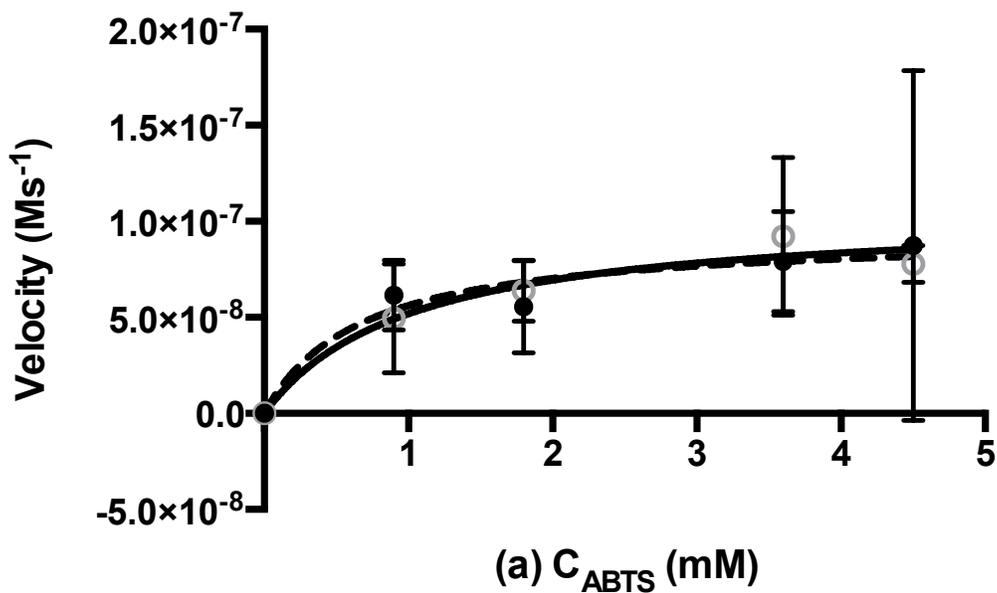
Figure 4.4 (a) Steady-state kinetics of γ-Fe$_2$O$_3$ (dashed line) and Fe-Au nanoparticles (black line) with H$_2$O$_2$ concentration at 5mM and varied ABTS concentration. (b) Hanes-Woolf plot of γ-Fe$_2$O$_3$ (blue) and Fe/Au nanoparticles (red). (Error bars represent S.D of the velocity mean)

Table 4.2   Comparison of the kinetic parameters of γ-Fe$_2$O$_3$ and Fe/Au nanoparticles.

Nanoparticles	Substrate	K_m (mM)	V_{max} (Ms^{-1})
γ-Fe$_2$O$_3$	H$_2$O$_2$	0.137	2.892×10^{-7}
	ABTS	0.674	9.400×10^{-8}
Fe/Au	H$_2$O$_2$	0.021	5.935×10^{-8}
	ABTS	1.019	9.226×10^{-8}

4.4.2 Development of nanocatalytic-based assay

In this subsection, development of a nanocatalytic-based assay is explored, particularly to detect 17β-estradiol in aqueous solution. It involves surface functionalization with an aptamer and surface modification with analytes by formation of a nanoparticles-analytes complex. The practicality of this assay was evaluated at different concentration of aptamer-tagged Fe/Au nanoparticles and 17β-estradiol. Then this assay was further tested for cross-reactivity analysis with related compounds and detection in tap water samples.

4.4.2.1 Analysis of aptamer-mediated conjugation

To introduce a probe aptamer that specifically binds to 17β-estradiol, the Fe/Au nanoparticle surface was initially modified with a thiolated aptamer (SH-apt). The probe aptamer that contained a fluorescent dye-labeled 17β-estradiol (fl-apt) was easily attached at the SH-apt complementary site as show by the underlined sequences in Table 4.1. This complementary site would help fl-apt to self-construct with thiolated-tagged nanoparticles by interaction between the nucleobases (A = T, G = C). After nanoparticles were successfully functionalized with the probe aptamer, Fe/Au-fl-apt would be able to "capture" the 17β-estradiol molecules in solution by conjugation at site-specific sequence, and subsequently form Fe/Au-17β-estradiol complexes. A schematic diagram of the surface functionalization with aptamers and formation of Fe/Au-17β-estradiol complex is shown in Figure 4.5.

To test the conjugation feasibility, two types of aptamer were introduced since each aptamer was tagged with unique labels; a thiol group for SH-apt and fluorescent dye; cyanine (Cy5.5) for fl-apt. The SH-apt would covalently attach to the Fe/Au nanoparticles based on the

Au-SH chemisorption interaction where the sulfur atom of a thiol contributes a lone pair of electrons to the empty orbitals of Au atoms at an interface (Sapsford et al., 2013). Detailed discussion on the charge transfer of the Au and -SH at the Fe/Au nanoparticles interface can be found in Chapter 3 (3.3.3). Another advantage of introducing a thiolated-aptamer is to avoid aptamer desorption from the nanoparticle's surface and loss the nanoparticle functionality. It had been reported that in the presence of targets, the aptamers become folded by binding to the targets and being desorbed from the surface of AuNPs (Liu et al., 2014c). Because of the strong interaction (covalent bond) between aptamer and nanoparticles (thiol-gold chemistry), the thiolated-aptamer will tightly bind at the surface, even though in the presence of targets. Thiol-gold bonds show high stability as reported by Krüger et al. (2001). They suggested that pulling a thiol attached to the Au surface could lead to Au-Au bond breakage. On the other hand, the attachment of the fl-apt would facilitate the conjugation process between nanoparticles and 17β-estradiol molecules due to the presence of 17β-estradiol site-specific sequence.

The attachment of the fl-apt to thiolated-tagged nanoparticles can be determined using cyanine dye, Cy5.5. This dye excites at 675 nm and emits at 695nm (Umezawa et al., 2009). The fluorescence emission intensity at 695nm was measured from the visible light absorption spectrum. Based on the results show in Figure 4.6, a low intensity was observed for Fe/Au-fl-apt at around 695nm as compared to the sample control (probe aptamer only). Still, we could observe a broad band ranging from 600 nm to 700 nm suggesting that the fl-apt was successfully attached to the thiolated-tagged nanoparticles and no obvious peak was observed for Fe/Au nanoparticles. The possible reason for its low absorbance intensity might be due to the quenching effect of

Fe/Au nanoparticles, as both Fe and Au nanoparticles can be efficient fluorescence quenchers as demonstrated by many analytical analysis studies (Raikar et al., 2011; Kang et al., 2011; Schneider and Decher, 2006).
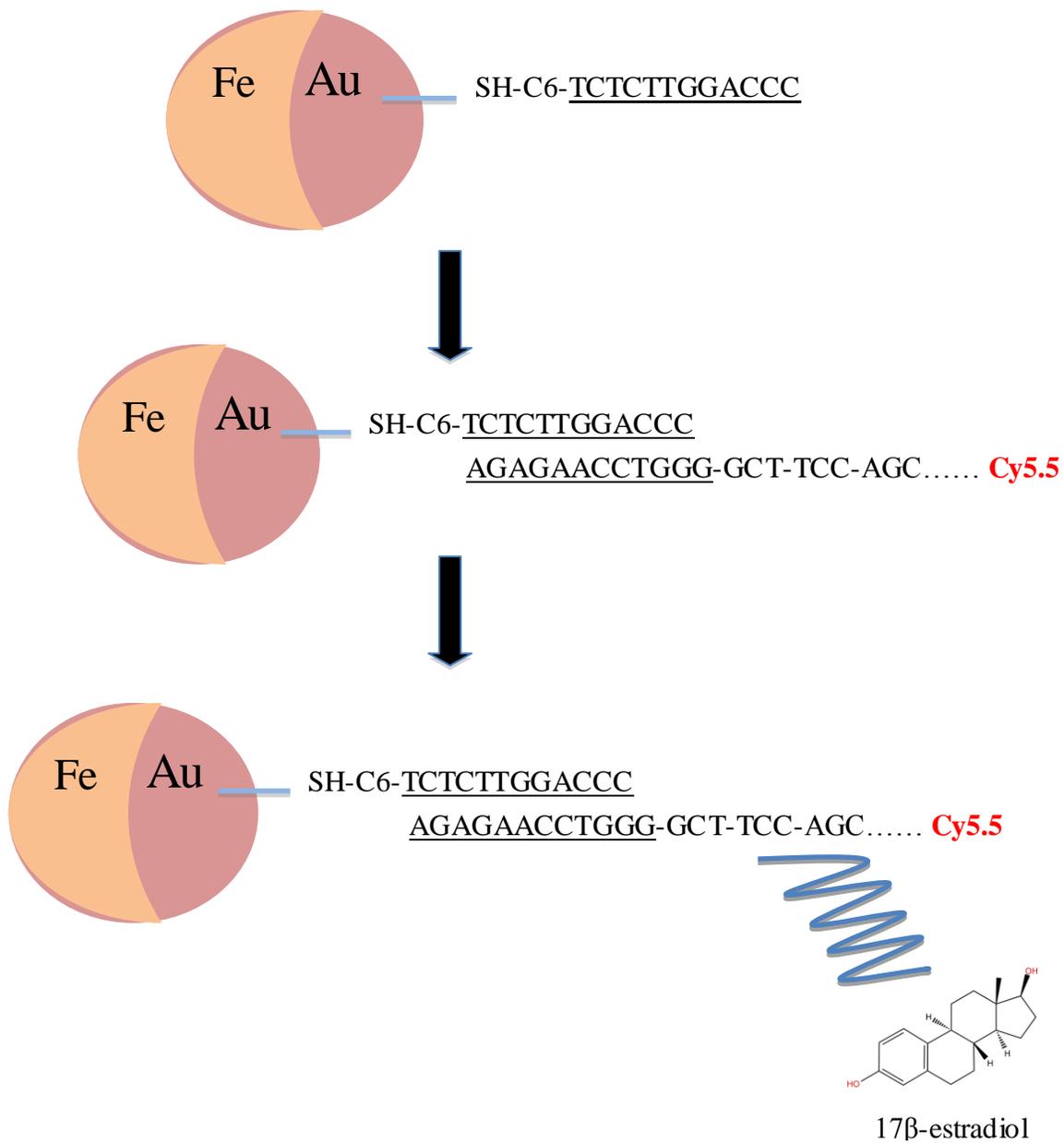
Figure 4.5 **A sequential attachment of thiolated aptamer (SH-apt) and probe aptamer (fl-apt) to functionalize Fe/Au nanoparticle surfaces followed by conjugation of 17β-estradiol at the site-specific sequence to generate Fe/Au-17β-estradiol complex.**
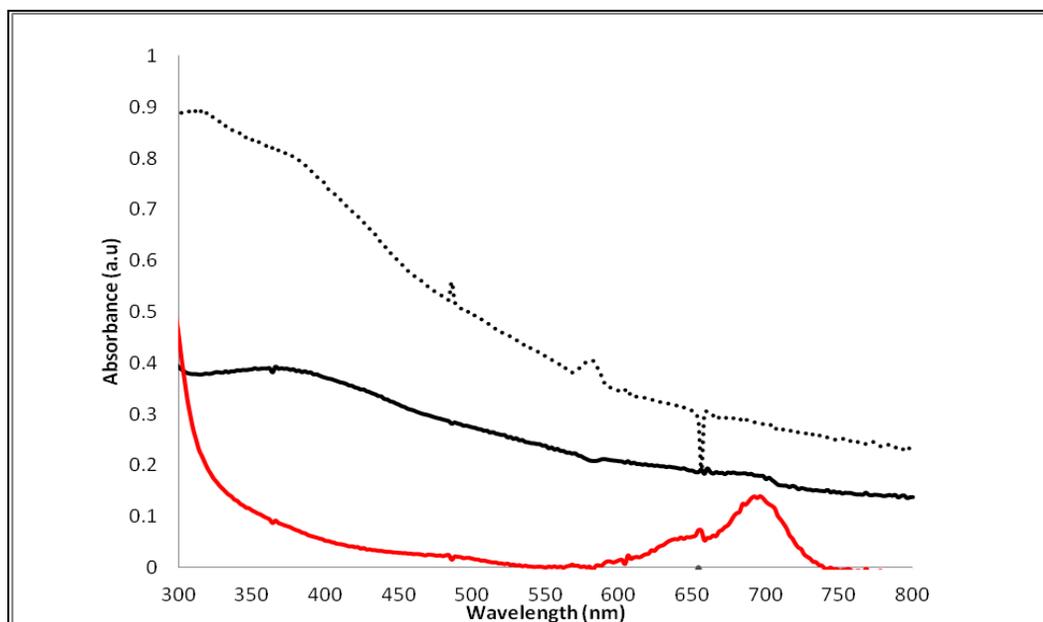
Figure 4.6 UV-Vis spectrophotometer measurement of Fe/Au nanoparticles (black dots), Fe/Au-fl-apt (solid black) and probe aptamer, fl-apt as a sample control (solid red).

4.4.2.2 Detection of 17β-estradiol

A simple nanocatalytic-based assay to detect 17β-estradiol was devised as illustrated in Figure 4.7. In general, this assay requires two simple steps, which are an immobilization process and a catalytic reaction process. The immobilization process is based on the conjugation of aptamer-tagged nanoparticles with 17β-estradiol. The bound 17β-estradiol formed a complex at the nanoparticle surface and this was easily separated from the solution using a permanent magnet due to the Fe/Au superparamagnetic property. Then, the catalytic property of Fe/Au-17β-estradiol was measured using the H_2O_2-ABTS system in a 96-well microplate. The absorbance signal was measured at 414nm as an indicator that oxidized ABTS ($ABTS_{ox}$) was present in the solution.

Results from Figure 4.8 present the absorbance intensity for Fe/Au nanoparticles, aptamer–tagged nanoparticles (Fe/Au-fl-apt) and nanoparticles-analytes complex (Fe/Au-17β-estradiol) within 5 min of the catalytic reaction. From this result, we can observe that a slight difference could be found after Fe/Au nanoparticles were functionalized with probe aptamer (Fe/Au-fl-apt). Inversely, the absorbance intensity was significantly decreased after nanoparticles-analytes complex was formed. Low absorbance intensity indicates that weak catalytic activity is involved. Thus, it clearly shows that the peroxidase activity of Fe/Au nanoparticles is disrupted or hindered by Fe/Au-17β-estradiol complex formation. This forms the basis of the assay, where a reduced signal should be proportional to an increase in 17β-estradiol concentration, and vice-versa.

The precision of this assay was evaluated by determination of the inter-batch coefficient of variability (CV) and this is presented in Table 4.3. Experimental results show that the CV for the nanoparticles-analytes complex was high, and this might be due to the heterogeneous attachment on the nanoparticles surface because the attachment of analytes to nanoparticles driven by the site-specific conjugation of aptamer at the nanoparticles surface.

The effect of surface functionalization with probe aptamer is negligible due to its low impact on the nanoparticles catalytic activity. Therefore, we could suggest that steric hindrance effects are most likely contributing to the disruption of nanoparticles catalytic activity. According to the literature, for small-molecules targets like 17β-estradiol, aptamers often form a cage surrounding the ligand (Long et al., 2008; Huang et al., 2003). Thus, it is speculated that when aptamer-tagged nanoparticles "captured" 17β-estradiol, the aptamer became folded and formed a cage surrounding the target. Assuming many cages were formed at the Fe/Au nanoparticles surface resulting in molecular crowding, its effect on the nanoparticles' catalytic activity is substantial. A study by Pitulice et al. (2013) revealed that the volume occupied by the crowding agent has a significant impact on the rate of ABTS reaction by H_2O_2 and catalyzed by HRP. The V_{max} and K_m of the Michaelis-Menten plot decay along with the growth of obstacle concentration.

It is known that interaction between the nanoparticles and substrate is important to ensure the catalytic process can occur, similar to enzyme-substrate interaction principals. The intermolecular steric hindrance considerably affects the catalytic activity of nanoparticles because the active center (catalytic site) is less accessible to the substrate molecules. Since the

substrates are unable to move into close proximity, interaction between nanoparticles and substrate molecules is interrupted causing weak apparent catalytic activity.

To further evaluate the feasibility of this assay, a serial dilution of 17β-estradiol (0.01 nM, 0.1 nM, 1.0 nM and 10 nM) was tested at different concentrations of aptamer-tagged nanoparticles (33 mg/mL, 17 mg/mL and 2.5 mg/mL). As expected, the absorbance intensity was inversely proportional to the 17β-estradiol concentrations as shown in Figure 4.9. This result suggested that increasing 17β-estradiol concentration would decrease the absorbance intensity causing by larger steric effects. We can also observe that, high absorbance intensity was obtained when aptamer-tagged nanoparticle concentrations were increased up to 33 mg/mL, which is similar with finding in Section 4.4.1 (Figure 4.2). At the same time, the inter-assay CV (%) for this concentration is comparabe to other concentrations (2.5 mg/mL and 17 mg/mL) resulting in low assay accuracy and precision.

17β-estradiol

Immobilization process

Wash and separate using permanent

Catalytic reaction

$H_2O_2 + ABTS_{(red)}$ $H_2O + ABTS_{(ox)}$

Measurement at 414nm

Fe/Au-fl-apt   Fe/Au-17β-estradiol
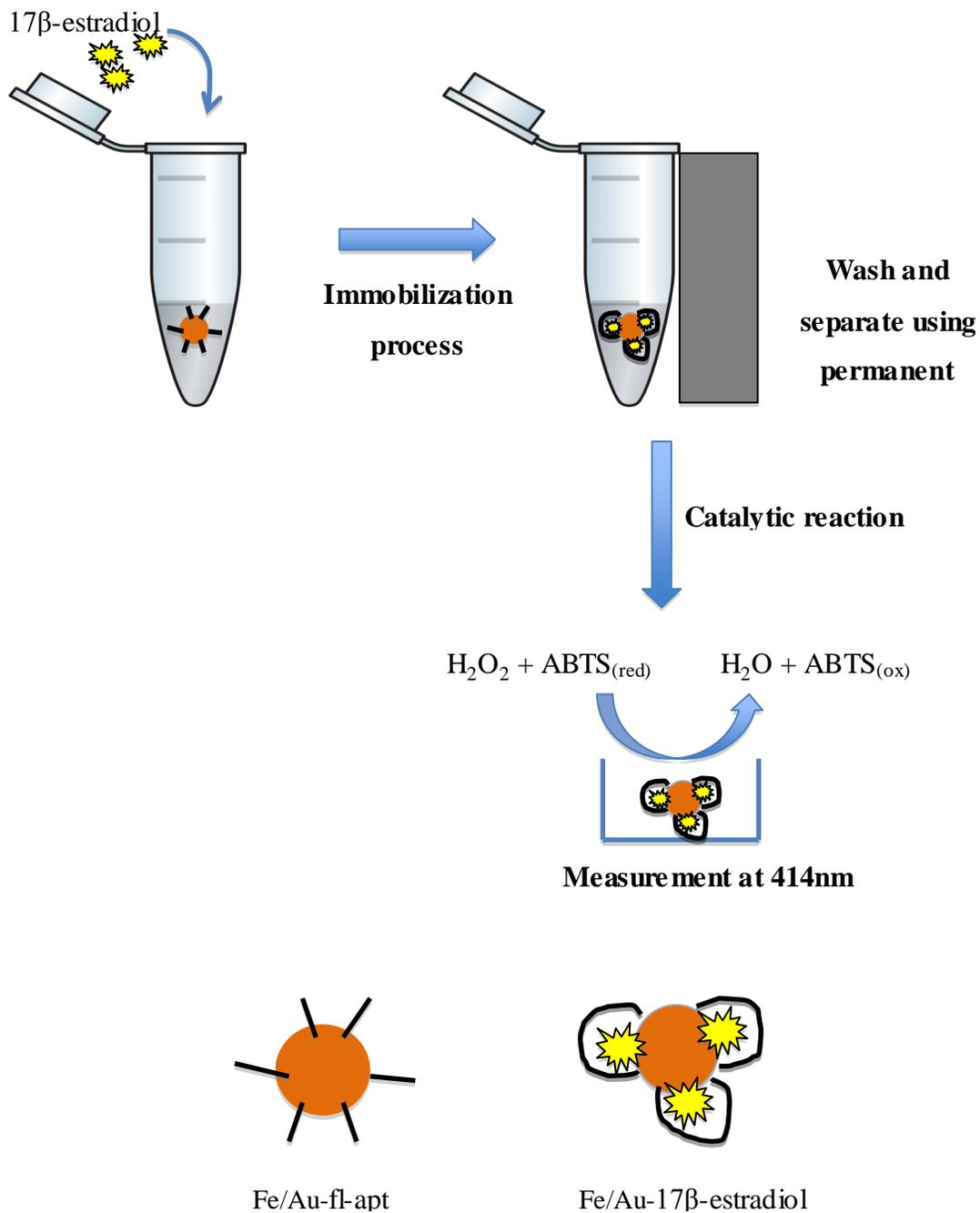
Figure 4.7   **Illustration of the detection strategy for a nanocatalytic-based assay that consists of two main steps i.e. an immobilization process and a catalytic reaction process, measured at 414 nm wavelength for 5 min of reaction.**

127
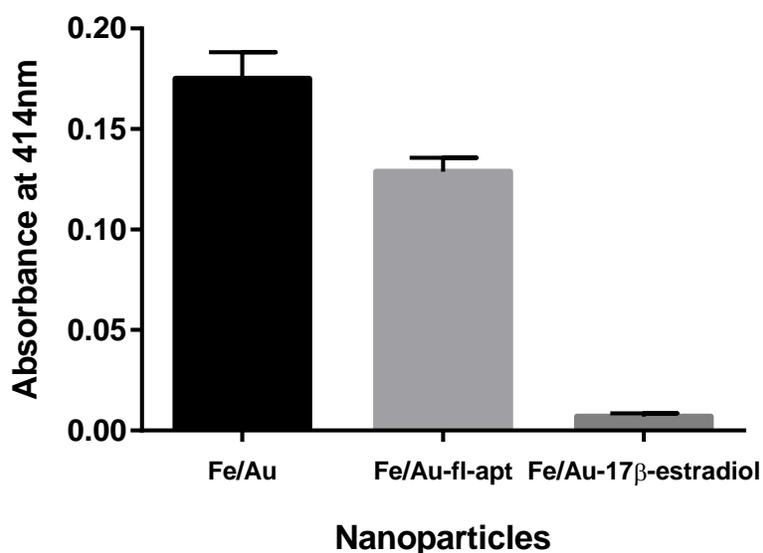
Figure 4.8   **Absorbance intensity at 414 nm for unmodified (Fe/Au) and modified nanoparticles (Fe/Au-fl-apt; Fe/Au-17β-estradiol) with each nanoparticles concentration approximately 12.5mg/mL. (Error bars represent S.D of the absorbance mean)**

Table 4.3   **Inter-assay of coefficient of variations (CV) for the unmodified and modified Fe/Au nanoparticles for absorbance at 414 nm**

Nanoparticles	Mean (n=3)	S.D	CV (%)
Fe/Au	0.175	0.013	8
Fe/Au-fl-apt	0.129	0.007	6
Fe/Au-17β-estradiol	0.007	0.002	22

In addition, to further analyze the assay sensitivity as well as the linear range of 17β-estradiol, the absorbance intensity at 414 nm was plotted with the log 17β-estradiol concentration as presented in Figure 4.10. Interestingly, absorbance data show that when lower amounts of aptamer-tagged nanoparticles are used, the detection assay shows high linearity. At low concentrations, a linear correlation coefficient of 0.999 was obtained as compared to other concentrations, suggesting a better sensitivity for 17β-estradiol detection. Due to its good sensitivity and detection, further evaluation for batch-to-batch reproducibility for two assay runs within different days for triplicate measurement was conducted and the results are shown in Table 4.5. A low CV (%) can be observed for 17β-estradiol concentration ranging between 0.01 nM to 1 nM indicating that the developed assay could be used repeatedly, and further revealed the possibility of batch preparation. However, when high concentrations (>10 nM) of 17β-estradiol was added into the solution, the detection assay show low accuracy and sensitivity due to the high inter- and intra-assay CV (%). A study by Atkinson et al., (2012) reported that 17β-estradiol was found at maximum concentrations in raw sewage (Ottawa and Cornwall, Ontario, Canada) at 66.9 ng/L. For this assay, the detection limit is ranging from ~3 ng/L to 272 ng/L (0.01 nM to 1nM) based on the calculation of 17β-estradiol molecular weight (272.4). Therefore, this assay shows a practical use for detection of 17β-estradiol in environment particularly in wastewater.

Based on the findings discussed above, we could draw a few conclusions on this newly developed nanocatalytic-based assay. The experimental results might indicate that this assay probably shows drawbacks when high concentrations of aptamer-tagged nanoparticles are used.

Notably, low concentrations of the aptamer-tagged nanoparticles used for detection of 17β-estradiol may ensure a higher sensitivity. It is most likely because of the excess aptamer concentration present in the solution results in a homogenous interaction between analytes and aptamer-tagged nanoparticles. Since the analyte is dependent on aptamer presence on the nanoparticles surface, optimization of the aptamer concentration is required for nanoparticles in higher concentration. We also suggest that 17β-estradiol concentrations ranging between 0.01 nM to 1 nM show considerably higher accuracy and reproducibility when tested with the assay. However, a study of optimized sensing conditions needs to be done, in order to improve the assay performance, as this is our first attempt to investigate the practicality of this assay.
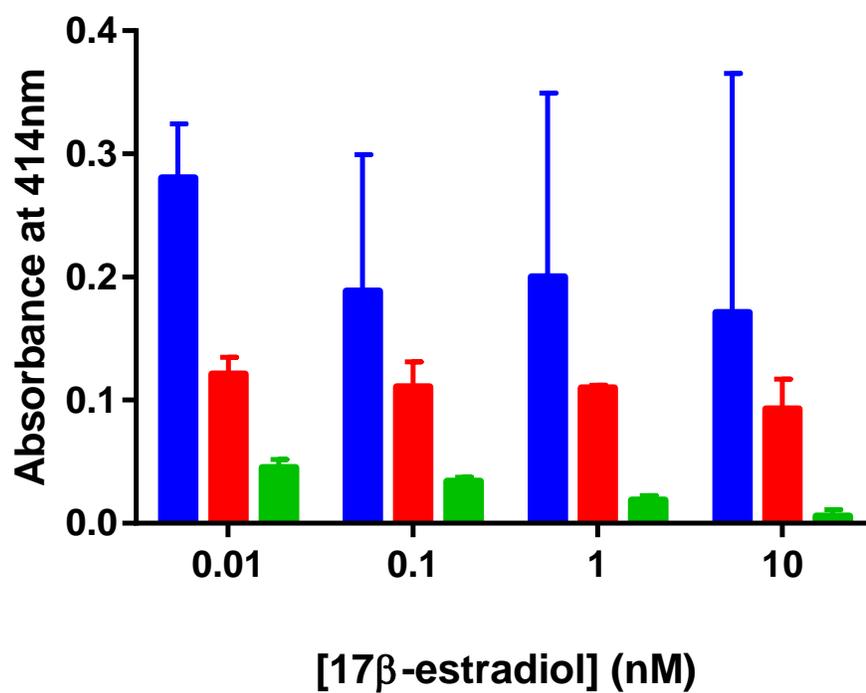
Figure 4.9   Serial dilution of 17β-estradiol at different aptamer-tagged nanoparticles concentration, 33 mg/mL (blue), 17 mg/mL (red) and 2.5 mg/mL (green). (Error bars represent S.D of the absorbance mean)

Table 4.4　　　**Inter-assay coefficients of variation (CV) of 17β-estradiol serial dilution at different aptamer-tagged nanoparticle concentrations.**

[Fe/Au-fl-apt] mg/mL	[17β-estradiol] (nM)	Mean (n=3)	S.D	CV (%)
33	0.01	0.280	0.044	16
	0.10	0.188	0.111	59
	1	0.200	0.150	75
	10	0.171	0.195	114
17	0.01	0.121	0.014	12
	0.10	0.111	0.020	18
	1	0.110	0.003	2
	10	0.093	0.024	26
2.5	0.01	0.045	0.007	15
	0.10	0.034	0.004	11
	1	0.019	0.004	20
	10	0.006	0.006	97
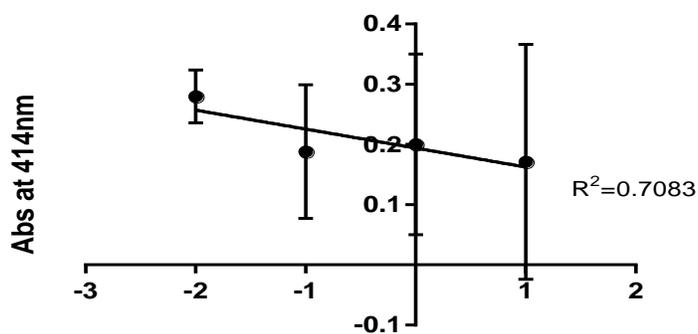
(a) LOG_{10} (17β-estradiol)
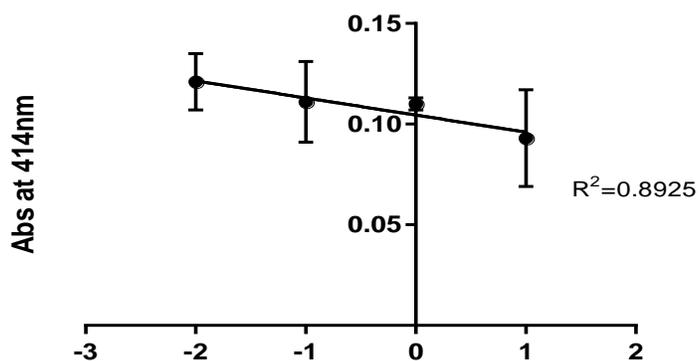
(b) LOG_{10} (17β-estradiol)
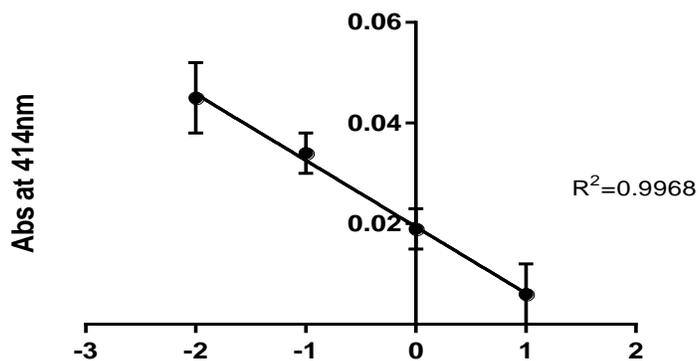
(c) LOG_{10} (17β-estradiol)

Figure 4.10   **The linearity of the detection assay for aptamer-tagged nanoparticle concentrations (a) 33 mg/mL, (b) 17 mg/mL and (c) 2.5 mg/mL. (Error bars represent S.D of the absorbance mean)**

133

Table 4.5   **Intra-assay coefficients of variation (CV) for serial dilutions of 17β-estradiol at 2.5 mg/mL of aptamer-tagged nanoparticles for batch-to-batch reproducibility determination.**

[17β-estradiol] (nM)	Mean (n=2)	S.D	CV (%)
0.01	0.047	0.003	7
0.10	0.029	0.008	26
1	0.018	0.001	4
10	0.012	0.009	77

4.4.2.3 Specificity test

To determine the specificity of the probe aptamer used in this study, several related endocrine disrupting chemicals (EDCs) such as carbaryl, 4NNP and estriol were studied by incubation with the Fe/Au nanoparticles. Then, the nanocatalytic-based assay was measured for each EDCs sample. As shown in Figure 4.11, the results from this assay show a slight absorbance difference between the blank control (Fe/Au-fl-apt) and ones containing other EDCs. In contrast, the absorbance declined substantially when 17β-estradiol was incubated with the nanoparticles, indicating a good selectivity of this assay. Therefore, the nanocatalytic-based assay using the probe aptamer attached on Fe/Au nanoparticles surface could specifically detect 17β-estradiol.

4.4.2.4 Tap water testing

As a preliminary study to evaluate the detection efficiency in real water samples, Fe/Au-fl-apt nanoparticles were tested with various concentrations of 17β-estradiol in tap water samples. For this experiment, two types of tap water were tested, non-filtered tap water (NF) and filtered tap water (F). The detection efficiency was calculated as shown previously in subsection 4.3.4.2. Based on this finding presented in Figure 4.12, the detection efficiency of Fe/Au-fl-apt nanoparticles show considerably good responses towards 17β-estradiol in filtered tap water compared to non-filtered tap water. The plausible reason is because the presence of other particles in non-filtered tap water that possibly interfere significantly the Fe/Au nanoparticles catalytic activity. Surprisingly, high detection efficiency of 17β-estradiol at concentration 10 nM was obtained for non-filtered tap water. Thus, this preliminary testing in tap water provides a good starting point for detection of 17β-estradiol in real water samples using Fe/Au-fl-apt nanoparticles.
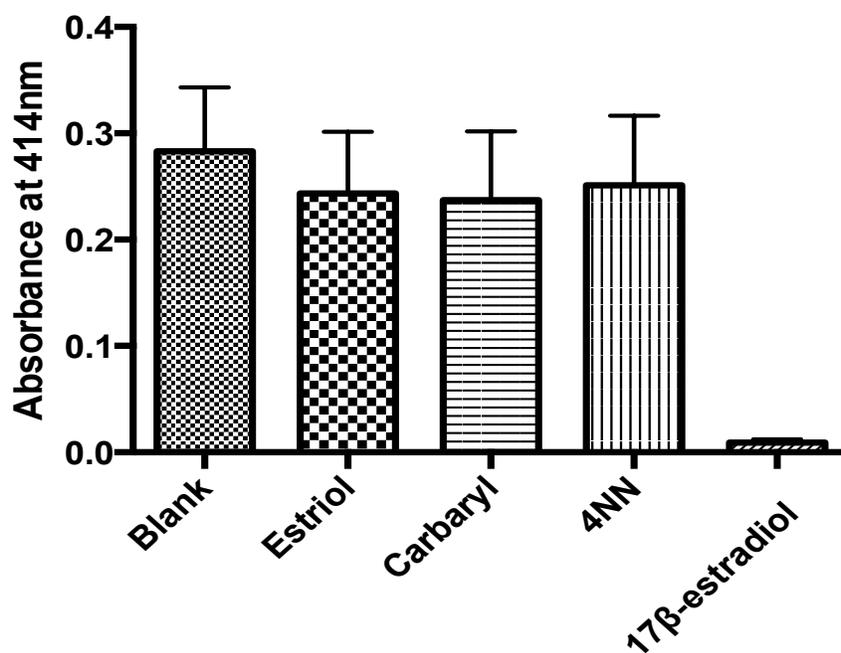
Figure 4.11 Cross-reactivity study with estriol, carbaryl and nonylphenol (4NNP). All the samples were evaluated at 100 nM of each EDCs with approximately 12.5 mg/mL of Fe/Au-fl-apt nanoparticles concentration. (Error bars represent S.D of the absorbance mean)
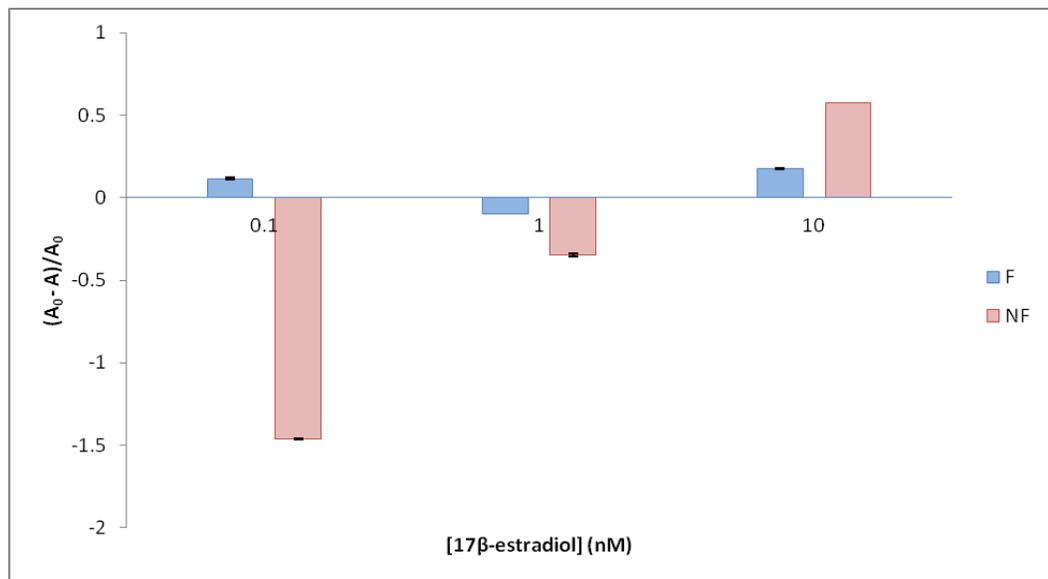
Figure 4.12 Detection efficiency $((A_0\text{-}A)/A_0)$ of Fe/Au-fl-apt nanoparticles with various concentration of 17β-estradiol in tap water samples. Two types of tap water samples were tested, non-filtered tap water (NF) and filtered tap water (F). All the samples were evaluated with approximately 12.5 mg/mL of Fe/Au-fl-apt nanoparticles concentration. (Error bars represent S.D of the absorbance mean)

4.5 Conclusions

In summary, we investigated the synthesized Fe/Au nanoparticles' intrinsic peroxidase-like activity and the potential manipulation of this interesting property for development of a nanocatalytic-based assay. A catalytic reaction by the Fe/Au nanoparticles for the oxidation of ABTS by H_2O_2 showed a typical Michaelis-Menten kinetic form and exhibited a good catalytic efficiency. We also functionalized the nanoparticles by attachment of a specific aptamer to "capture" a target analyte, 17β-estradiol that would form a nanoparticles-analytes complex. The formation of this complex significantly influenced and decreased the nanoparticles' catalytic activity as shown by drastic declines in the absorbance intensity. We suggest that steric effects might be a plausible reason for this phenomenon since the active center, which is the catalytic site, is less accessible to the substrate molecules once the target analyte has complexed with the nanoparticle. Our study provides a new way of utilization of the nanoparticles' peroxidase-like activity for development of a simple, rapid and sensitive detection assay that appears to specifically detect 17β-estradiol in aqueous solution.

References

Atkinson SK, Mariatt VL, Kimpe LE, Lean DRS, Trudeau VL, and Blais JM. (2012) The occurance of steroidal estrogens in south-eastern Ontario Wastewater treatment plants. *Sci of The Tot Env* (430): 119-125

Chen W, Chen J, Liu AL, Wang LM, Li GW, and Lin XH. (2011) Peroxidase-Like Activity of Cupric Oxide Nanoparticle. *Chem Cat Chem* (3): 1151 – 1154

Fujii T, De Groot FMF, Sawatzky GA, Voogt FC, Hibma T, Okada K, and Fujii K. (1999) In situ XPS analysis of various iron oxide films grown by NO_2 -assisted molecular-beam epitaxy. *Phy Rev B* 59(4): 3195-3202

Gao L, Zhuang J, Nie L, Zhang Jinbin, Zhang Y, Gu N, Wang T, Feng J, Yang D, Perrett S, and Yan X. (2007) Intrinsic peroxidase-like activity of ferromagnetic nanoparticles. *Nat Nanotech* (2): 577 - 583

He W, Wu X, Liu J, Hu X, Zhang K, Hou S, Zhou W, and Xie S. (2010) Design of AgM Bimetallic Alloy Nanostructures (M = Au, Pd, Pt) with Tunable Morphology and Peroxidase-Like Activity. *Chem Mater* 22(9): 2988–2994

Huang DB, Vu D, Cassiday LA, Zimmerman JM, Maher LJ, and Ghosh G. (2003) Crystal structure of NF-κB (p50)2 complexed to a high-affinity RNA aptamer. *Proc of the Nat Acad of Sci of the USA, 5* 100(16): 9268-73

Jv Y, Li B, and Cao R. (2010) Positivley-charged Gold Nanoparticles as Peroxidase Mimic and their Application in Hydrogen Peroxidase and Glucose detection. *Chem Commun* (46): 8017-8019

Kang KA, Wang J, Jasinski JB, and Achilefu S. (2011) Fluorescence Manipulation by Gold Nanoparticles: From Complete Quenching to Extensive Enhancement. *J of Nanobiotech* 2011, 9(16): 1-13

Kim YS, Jung HS, Matsuura T, Lee HY, Kawai T, Gu MB. (2007) Electrochemical detection of 17β-estradiol using DNA aptamer immobilized gold electrode chip. *Biosens and Bioelect* (22): 2525–2531

Krüger D, Fuchs H, Rousseau R, Marx D, and Parrinello M. (2001) Interaction of short-chain alkane thiols and thiolates with small gold clusters: Adsorption structures and energetics The Journal of Chemical Physics 115(10): 4776

Liang M, Fan K, Pan Y, Jiang H, Wang F, Yang D, Lu D, Feng J, Zhao J, Yang L, and Yan X. (2013) Fe_3O_4 magnetic nanoparticle peroxidase mimetic-based colorimetric assay for the rapid detection of organophosphorus pesticide and nerve agent. *Anal Chem* 85(1): 308-12

Liu Y, and Yu F. (2011) Substrate-specific modifications on magnetic iron oxide nanoparticles as an artificial peroxidase for improving sensitivity in glucose detection Nanotechnology (22): 145704

Liu Y, Zhu G, Yang J, Yuan A, and Shen X. (2014a) Peroxidase-Like Catalytic Activity of Ag_3PO_4 Nanocrystals Prepared by a Colloidal Route. *PLOS ONE* 9(10): 1-7

Liu Y, Yuan M, Qiao L, and Guo R. (2014b) An efficient colorimetric biosensor for glucose based on peroxidase-like protein-Fe3O4 and glucose oxidase nanocomposites. *Biosens & Bioelect* (52): 391-396

Liu J, Bai W, Niu S, Zhu C, Yang S, and Chen A. (2014c) Highly sensitive colorimetric detection of 17β-estradiol using split DNA aptamers immobilized on unmodified gold nanoparticles. *Sci Rep* 4(7571)

Liu Y, Wang C, Cai N, Long S, and Yu F. (2014d) Negatively charged gold nanoparticles as an intrinsic peroxidase mimic and their applications in the oxidation of dopamine. *J Mater Sci* 49(20): 7143-7150

Long SB, Long MB, White RR, and Sullenger BA. (2008) Crystal structure of an RNA aptamer bound to thrombin. *RNA* 14(12): 2504-12

Raikar US, Tangod VB, Mastiholi BM, and Fulari VJ. (2011) Fluorescence quenching using plasmonic gold nanoparticles. *Opt Comm* 284(19): 4761-4765

Sapsford KE, Algar WR, Berti L, Gemmill KB, Casey BJ, Oh E, Stewart MH, and Medintz IL. (2013) Functionalizing nanoparticles with biological molecules: Developing chemistries that facilitate nanotechnology. *Chem Rev* 113(3): 1904–2074

Schneider G, and Decher G. (2006) Distance-Dependent Fluorescence Quenching on Gold Nanoparticles Ensheathed with Layer-by-Layer Assembled Polyelectrolytes. *Nano Lett* 6(3): 530–536

Sun H, Jiao X, Han Y, Jiang Z, and Chen D. (2013) Synthesis of Fe_3O_4-Au Nanocomposites with Enhanced Peroxidase-Like Activity. *Eur J Inorg Chem* 109–114

Umezawa K, Matsui A, Nakamura Y, Citterio D, and Suzuki K. (2009) Bright, Color Tunable Fluorescent Dyes in the Vis/NIR Region: Establishment of New "Tailor Made" Multicolor Fluorophores Based on Borondipyrromethene. *Chem – A Eur J* 15(5): 1096-1106

Voinov MA, Pagan JOS, Morrison E, Smirnova TI, and Smirnov AI. (2011) Surface-Mediated Production of Hydroxyl Radicals as a Mechanism of Iron Oxide Nanoparticle Biotoxicity. *J Am Chem Soc* 133(1): 35-41

Wang J, Wang F, and Dong S. (2009) Methylene blue as an indicator for sensitive electrochemical detection of adenosine based on aptamer switch. *J of Electro Chem* (626): 1-5

Yu F, Huang Y, Cole AJ, and Yang VC. (2009) The artificial peroxidase activity of magnetic iron oxide nanoparticles and its application to glucose detection. *Biomater* 30(27): 4716-4722

Zhang XQ, Gong SW, Zhang Y, Yang T, Wang CY, and Gu N. (2010) Prussian blue modified iron oxide magnetic nanoparticles and their high peroxidase-like activity. *J Matter Chem* (20): 5110-5116

Chapter 5
Overall Conclusions and Recommendations

5.1   Conclusions

The work in this thesis highlighted the manipulation of heterogeneous Fe/Au nanoparticles' physiochemical property for application in nanosensor systems. Furthermore, the synergetic effect of this nanoparticle greatly enhanced the individual nanoparticle property and lead to multifunctionality. In this study, Fe/Au nanoparticles showed a useful ability as biomolecules supporting materials as well as a good peroxidase-like catalytic activity, leading to the development of a nanocatalytic-based assay. The marked features of this work are as follow:

1.   The IONPs surface charge was easily tuned using pH adjustment, thus making it possible for electrostatic -self -assembly technique with AuNPs. The electrostatic, combined with the magnetic, interaction was the main driving force for the formation of heterogeneous nanoparticles, IONPs-AuNPs.

2.   The formation of IONPs-AuNPs show a blue-shift phenomenon as observed for localized plasmon resonance of AuNPs. It might be due to the particles coalescence and recrystallization as the nanoparticles became more spherical. Furthermore, characterization analysis reveals the formation of a metastable alloy-like morphology (Fe/Au).

3.   The colorimetric assay for detection of glucose using immobilized glucose oxidase (GOx) on the Fe/Au surface showed that an increase in absorbance correlates with the glucose concentration with a linear range from 20 μM to 100 μM.

4. The synthesized Fe/Au nanoparticles show intrinsic peroxidase-like activity that follows typical Michaelis-Menten kinetic. The catalytic activity was measured spectrophotometricly at 414 nm using H_2O_2-ABTS colorimetric system.

5. A nanocatalytic-based assay was developed based on two fundamental steps, the immobilization and the catalytic reaction process. A specific aptamer was attached at the Fe/Au nanoparticles' surface in order to form a nanoparticles-analytes complex (Fe/Au-17β-estradiol). The catalytic activity was significantly inhibited with an increase of Fe/Au-17β-estradiol concentration, and this could be used as the basis for a simple colorimetric assay.

6. The utilization of the nanoparticles' peroxidase-like activity provides a new way for development of a simple, rapid and sensitive detection assay that appears to specifically detect 17β-estradiol in aqueous solution ranging from 0.01 nM to 1 nM with considerably higher accuracy and reproducility without interference from other selected EDCs (i.e. estriol, carbaryl, and 4NN).

7. In addition, detection efficiency $((A_0-A)/A_0)$ of Fe/Au-fl-apt nanoparticles show considerably good responses towards 17β-estradiol in filtered tap water compared to non-filtered tap water and provides a good basis for detection of 17β-estradiol in real water samples using Fe/Au-fl-apt nanoparticles.

5.2 Recommendation for future work

The heterogeneous Fe/Au nanoparticles undoubtedly provide an interesting physiochemical property, especially the peroxidase-like catalytic activity for application in nanosensor systems. Therefore, some of the work presented here can be extended in certain major directions, such as heterostructure formation and optimization of nanocatalytic-based assay.

The Fe/Au nanoparticles' catalytic activity is a structure-sensitive property. Hence, the nanoparticle morphology might affect the catalytic activity. To investigate this phenomenon, other nanoparticle morphologies such as core-shell and dumbbell, should be explored. The electrostatic -self -assembly technique is still in its infancy stage, and thus an optimized condition with controllability of the synthesis should be investigated. Furthermore, modification of γ-Fe_2O_3 is needed since it shows a weak catalytic activity. A surface modification agent like Prussian blue (PB) can be utilize in order to increase the catalytic activity, thus adding of PB into Fe/Au nanoparticles might enhance the catalytic activity. In addition, a study on size-dependent nanoparticles and their impact on catalytic activity can also be carry out.

An optimized condition for surface functionalization using aptamer needs to be carried out since this specific handle was Au dependent. This is the first attempt for development of nanocatalytic-based assay, thus, characterization and assay optimization on the sensing capability and efficiency need to be extensively performed.

Appendix A

Optimization of IONPs coated with AuNPs using poly (allylamine hydrochloride) for layer by layer assembly technique

Summary

Background: Polyelectrolytes (ionic polymers) have been introduced in the LbL assembly technique as an alternated adsorption of oppositely charged polymers. It modifies surfaces and colloids by exploiting electrostatic attraction for their deposition. This process is versatile as it can be deposited repeatedly and is able to generate a multilayered coating. In this optimization study, a weak cationic polyelectrolytes poly (allylamine hydrochloride) (PAH) with molecular weight, ~ 65 000 are selected for LbL assembly technique and it can be easily tuned by simple pH adjustments. The PAH chemical structure is shown in Figure A1.
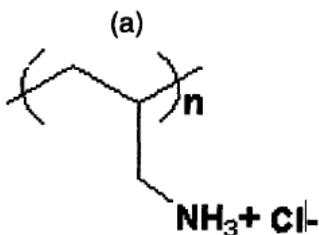
Figure A1   Chemicals structure of the weak polyelectrolyte, PAH

Methods: IONPs were synthesized using a reverse co-precipitation method and then were treated with PAH and were incubated overnight in dark. AuNPs were synthesized using the Turkevish method followed by microwave-assisted irradiation. Then, AuNPs were added into the

IONPs/PAH solution and were incubated overnight in dark. Finally, the IONPs/PAH/AuNPs were incubated with another layer of PAH and were incubated overnight in dark to form IONPs/PAH/AuNPs/PAH. This interaction is based on the opposite interfacial charges exhibited between the anionic nanoparticles (citrate-capped IONPs and citrate-capped AuNPs) and cationic polyelectrolytes.

Results: For this study, the magnetic (IONPs) and plasmonic properties (AuNPs) were observed. A simple analytical signal using a UV-Vis spectrophotometer was used based on the deposition of AuNPs into the IONPs nanoparticles. However, in this study, we are unable to observe any magnetic and plasmonic properties for IONPs/PAH/AuNPs/PAH. The nanoparticles show aggregation and no interaction was observed with the permanent magnet. In addition, no blue or red shift was observed as an indicator of the deposition of multilayer coatings on AuNPs.

Conclusions: The LbL technique using cationic polyelectrolyte (PAH) with the alternate deposition of citrate-capped IONPs and citrate-capped AuNPs was unsuccessful. This might be due to the pH of weak polyelectrolyte solutions (PAH). A controlled pH is an extremely important parameter when assembling the core and shell structure. Unlike strong polyelectrolytes, which remain charged over the entire pH range, the degree of ionization of weak polyelectrolytes depends greatly on solution pH. Furthermore, the deposition of PAH induced particles aggregation due to the surface modification with polyelectrolytes, hence magnetic and plasmonic properties of IONPs and AuNPs unable to be observed.

146